

Search for new phenomena in final states with an energetic jet and large missing transverse momentum in pp collisions at $\sqrt{s} = 13$ TeV using the ATLAS detector

M. Aaboud *et al.**

(ATLAS Collaboration)

(Received 27 April 2016; published 22 August 2016)

Results of a search for new phenomena in final states with an energetic jet and large missing transverse momentum are reported. The search uses proton-proton collision data corresponding to an integrated luminosity of 3.2 fb^{-1} at $\sqrt{s} = 13$ TeV collected in 2015 with the ATLAS detector at the Large Hadron Collider. Events are required to have at least one jet with a transverse momentum above 250 GeV and no leptons. Several signal regions are considered with increasing missing-transverse-momentum requirements between $E_T^{\text{miss}} > 250$ GeV and $E_T^{\text{miss}} > 700$ GeV. Good agreement is observed between the number of events in data and Standard Model predictions. The results are translated into exclusion limits in models with large extra spatial dimensions, pair production of weakly interacting dark-matter candidates, and the production of supersymmetric particles in several compressed scenarios.

DOI: [10.1103/PhysRevD.94.032005](https://doi.org/10.1103/PhysRevD.94.032005)

I. INTRODUCTION

Events with an energetic jet and large missing transverse momentum \vec{p}_T^{miss} (with magnitude E_T^{miss}) in the final state constitute a clean and distinctive signature in searches for new physics beyond the Standard Model (SM) at colliders. Such signatures are referred to as monojetlike in this paper. In particular, monojet (as well as monophoton and mono- W/Z) final states have been studied at the Large Hadron Collider (LHC) [1–15] in the context of searches for large extra spatial dimensions (LED), supersymmetry (SUSY), and weakly interacting massive particles (WIMPs) as candidates for dark matter.

The Arkani-Hamed, Dimopoulos, and Dvali (ADD) model for LED [16] explains the large difference between the electroweak unification scale at $O(10^2)$ GeV and the Planck scale $M_{\text{Pl}} \sim O(10^{19})$ GeV by postulating the presence of n extra spatial dimensions of size R , and defining a fundamental Planck scale in $4 + n$ dimensions, M_D , given by $M_{\text{Pl}}^2 \sim M_D^{2+n} R^n$. An appropriate choice of R for a given n yields a value of M_D at the electroweak scale. The extra spatial dimensions are compactified, resulting in a Kaluza–Klein tower of massive graviton modes. If produced in high-energy collisions in association with an energetic jet, these graviton modes escape detection leading to a monojetlike signature in the final state.

Supersymmetry [17–25] is a theory for physics beyond the SM that naturally solves the hierarchy problem and

provides a possible candidate for dark matter in the Universe. SUSY enlarges the SM spectrum of particles by introducing a new supersymmetric partner (sparticle) for each particle in the SM. In particular, a new scalar field is associated with each left- or right-handed quark state and, ignoring intergenerational mixing, two squark mass eigenstates \tilde{q}_1 and \tilde{q}_2 result from the mixing of the scalar fields for a particular flavor.

In some SUSY scenarios, a significant mass difference between the two eigenstates in the bottom squark (sbottom) and top squark (stop) sectors can occur, leading to rather light sbottom \tilde{b}_1 and stop \tilde{t}_1 mass states. In addition, naturalness arguments suggest that the third generation squarks should be light, with masses below about 1 TeV [26]. In a generic supersymmetric extension of the SM that assumes R-parity conservation [27–31], sparticles are produced in pairs and the lightest supersymmetric particle (LSP) is stable. In this paper the LSP is assumed to be the lightest neutralino¹ $\tilde{\chi}_1^0$.

The results from the monojetlike analysis are interpreted in terms of searches for squark production using simplified models in compressed scenarios for which the mass difference $\Delta m \equiv m_{\tilde{q}} - m_{\tilde{\chi}_1^0}$ is small. Three separate processes are considered: stop pair production, where the stop decays to a charm quark and the LSP ($\tilde{t}_1 \rightarrow c + \tilde{\chi}_1^0$); sbottom pair production with $\tilde{b}_1 \rightarrow b + \tilde{\chi}_1^0$; and squark pair production, with $\tilde{q} \rightarrow q + \tilde{\chi}_1^0$ ($q = u, d, c, s$). For relatively small Δm , both the transverse momenta of the quark jets and the E_T^{miss}

*Full author list given at the end of the article.

Published by the American Physical Society under the terms of the *Creative Commons Attribution 3.0 License*. Further distribution of this work must maintain attribution to the author(s) and the published article's title, journal citation, and DOI.

¹Neutralinos $\tilde{\chi}_j^0$ ($j = 1, 2, 3, 4$ in the order of increasing mass) and charginos $\tilde{\chi}_j^\pm$ ($j = 1, 2$) are SUSY mass eigenstates formed from the mixing of the SUSY partners to the Higgs and electroweak gauge bosons.

in the final state are low, making it difficult to extract the signal from the large multijet background. In this study, the event selection makes use of the presence of initial-state radiation jets to identify signal events (see Fig. 1, left). In this case, the squark-pair system is boosted, leading to larger E_T^{miss} .

A nonbaryonic dark matter component in the Universe is commonly used to explain a range of astrophysical measurements (see, for example, Ref. [32] for a review). Since none of the SM particles are adequate dark matter candidates, the existence of a new particle is often hypothesized. Weakly interacting massive particles are one such class of particle candidates [33] that can be searched for at the LHC. Such a new particle would result in the correct relic density values for nonrelativistic matter in the early Universe [34], as measured by the Planck [35] and WMAP [36] satellites, if its mass is between a few GeV and one TeV and if it has electroweak-scale interaction cross sections. Many new particle-physics models such as SUSY [17–25] also predict WIMPs.

In contrast to the Run-1 analyses with the monojetlike final state [37], the results of this analysis are not interpreted in terms of the effective-field-theory models [38]. Simplified models are used instead, providing a more complete framework that involves new mediator particles between the SM and the dark sector [39–42]. The predictions from simplified models coincide with those obtained by using an effective-field-theory approach when the mediator mass considered is above 10 TeV [43]. Here a model with an s -channel exchange of a spin-1 mediator particle with axial-vector couplings is considered, connecting the quarks to WIMPs of a Dirac fermion type. This is referred to as a leptophobic Z' -like model, and is defined by four free parameters: the WIMP mass m_χ , the mediator mass m_A , the coupling of the mediator to WIMPs (g_χ) and the flavor-universal coupling to quarks (g_q). Couplings to other SM particles are not allowed and the minimal mediator width is taken, defined in accord with Ref. [41] as

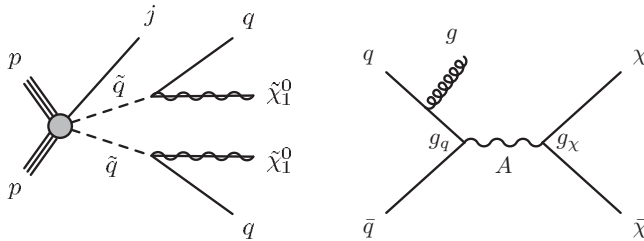


FIG. 1. Left: a generic diagram for the pair production of squarks with the decay mode $\tilde{q} \rightarrow q + \tilde{\chi}_1^0$. Right: diagram for the pair production of weakly interacting massive particles, with a leptophobic Z' -like mediator A with axial-vector couplings exchanged in the s -channel. The presence of a jet from initial-state radiation is indicated for both processes for illustration purposes.

$$\Gamma_{\min} = \frac{g_\chi^2 m_A}{12\pi} \beta_\chi^3 \theta(m_A - 2m_\chi) + \sum_q \frac{3g_q^2 m_A}{12\pi} \beta_q^3 \theta(m_A - 2m_q), \quad (1)$$

where $\theta(x)$ denotes the Heaviside step function and $\beta_f = \sqrt{1 - \frac{4m_f^2}{m_A^2}}$ is the velocity of the fermion f with mass m_f in the mediator rest frame. The sum runs over all quark flavors. The monojetlike signature in this model emerges from initial-state radiation of a gluon as shown in Fig. 1 (right).

The paper is organized as follows. The ATLAS detector is described in the next section. Section III provides details of the simulations used in the analysis for background and signal processes. Section IV discusses the reconstruction of jets, leptons, and missing transverse momentum, while Sec. V describes the event selection. The estimation of background contributions and the study of systematic uncertainties are discussed in Secs. VI and VII. The results are presented in Sec. VIII and are interpreted in terms of limits in models for ADD LED, SUSY in compressed scenarios, and WIMP pair production. Finally, Sec. IX is devoted to the conclusions.

II. EXPERIMENTAL SETUP

The ATLAS detector [44] covers almost the whole solid angle² around the collision point with layers of tracking detectors, calorimeters, and muon chambers. The ATLAS inner detector covers the pseudorapidity range $|\eta| < 2.5$. It consists of a silicon pixel detector, a silicon microstrip detector, and a straw tube tracker that also measures transition radiation for particle identification, all immersed in a 2 T axial magnetic field produced by a solenoid. During the first LHC long shutdown, a new tracking layer, known as the insertable B-layer [45], was added at a radius of 33 mm.

High-granularity lead/liquid-argon (LAr) electromagnetic sampling calorimeters cover the pseudorapidity range $|\eta| < 3.2$. The hadronic calorimetry in the range $|\eta| < 1.7$ is provided by a steel/scintillator-tile calorimeter, consisting of a large barrel and two smaller extended barrel cylinders, one on either side of the central barrel. In the endcaps

²The ATLAS experiment uses a right-handed coordinate system with its origin at the nominal interaction point (IP) in the center of the detector and the z axis along the beam pipe. The x axis points from the IP to the center of the LHC ring, and the y axis points upward. The azimuthal angle ϕ is measured around the beam axis, and the polar angle θ is measured with respect to the z axis. The transverse energy is defined as $E_T = E \sin \theta$, the transverse momentum as $p_T = p \sin \theta$, and the pseudorapidity as $\eta = -\ln[\tan(\theta/2)]$. The rapidity is defined as $y = 0.5 \times \ln[(E + p_z)/(E - p_z)]$, where E denotes the energy and p_z is the component of the momentum along the beam direction.

($|\eta| > 1.5$), copper/LAr and tungsten/LAr hadronic calorimeters match the outer $|\eta|$ limits of the endcap electromagnetic calorimeters. The LAr forward calorimeters provide both the electromagnetic and hadronic energy measurements, and extend the coverage to $|\eta| < 4.9$.

The muon spectrometer measures the deflection of muons in the magnetic field provided by large superconducting air-core toroid magnets in the pseudorapidity range $|\eta| < 2.7$, instrumented with separate trigger and high-precision tracking chambers. Over most of the η range, a measurement of the track coordinates in the bending direction of the magnetic field is provided by monitored drift tubes. Cathode strip chambers with higher granularity are used in the innermost plane over $2.0 < |\eta| < 2.7$. The muon fast trigger detectors cover the pseudorapidity range $|\eta| < 2.4$ and provide a measurement of the coordinate in the nonbending plane.

The data were collected using an online two-level trigger system [46] that selects events of interest and reduces the event rate from several MHz to about 1 kHz for recording and offline processing.

III. MONTE CARLO SIMULATION

Monte Carlo (MC) simulated event samples are used to compute detector acceptance and reconstruction efficiencies, determine signal and background contributions, and estimate systematic uncertainties in the final results. Background contributions from multijet processes are determined directly from data.

A. Background simulation

The expected background to the monojetlike signature is dominated by $Z(\rightarrow \nu\bar{\nu}) + \text{jets}$ and $W + \text{jets}$ production with $W(\rightarrow \tau\nu) + \text{jets}$ being the largest $W + \text{jets}$ background, and includes small contributions from $Z/\gamma^*(\rightarrow \ell^+\ell^-) + \text{jets}$ ($\ell = e, \mu, \tau$), multijet, $t\bar{t}$, single-top, and diboson (WW, WZ, ZZ) processes. Contributions from top production associated with additional vector bosons ($t\bar{t} + W, t\bar{t} + Z, \text{ or } t + Z + q/b$ processes) are negligible.

Events containing W or Z bosons with associated jets are simulated using the SHERPA-2.1.1 [47] generator. Matrix elements (ME) are calculated for up to two partons at next-to-leading order (NLO) and four partons at leading order (LO) using the COMIX [48] and OPENLOOPS [49] matrix element generators and merged with the SHERPA parton shower (PS) [50] using the ME + PS@NLO prescription [51]. The CT10 [52] parton distribution function (PDF) set is used in conjunction with a dedicated parton shower tuning developed by the authors of SHERPA. The MC predictions are initially normalized to next-to-next-to-leading-order (NNLO) perturbative QCD (pQCD) predictions according to DYNLO [53,54] using MSTW2008 90% C.L. NNLO PDF sets [55].

For the generation of $t\bar{t}$ and single top quarks in the Wt channel and s channel the POWHEG-BOX v2 [56] generator with the CT10 PDF sets in the matrix element calculations is used. Electroweak t -channel single top-quark events are generated using the POWHEG-BOX v1 generator. This generator uses the four-flavor scheme for the calculations of NLO matrix elements with the fixed four-flavor PDF set CT10. The parton shower, fragmentation, and underlying event are simulated using PYTHIA-6.428 [57] with the CTEQ6L1 [58] PDF sets and the corresponding Perugia 2012 set of tuned parameters (P2012 tune) [59]. The top-quark mass is set to 172.5 GeV. The EVTGEN v.1.2.0 program [60] is used to model the decays of the bottom and charm hadrons. Finally, diboson samples ($WW, WZ, \text{ and } ZZ$ production) are generated using SHERPA-2.1.1 with CT10 PDFs and are normalized to NLO pQCD predictions [61]. The diboson samples are also generated using POWHEG interfaced to PYTHIA-8.186 and using CT10 PDFs for studies of systematic uncertainties.

B. Signal simulation

Simulated samples for the ADD LED model with different numbers of extra dimensions in the range $n = 2-6$ and M_D in the range 2–5 TeV are generated using PYTHIA-8.165 with NNPDF23LO [62] PDFs. The renormalization scale is set to the geometric mean of the transverse mass of the two produced particles, $\sqrt{(p_{T,G}^2 + m_G^2)(p_{T,p}^2 + m_p^2)}$, where m_G and $p_{T,G}$ (m_p and $p_{T,p}$) denote, respectively, the mass and the transverse momentum of the graviton (parton) in the final state. The factorization scale is set to the minimum transverse mass $\sqrt{m^2 + p_T^2}$ of the graviton and the parton.

SUSY signals for stop pair production with $\tilde{t}_1 \rightarrow c + \tilde{\chi}_1^0$, for sbottom pair production decaying as $\tilde{b}_1 \rightarrow b + \tilde{\chi}_1^0$, and for the production of squark pairs from the first two squark generations with $\tilde{q} \rightarrow q + \tilde{\chi}_1^0$ ($q = u, d, c, s$) are considered. Events are generated with MG5_aMC@NLO v5.2.2.3 [63] interfaced to PYTHIA-8.186 with the ATLAS A14 [64] tune for the modeling of the squark decay, and the parton showering, hadronization, and underlying event. The matrix element calculation is performed at tree level, and includes the emission of up to two additional partons. The renormalization and factorization scales are set to the sum of transverse masses of all final state particles. The PDF used for the generation is NNPDF23LO. The ME-PS matching is done using the CKKW-L [65] prescription, with a matching scale set to one quarter of the pair-produced superpartner mass. Simulated samples with squark masses in the range between 250 and 700 GeV and Δm varying between 5 and 25 GeV are produced. Signal cross sections are calculated to NLO in the strong coupling constant, adding the resummation of soft gluon emission at next-to-leading-logarithmic (NLO + NLL) accuracy [66–68]. The nominal cross section and its uncertainty are taken from an envelope of

cross-section predictions using different PDF sets and factorization and renormalization scales, as described in Ref. [69].

WIMP signals are simulated in POWHEG-BOX v2 [70–72] using revision 3049 of the DMV model implementation of WIMP pair production with s -channel spin-1 mediator exchange at NLO precision including parton showering effects, introduced in Ref. [73]. Renormalization and factorization scales are set to $H_T/2$ on an event-by-event basis, where $H_T = \sqrt{m_{\chi\chi}^2 + p_{T,j1}^2} + p_{T,j1}$ is defined by the invariant mass of the WIMP pair ($m_{\chi\chi}$) and the transverse momentum of the hardest jet ($p_{T,j1}$). A Breit-Wigner distribution is chosen to describe the mediator propagator. Events are generated using the NNPDF30NLO [74] parton distribution functions and interfaced to PYTHIA-8.205 with the ATLAS A14 tune for parton showering. Couplings of the mediator to WIMPs and quarks are set to $g_\chi = 1$ and $g_q = 1/4$, leading to narrow mediators with Γ_{\min}/m_A up to about 5%. A grid of samples is produced for WIMP masses ranging from 1 GeV to 1 TeV and mediator masses between 10 GeV and 2 TeV.³

Differing pileup (multiple proton-proton interactions in the same or neighboring bunch crossings) conditions as a function of the instantaneous luminosity are taken into account by overlaying simulated minimum-bias events generated with PYTHIA onto the hard-scattering process. The MC-generated samples are processed with a full ATLAS detector simulation [75] based on the GEANT4 program [76]. The simulated events are reconstructed and analyzed with the same analysis chain as for the data, using the same trigger and event selection criteria.

IV. RECONSTRUCTION OF PHYSICS OBJECTS

Jets are reconstructed from energy deposits in the calorimeters using the anti- k_r jet algorithm [77] with the radius parameter (in y - ϕ space) set to 0.4. The measured jet transverse momentum is corrected for detector effects, including the noncompensating character of the calorimeter, by weighting energy deposits arising from electromagnetic and hadronic showers differently. In addition, jets are corrected for contributions from pileup, as described in Ref. [78]. Jets with corrected $p_T > 20$ GeV and $|\eta| < 2.8$ are initially considered in the analysis. Track-based variables to suppress pileup jets have been developed. A combination of two such variables called the jet-vertex tagger is constructed. In order to remove jets originating from pileup collisions, for central jets ($|\eta| < 2.4$) with $p_T < 50$ GeV a significant fraction of the tracks associated with

³In the generation of the samples, the *bornkmin* and *bornsupfact* MC parameters [70] are set to 150 GeV and 1 TeV, respectively, in order to suppress the generation of events at low E_T^{miss} .

each jet must have an origin compatible with the primary vertex, as defined by the jet-vertex tagger [79].

The presence of leptons (electrons or muons) in the final state is used in the analysis to define control samples and to reject background contributions in the signal regions (see Secs. V and VI). Electron candidates are initially required to have $p_T > 20$ GeV and $|\eta| < 2.47$, and to satisfy the loose electron shower shape and track selection criteria described in Refs. [80,81]. Overlaps between identified electrons and jets in the final state are resolved. Jets are discarded if their separation $\Delta R = \sqrt{(\Delta\eta)^2 + (\Delta\phi)^2}$ from an identified electron is less than 0.2. The electrons separated by ΔR between 0.2 and 0.4 from any remaining jet are removed.

Muon candidates are formed by combining information from the muon spectrometer and inner tracking detectors as described in Ref. [80] and are required to have $p_T > 10$ GeV and $|\eta| < 2.5$. Jets with $p_T > 20$ GeV and less than three tracks with $p_T > 0.4$ GeV associated with them are discarded if their separation ΔR from an identified muon is less than 0.4. The muon is discarded if it is matched to a jet that has at least three tracks associated with it.

The E_T^{miss} is reconstructed using all energy deposits in the calorimeter up to pseudorapidity $|\eta| = 4.9$. Clusters associated with either electrons or photons with $p_T > 20$ GeV and those associated with jets with $p_T > 20$ GeV make use of the corresponding calibrations for these objects. Softer jets and clusters not associated with these objects are calibrated using tracking information [82]. As discussed below, in this analysis the E_T^{miss} is not corrected for the presence of muons in the final state.

V. EVENT SELECTION

The data sample considered in this paper was collected with tracking detectors, calorimeters, muon chambers, and magnets fully operational, and corresponds to a total integrated luminosity of 3.2 fb^{-1} . The data were selected online using a trigger logic that selects events with E_T^{miss} above 70 GeV, as computed at the final stage of the two-level trigger system of ATLAS. With the final analysis requirements, the trigger selection is fully efficient for $E_T^{\text{miss}} > 250$ GeV, as determined using a data sample with muons in the final state. The following selection criteria, summarized in Table I, are applied in the signal regions.

- (i) Events are required to have a reconstructed primary vertex for the interaction with at least two associated tracks with $p_T > 0.4$ GeV and consistent with the beamspot envelope; when more than one such vertex is found, the vertex with the largest summed p_T^2 of the associated tracks is chosen.
- (ii) Events are required to have $E_T^{\text{miss}} > 250$ GeV. The analysis selects events with a leading (highest p_T) jet with $p_T > 250$ GeV and $|\eta| < 2.4$ in the final state. A maximum of four jets with $p_T > 30$ GeV and

TABLE I. Event selection criteria applied, as described in Sec. V.

Selection criteria							
Primary vertex							
$E_T^{\text{miss}} > 250$ GeV							
Leading jet with $p_T > 250$ GeV and $ \eta < 2.4$							
At most four jets with $p_T > 30$ GeV and $ \eta < 2.8$							
$\Delta\phi(\text{jet}, \vec{p}_T^{\text{miss}}) > 0.4$							
Jet quality requirements							
No identified muons with $p_T > 10$ GeV or electrons with $p_T > 20$ GeV							
Inclusive signal region	IM1	IM2	IM3	IM4	IM5	IM6	IM7
E_T^{miss} (GeV)	> 250	> 300	> 350	> 400	> 500	> 600	> 700
Exclusive signal region	EM1	EM2	EM3	EM4	EM5	EM6	
E_T^{miss} (GeV)	[250–300]	[300–350]	[350–400]	[400–500]	[500–600]	[600–700]	

$|\eta| < 2.8$ are allowed. A separation in the azimuthal plane of $\Delta\phi(\text{jet}, \vec{p}_T^{\text{miss}}) > 0.4$ between the missing transverse momentum direction and each selected jet is required. This requirement reduces the multijet background contribution where the large E_T^{miss} originates mainly from jet energy mismeasurement.

- (iii) Events are rejected if they contain any jet inconsistent with the requirement that they originate from a proton-proton collision. Jet quality selection criteria [83] involve quantities such as the pulse shape of the energy depositions in the cells of the calorimeters, electromagnetic fraction in the calorimeter, calorimeter sampling fraction, or charged-particle fraction.⁴ The loose criteria are applied to all jets with $p_T > 20$ GeV and $|\eta| < 2.8$, dealing efficiently with coherent noise and electronic noise bursts in the calorimeter producing anomalous energy depositions [84]. Noncollision backgrounds, i.e. energy depositions in the calorimeters due to muons of beam-induced or cosmic-ray origin, are further suppressed by applying the tight selection criteria to the leading jet: the ratio of the jet charged-particle fraction to the calorimeter sampling fraction,⁵ $f_{\text{ch}}/f_{\text{max}}$, is required to be larger than 0.1. These requirements have a negligible effect on the signal efficiency.
- (iv) Events with identified muons with $p_T > 10$ GeV or electrons with $p_T > 20$ GeV in the final state are vetoed.

Inclusive (IM1–IM7) and exclusive (EM1–EM6) signal regions are considered with increasing E_T^{miss} thresholds from 250 to 700 GeV (see Table I). The use of inclusive

E_T^{miss} signal regions follows the Run 1 strategy, where the results are translated into model-independent cross section upper limits for the production of new physics. The use of exclusive E_T^{miss} signal regions effectively explores information from the shape of the E_T^{miss} distribution (see Secs. VID and VIII) and enhances the sensitivity to the different new physics models.

VI. BACKGROUND ESTIMATION

The $W + \text{jets}$, $Z(\rightarrow \nu\bar{\nu}) + \text{jets}$, $Z/\gamma^*(\rightarrow \tau^+\tau^-) + \text{jets}$, and $Z/\gamma^*(\rightarrow \mu^+\mu^-) + \text{jets}$ backgrounds are constrained using MC samples normalized with data in selected control regions. The normalization factors are extracted simultaneously using a global fit that includes systematic uncertainties, to properly take into account correlations.

A $W(\rightarrow \mu\nu) + \text{jets}$ control sample is used to define normalization factors for $W(\rightarrow \mu\nu) + \text{jets}$ and $Z(\rightarrow \nu\bar{\nu}) + \text{jets}$ processes. As discussed in Sec. VID, the use of the $W(\rightarrow \mu\nu) + \text{jets}$ control sample to constrain the normalization of the $Z(\rightarrow \nu\bar{\nu}) + \text{jets}$ process translates into a reduced uncertainty in the estimation of the main irreducible background contribution, due to a partial cancellation of systematic uncertainties and the statistical power of the $W(\rightarrow \mu\nu) + \text{jets}$ control sample in data, which is about seven times larger than the $Z/\gamma^*(\rightarrow \mu^+\mu^-) + \text{jets}$ control sample. A $W(\rightarrow e\nu) + \text{jets}$ control sample is used to constrain the normalization of the $W(\rightarrow e\nu) + \text{jets}$ and $W(\rightarrow \tau\nu) + \text{jets}$ background processes. For the latter, this is motivated by the fact that the τ lepton in the $W(\rightarrow \tau\nu) + \text{jets}$ background process mainly decays hadronically leading to a final-state topology in the detector similar to that of the $W(\rightarrow e\nu) + \text{jets}$ sample. A small $Z/\gamma^*(\rightarrow \tau^+\tau^-) + \text{jets}$ background contribution is also constrained using the $W(\rightarrow e\nu) + \text{jets}$ control sample. Uncertainties related to the difference between $W + \text{jets}$ and $Z + \text{jets}$ final states, leading to potential differences in event kinematics and selection acceptances and efficiencies, are discussed in Sec. VII. Finally, a $Z/\gamma^*(\rightarrow \mu^+\mu^-) + \text{jets}$ control sample is

⁴The charged-particle fraction is defined as $f_{\text{ch}} = \sum p_T^{\text{track,jet}} / p_T^{\text{jet}}$, where $\sum p_T^{\text{track,jet}}$ is the scalar sum of the transverse momenta of tracks associated with the primary vertex within a cone of radius $\Delta R = 0.4$ around the jet axis, and p_T^{jet} is the transverse momentum as determined from calorimetric measurements.

⁵ f_{max} denotes the maximum fraction of the jet energy collected by a single calorimeter layer.

TABLE II. Summary of the methods and control samples used to constrain the different background contributions in the signal regions.

Background process	Method	Control sample
$Z(\rightarrow \nu\bar{\nu}) + \text{jets}$	MC and control samples in data	$W(\rightarrow \mu\nu)$
$W(\rightarrow e\nu) + \text{jets}$	MC and control samples in data	$W(\rightarrow e\nu)$
$W(\rightarrow \tau\nu) + \text{jets}$	MC and control samples in data	$W(\rightarrow e\nu)$
$W(\rightarrow \mu\nu) + \text{jets}$	MC and control samples in data	$W(\rightarrow \mu\nu)$
$Z/\gamma^*(\rightarrow \mu^+\mu^-) + \text{jets}$	MC and control samples in data	$Z/\gamma^*(\rightarrow \mu^+\mu^-)$
$Z/\gamma^*(\rightarrow \tau^+\tau^-) + \text{jets}$	MC and control samples in data	$W(\rightarrow e\nu)$
$Z/\gamma^*(\rightarrow e^+e^-) + \text{jets}$	MC only	
$t\bar{t}$, single top	MC only	
Diboson	MC only	
Multijets	data driven	
Noncollision	data driven	

used to constrain the $Z/\gamma^*(\rightarrow \mu^+\mu^-) + \text{jets}$ background contribution.

The remaining SM backgrounds from $Z/\gamma^*(\rightarrow e^+e^-) + \text{jets}$,⁶ $t\bar{t}$, single top, and dibosons are determined using MC simulated samples, while the multijet background contribution is extracted from data. The contributions from noncollision backgrounds are estimated in data using the beam-induced background identification techniques described in Ref. [84].

The methodology and the samples used for estimating the background are summarized in Table II. In the following subsections, details of the definition of the $W/Z + \text{jets}$ control regions and of the data-driven determination of the multijet and beam-induced backgrounds are given. This is followed by a description of the background fits.

A. $W/Z + \text{jets}$ background

Control samples in data, with identified electrons or muons in the final state and with requirements on the jet p_T and E_T^{miss} identical to those in the signal regions, are used to determine the $W(\rightarrow \ell\nu) + \text{jets}$ ($\ell = e, \mu, \tau$), $Z(\rightarrow \nu\bar{\nu}) + \text{jets}$, and $Z/\gamma^*(\rightarrow \ell^+\ell^-) + \text{jets}$ ($\ell = \mu, \tau$) background contributions. The $Z/\gamma^*(\rightarrow e^+e^-) + \text{jets}$ background contribution is tiny and it is determined from MC simulation. The E_T^{miss} -based online trigger used in the analysis does not include muon information in the E_T^{miss} calculation. This allows the collection of $W(\rightarrow \mu\nu) + \text{jets}$ and $Z/\gamma^*(\rightarrow \mu^+\mu^-) + \text{jets}$ control samples with the same trigger as for the signal regions.

A $W(\rightarrow \mu\nu) + \text{jets}$ control sample is selected by requiring a muon consistent with originating from the primary vertex with $p_T > 10$ GeV, and transverse mass in the range

$30 \text{ GeV} < m_T < 100 \text{ GeV}$. The transverse mass $m_T = \sqrt{2p_T^\ell p_T^\nu [1 - \cos(\phi^\ell - \phi^\nu)]}$ is defined by the lepton and neutrino transverse momenta, where the (x, y) components of the neutrino momentum are taken to be the same as the corresponding \vec{p}_T^{miss} components. Events with identified electrons in the final state are vetoed. Similarly, a $Z/\gamma^*(\rightarrow \mu^+\mu^-) + \text{jets}$ control sample is selected by requiring the presence of two muons with $p_T > 10$ GeV and invariant mass in the range $66 \text{ GeV} < m_{\mu\mu} < 116 \text{ GeV}$. In the $W(\rightarrow \mu\nu) + \text{jets}$ and $Z/\gamma^*(\rightarrow \mu^+\mu^-) + \text{jets}$ control regions, the E_T^{miss} is not corrected for the presence of the muons in the final state, motivated by the fact that these control regions are used to estimate the $Z(\rightarrow \nu\bar{\nu}) + \text{jets}$ and the $Z/\gamma^*(\rightarrow \mu^+\mu^-) + \text{jets}$ backgrounds, respectively, in the signal regions with no identified muons.

Finally, a $W(\rightarrow e\nu) + \text{jets}$ dominated control sample is defined with an isolated electron candidate with $p_T > 20$ GeV, selected with tight or medium selection criteria [80,81] depending on p_T , and no additional identified leptons in the final state. The E_T^{miss} calculation includes the contribution of the energy cluster from the identified electron in the calorimeter (no attempt is made to subtract it), since $W(\rightarrow e\nu) + \text{jets}$ processes contribute to the background in the signal regions when the electron is not identified.

Monte Carlo based scale factors, determined from the SHERPA simulation, are defined for each of the signal selections to estimate the different background contributions in the signal regions. As an illustration, in the case of the dominant $Z(\rightarrow \nu\bar{\nu}) + \text{jets}$ background process its contribution to a given signal region $N_{\text{signal}}^{Z(\rightarrow \nu\bar{\nu})}$ is determined using the $W(\rightarrow \mu\nu) + \text{jets}$ control sample in data according to

$$N_{\text{signal}}^{Z(\rightarrow \nu\bar{\nu})} = (N_{W(\rightarrow \mu\nu), \text{control}}^{\text{data}} - N_{W(\rightarrow \mu\nu), \text{control}}^{\text{non-W}}) \times \frac{N_{\text{signal}}^{\text{MC}(Z(\rightarrow \nu\bar{\nu}))}}{N_{W(\rightarrow \mu\nu), \text{control}}^{\text{MC}}}, \quad (2)$$

⁶In the course of the analysis, the use of an additional $Z/\gamma^*(\rightarrow e^+e^-) + \text{jets}$ control sample was explored for constraining the $Z/\gamma^*(\rightarrow e^+e^-) + \text{jets}$ and $Z(\rightarrow \nu\bar{\nu}) + \text{jets}$ background contributions, leading to an insignificant improvement in the background determination.

TABLE III. Data and background predictions in the control regions before and after the fit is performed for the IM1 selection. The background predictions include both the statistical and systematic uncertainties. The individual uncertainties are correlated, and do not necessarily add in quadrature to the total background uncertainty.

IM1 control regions	$W(\rightarrow e\nu)$	$W(\rightarrow \mu\nu)$	$Z/\gamma^*(\rightarrow \mu^+\mu^-)$
Observed events (3.2 fb^{-1})	3559	10481	1488
SM prediction (postfit)	3559 ± 60	10480 ± 100	1488 ± 39
Fitted $W(\rightarrow e\nu)$	2410 ± 140	0.4 ± 0.1	–
Fitted $W(\rightarrow \mu\nu)$	2.4 ± 0.3	8550 ± 330	1.8 ± 0.3
Fitted $W(\rightarrow \tau\nu)$	462 ± 27	435 ± 28	0.14 ± 0.02
Fitted $Z/\gamma^*(\rightarrow e^+e^-)$	0.5 ± 0.1	–	–
Fitted $Z/\gamma^*(\rightarrow \mu^+\mu^-)$	0.02 ± 0.02	143 ± 10	1395 ± 41
Fitted $Z/\gamma^*(\rightarrow \tau^+\tau^-)$	30 ± 2	22 ± 4	0.5 ± 0.1
Fitted $Z(\rightarrow \nu\bar{\nu})$	1.8 ± 0.1	2.3 ± 0.2	–
Expected $t\bar{t}$, single top	500 ± 150	1060 ± 330	42 ± 13
Expected dibosons	150 ± 13	260 ± 25	48 ± 5
MC exp. SM events	3990 ± 320	10500 ± 710	1520 ± 98
Fit input $W(\rightarrow e\nu)$	2770 ± 210	0.4 ± 0.1	–
Fit input $W(\rightarrow \mu\nu)$	2.4 ± 0.3	8500 ± 520	1.8 ± 0.2
Fit input $W(\rightarrow \tau\nu)$	531 ± 39	500 ± 34	0.16 ± 0.03
Fit input $Z/\gamma^*(\rightarrow e^+e^-)$	0.5 ± 0.1	–	–
Fit input $Z/\gamma^*(\rightarrow \mu^+\mu^-)$	0.02 ± 0.02	146 ± 13	1427 ± 92
Fit input $Z/\gamma^*(\rightarrow \tau^+\tau^-)$	34 ± 3	25 ± 4	0.6 ± 0.1
Fit input $Z(\rightarrow \nu\bar{\nu})$	1.8 ± 0.1	2.2 ± 0.1	–
Fit input $t\bar{t}$, single top	500 ± 160	1060 ± 340	42 ± 13
Fit input dibosons	150 ± 13	260 ± 25	48 ± 5

TABLE IV. Data and SM background prediction, before and after the fit, in the $W(\rightarrow e\nu)$ control region for the different selections. For the SM predictions both the statistical and systematic uncertainties are included.

Inclusive selection	IM1	IM2	IM3	IM4	IM5	IM6	IM7
Observed events (3.2 fb^{-1})	3559	1866	992	532	183	72	32
SM prediction (postfit)	3559 ± 60	1866 ± 43	992 ± 32	532 ± 23	183 ± 14	72 ± 8	32 ± 6
SM prediction (prefit)	3990 ± 320	2110 ± 170	1142 ± 94	654 ± 54	216 ± 19	85 ± 8	34 ± 3
Exclusive selection	EM1	EM2	EM3	EM4	EM5	EM6	
Observed events (3.2 fb^{-1})	1693	874	460	349	111	40	
SM prediction (postfit)	1693 ± 41	874 ± 30	460 ± 21	349 ± 19	111 ± 11	40 ± 6	
SM prediction (prefit)	1880 ± 150	971 ± 79	488 ± 40	439 ± 36	131 ± 12	50 ± 5	

where $N_{\text{signal}}^{\text{MC}(Z(\rightarrow \nu\bar{\nu}))}$ denotes the background predicted by the MC simulation in the signal region, and $N_{W(\rightarrow \mu\nu),\text{control}}^{\text{data}}$, $N_{W(\rightarrow \mu\nu),\text{control}}^{\text{MC}}$, and $N_{W(\rightarrow \mu\nu),\text{control}}^{\text{non-W}}$ denote, in the control region, the number of data events, the number of $W(\rightarrow \mu\nu) + \text{jets}$ candidates from MC simulation, and the non- $W(\rightarrow \mu\nu)$ background contribution, respectively. The $N_{W(\rightarrow \mu\nu),\text{control}}^{\text{non-W}}$ term refers mainly to top-quark and diboson processes, but also includes contributions from other $W/Z + \text{jets}$ processes. Multijets and noncollision backgrounds in the control regions are negligible.

As discussed in Sec. VID, a global simultaneous likelihood fit to all the control regions is used to determine the normalization factors.

B. Multijets background

The multijet background with large $E_{\text{T}}^{\text{miss}}$ mainly originates from the misreconstruction of the energy of a jet in the calorimeter and to a lesser extent is due to the presence of neutrinos in the final state from heavy-flavor hadron decays. In this analysis, the multijet background is determined from data, using the jet smearing method as described in Ref. [85], which relies on the assumption that the $E_{\text{T}}^{\text{miss}}$ of multijet events is dominated by fluctuations in the jet response in the detector which can be measured in the data. For the IM1 and EM1 selections, the multijets background constitutes about 0.5% of the total background, and is negligible for the other signal regions.

TABLE V. Data and SM background prediction, before and after the fit, in the $W(\rightarrow \mu\nu)$ control region for the different selections. For the SM predictions both the statistical and systematic uncertainties are included.

Inclusive selection	IM1	IM2	IM3	IM4	IM5	IM6	IM7
Observed events (3.2 fb^{-1})	10481	6279	3538	1939	677	261	95
SM prediction (postfit)	10480 ± 100	6279 ± 79	3538 ± 60	1939 ± 44	677 ± 26	261 ± 16	95 ± 10
SM prediction (prefit)	10500 ± 710	6350 ± 460	3560 ± 280	2010 ± 160	700 ± 57	256 ± 23	106 ± 9
Exclusive selection	EM1	EM2	EM3	EM4	EM5	EM6	
Observed events (3.2 fb^{-1})	4202	2741	1599	1262	416	166	
SM prediction (postfit)	4202 ± 65	2741 ± 52	1599 ± 40	1262 ± 36	416 ± 20	166 ± 13	
SM prediction (prefit)	4140 ± 260	2800 ± 190	1540 ± 120	1310 ± 100	444 ± 35	150 ± 14	

TABLE VI. Data and SM background prediction, before and after the fit, in the $Z/\gamma^*(\rightarrow \mu^+\mu^-)$ control region for the different selections. For the SM predictions both the statistical and systematic uncertainties are included.

Inclusive selection	IM1	IM2	IM3	IM4	IM5	IM6	IM7
Observed events (3.2 fb^{-1})	1488	877	505	293	100	33	15
SM prediction (postfit)	1488 ± 39	877 ± 30	505 ± 22	293 ± 17	100 ± 10	33 ± 6	15 ± 4
SM prediction (prefit)	1520 ± 98	910 ± 59	487 ± 34	271 ± 19	89 ± 7	32 ± 3	13 ± 1
Exclusive selection	EM1	EM2	EM3	EM4	EM5	EM6	
Observed events (3.2 fb^{-1})	611	372	212	193	67	18	
SM prediction (postfit)	611 ± 25	372 ± 19	212 ± 15	193 ± 14	67 ± 8	18 ± 4	
SM prediction (prefit)	610 ± 42	422 ± 36	217 ± 15	182 ± 13	57 ± 4	19 ± 2	

C. Noncollision background

Noncollision backgrounds represent a significant portion of data acquired by E_T^{miss} triggers. These backgrounds resemble the topology of monojetlike final states and a dedicated strategy with a suppression power of approximately 10^3 is needed in order to reduce these backgrounds to a subpercent level. This is achieved by the jet quality selection criteria described in Sec. V. The rate of jets due to cosmic-ray muons surviving this selection, as measured in dedicated cosmic ray data sets, is found to be negligible compared to the rate of data in the monojetlike signal regions. The main source of residual noncollision backgrounds is therefore beam-induced muons originating in the particle cascades due to beam halo protons intercepting the LHC collimators. The noncollision background is estimated using a method that identifies beam-induced muons based on the spatial matching of calorimeter clusters to muon track segments, reconstructed in the muon-system endcaps and pointing in a direction nearly parallel to the beam pipe [84]. The number of events where the reconstructed objects satisfy the identification criteria is corrected for the efficiency of this method. The efficiency is evaluated in a dedicated beam-induced background-enhanced region defined by inverting the tight jet quality selection imposed on the leading jet.

The results indicate an almost negligible contribution from noncollision backgrounds in the signal regions. As an

example, 110 and 19 noncollision background events are estimated in the IM1 and EM3 signal regions, respectively, with no sign of noncollision backgrounds at $E_T^{\text{miss}} > 500 \text{ GeV}$. This constitutes about 0.5% of the total background for the IM1 and EM3 selections.

D. Background fits

The use of control regions to constrain the normalization of the dominant background contributions from $Z(\rightarrow \nu\bar{\nu}) + \text{jets}$ and $W + \text{jets}$ significantly reduces the relatively large theoretical and experimental systematic uncertainties, of the order of 20%–40%, associated with purely MC-based background predictions in the signal regions. A complete study of systematic uncertainties is carried out, as detailed in Sec. VII. To determine the final uncertainty in the total background, all systematic uncertainties are treated as nuisance parameters with Gaussian shapes in a fit based on the profile likelihood method [86] and which takes into account correlations among systematic variations. The likelihood also takes into account cross-contamination between different background sources in the control regions.

A simultaneous likelihood fit to the $W(\rightarrow \mu\nu) + \text{jets}$, $W(\rightarrow e\nu) + \text{jets}$, and $Z/\gamma^*(\rightarrow \mu^+\mu^-) + \text{jets}$ control regions is performed to normalize and constrain the corresponding background estimates in the signal regions. Background-only fits are performed separately in each of the inclusive regions IM1–IM7, as described in Sec. V. In addition, a fit

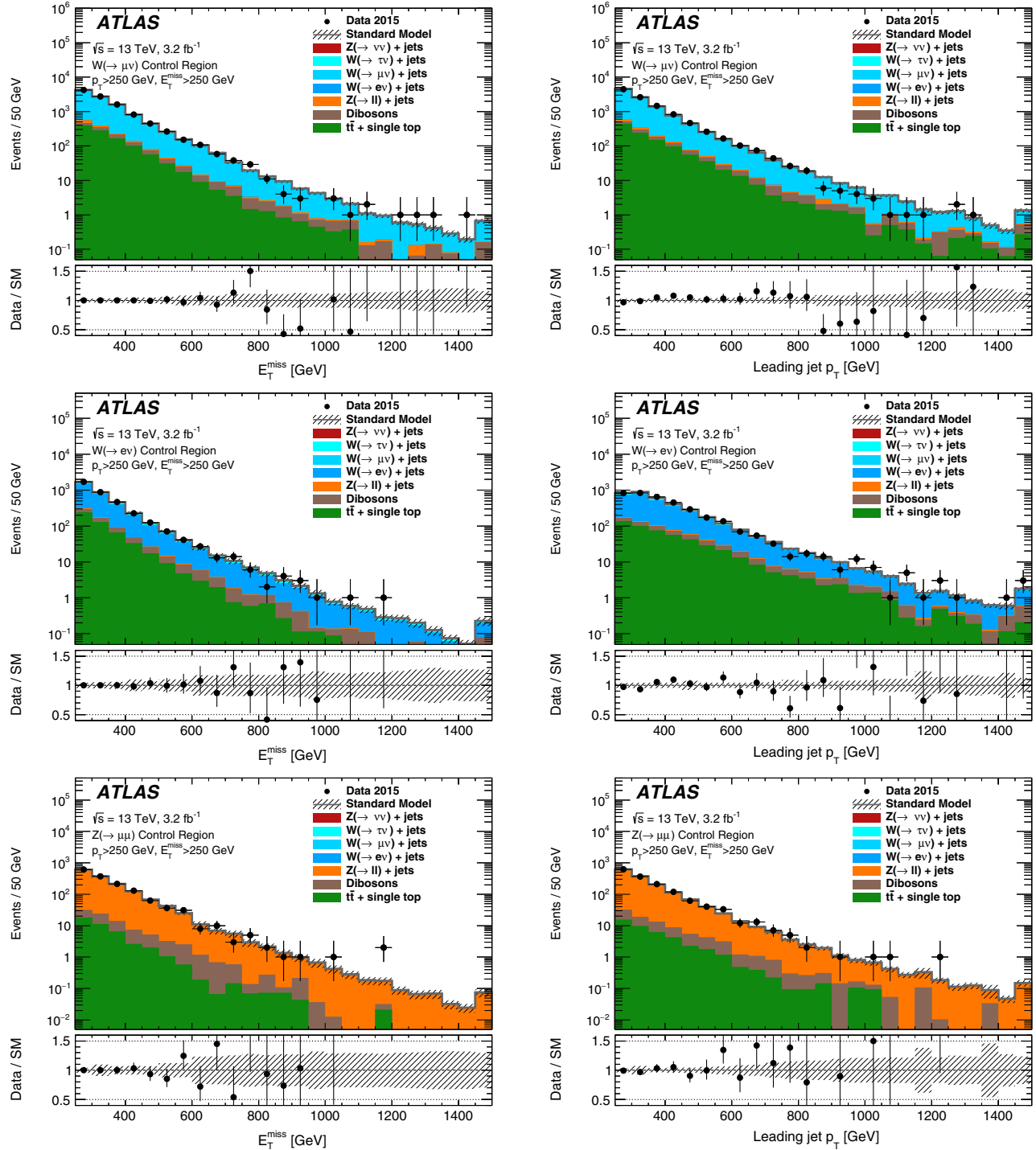


FIG. 2. The measured E_T^{miss} and leading-jet p_T distributions in the $W(\rightarrow \mu\nu) + \text{jets}$ (top), $W(\rightarrow e\nu) + \text{jets}$ (middle), and $Z/\gamma^*(\rightarrow \mu^+\mu^-) + \text{jets}$ (bottom) control regions, for the IM1 selection, compared to the background predictions. The latter include the global normalization factors extracted from the fit as performed in exclusive E_T^{miss} bins. The error bands in the ratios include the statistical and experimental uncertainties in the background predictions as determined by the global fit to the data in the control regions. The contributions from multijets and noncollision backgrounds are negligible and are not shown in the figures.

simultaneously using all the exclusive E_T^{miss} regions EM1–EM6 and IM7 is performed. In this case, normalization factors are considered separately in each exclusive E_T^{miss} region, which effectively employs information from the shape of the E_T^{miss} distribution to enhance the sensitivity of the analysis to the presence of new phenomena.

The results of the background-only fit in the control regions are presented in detail in Table III for the IM1 selection. Tables IV–VI collect the results for the total background predictions in each of the control regions for the inclusive and exclusive E_T^{miss} selections. As the tables indicate, the W/Z + jets background predictions receive multiplicative normalization factors that vary in the range between 0.8 and 1.2, depending on the process and the kinematic selection. Good agreement is observed between the normalization factors obtained by using inclusive or exclusive E_T^{miss} regions.

Figure 2 shows, for the IM1 monojetlike kinematic selection and in the different control regions, the distributions of the E_T^{miss} and the leading-jet p_T in data and MC simulation. The MC predictions include data-driven normalization factors as extracted from the global fit that considers exclusive E_T^{miss} bins. Altogether, the MC simulation provides a good description of the shape of the measured distributions in the different control regions.

In the analysis, the control regions are defined using the same requirements for E_T^{miss} , leading jet p_T , event topologies, and jet vetoes as in the signal regions, such that no extrapolation in E_T^{miss} or jet p_T is needed from control to signal regions. Agreement between data and background predictions is confirmed in a low- p_T validation region defined using the same monojetlike selection criteria with E_T^{miss} limited to the range 150–250 GeV.

VII. SYSTEMATIC UNCERTAINTIES

In this section the impact of each source of systematic uncertainty on the total background prediction in the signal regions, as determined via the global fits explained in Sec. VID, is discussed. Here, the case of the inclusive E_T^{miss} selections is presented. Similar studies are carried out in exclusive E_T^{miss} bins. The correlation of systematic uncertainties across E_T^{miss} bins is properly taken into account. Finally, the experimental and theoretical uncertainties in the signal yields are discussed.

A. Background systematic uncertainties

Uncertainties in the absolute jet and E_T^{miss} energy scales and resolutions [78] translate into an uncertainty in the total background which varies between $\pm 0.5\%$ for IM1 and $\pm 1.6\%$ for IM7. Uncertainties related to jet quality requirements, pileup description and corrections to the jet p_T and E_T^{miss} introduce a $\pm 0.2\%$ to $\pm 0.9\%$ uncertainty in the background predictions. Uncertainties in the simulated

lepton identification and reconstruction efficiencies, energy/momentum scale and resolution translate into an uncertainty in the total background which varies between $\pm 0.1\%$ and $\pm 1.4\%$ for the IM1 and between $\pm 0.1\%$ and $\pm 2.6\%$ for the IM7 selections, respectively.

Variations of the renormalization, factorization, and parton-shower matching scales and PDFs in the SHERPA W/Z + jets background samples translate into a $\pm 1.1\%$ to $\pm 1.3\%$ uncertainty in the total background. Model uncertainties, related to potential differences between W + jets and Z + jets final states, affecting the normalization of the dominant $Z(\rightarrow \nu\bar{\nu})$ + jets background and the small $Z/\gamma^*(\rightarrow \tau^+\tau^-)$ + jets background contribution as determined in $W(\rightarrow \mu\nu)$ + jets and $W(\rightarrow e\nu)$ + jets control regions, are studied in detail. This includes uncertainties related to PDFs and renormalization and factorization scale settings, the parton-shower parameters and the hadronization model used in the MC simulation, and the dependence on the lepton reconstruction and acceptance. As a result, an additional $\pm 3\%$ uncertainty in the $Z(\rightarrow \nu\bar{\nu})$ + jets and $Z/\gamma^*(\rightarrow \tau^+\tau^-)$ + jets contributions is included for all the selections. In addition, the effect from NLO electroweak corrections on the W + jets to Z + jets ratio is taken into account [87–89]. Dedicated parton-level calculations are performed with the same E_T^{miss} and leading-jet- p_T requirements as in the IM1–IM7 signal regions. The studies suggest an effect on the W + jets to Z + jets ratio which varies between about $\pm 1.9\%$ for IM1 and $\pm 5.2\%$ for IM7, although the calculations suffer from large uncertainties, mainly due to our limited knowledge of the photon PDFs in the proton. In this analysis, these results are adopted as an additional uncertainty in the $Z(\rightarrow \nu\bar{\nu})$ + jets and $Z/\gamma^*(\rightarrow \tau^+\tau^-)$ + jets contributions. Altogether, this translates into an uncertainty in the total background which varies from $\pm 2.0\%$ and $\pm 3.0\%$ for the IM1 and IM5 selections, respectively, to about $\pm 3.9\%$ for the IM7 selection.

Theoretical uncertainties in the predicted background yields for top-quark-related processes include uncertainties on the absolute $t\bar{t}$ and single-top production cross sections; variations in the set of parameters that govern the parton showers and the amount of initial- and final-state soft gluon radiation; and uncertainties due to the choice of renormalization and factorization scales and PDFs. This introduces an uncertainty in the total background prediction which varies between $\pm 2.7\%$ and $\pm 3.3\%$ for the IM1 and IM7 selections, respectively. Uncertainties in the diboson contribution are estimated using different MC generators and translate into an uncertainty in the total background in the range between $\pm 0.05\%$ and $\pm 0.4\%$. A $\pm 100\%$ uncertainty in the multijet and noncollision background estimations is adopted, leading to a $\pm 0.2\%$ uncertainty in the total background for the IM1 selection. Statistical uncertainties related to the data control regions and simulation samples lead to an additional uncertainty in the final background estimates in the signal regions which varies between

TABLE VII. Data and SM background predictions in the signal region for several inclusive and exclusive E_T^{miss} selections. For the SM prediction both the statistical and systematic uncertainties are included. In each signal region, the individual uncertainties for the different background processes can be correlated, and do not necessarily add in quadrature to the total background uncertainty.

Signal region	IM1	EM3	EM5	IM7
Observed events (3.2 fb^{-1})	21447	2939	747	185
SM prediction	21730 ± 940	3210 ± 170	686 ± 50	167 ± 20
$W(\rightarrow e\nu)$	1710 ± 170	228 ± 26	37 ± 7	7 ± 2
$W(\rightarrow \mu\nu)$	1950 ± 170	263 ± 28	44 ± 8	11 ± 2
$W(\rightarrow \tau\nu)$	3980 ± 310	551 ± 47	101 ± 15	19 ± 4
$Z/\gamma^*(\rightarrow e^+e^-)$	0.01 ± 0.01	–	–	–
$Z/\gamma^*(\rightarrow \mu^+\mu^-)$	76 ± 30	9 ± 5	5 ± 2	2 ± 1
$Z/\gamma^*(\rightarrow \tau^+\tau^-)$	48 ± 7	5 ± 1	0.9 ± 0.2	0.2 ± 0.1
$Z(\rightarrow \nu\bar{\nu})$	12520 ± 700	1940 ± 130	443 ± 42	109 ± 18
$t\bar{t}$, single top	780 ± 240	108 ± 32	19 ± 7	3 ± 1
Dibosons	506 ± 48	82 ± 8	36 ± 5	15 ± 2
Multijets	51 ± 50	6 ± 6	1 ± 1	0.4 ± 0.4
Noncollision background	110 ± 110	19 ± 19	–	–

TABLE VIII. Data and SM background predictions in the signal region for the different selections. For the SM predictions both the statistical and systematic uncertainties are included.

Signal region	IM1	IM2	IM3	IM4	IM5	IM6	IM7
Observed events (3.2 fb^{-1})	21447	11975	6433	3494	1170	423	185
SM prediction	21730 ± 940	12340 ± 570	6570 ± 340	3390 ± 200	1125 ± 77	441 ± 39	167 ± 20
Signal region	EM1	EM2	EM3	EM4	EM5	EM6	
Observed events (3.2 fb^{-1})	9472	5542	2939	2324	747	238	
SM prediction	9400 ± 410	5770 ± 260	3210 ± 170	2260 ± 140	686 ± 50	271 ± 28	

$\pm 2.5\%$ for the IM1 and $\pm 10\%$ for the IM7 selections. Finally, the impact of the uncertainty in the integrated luminosity, which partially cancels in the data-driven determination of the SM background, is negligible.

B. Signal systematic uncertainties

Several sources of systematic uncertainty in the predicted signal yields are considered for each of the models of new physics. The uncertainties are computed separately for each signal region by varying the model parameters (see Sec. VIII).

Experimental uncertainties include those related to the jet and E_T^{miss} reconstruction, energy scales and resolutions; and the $\pm 5\%$ uncertainty in the integrated luminosity, derived following a methodology similar to that detailed in Ref. [90], from a calibration of the luminosity scale using x - y beam-separation scans performed in August 2015. Other uncertainties related to the jet quality requirements are negligible ($< 1\%$).

Uncertainties affecting the signal acceptance, related to the generation of the signal samples, include uncertainties in the modeling of the initial- and final-state gluon radiation, as determined using simulated samples with modified parton-shower parameters (by factors of two or one half) that enhance or suppress the parton radiation; uncertainties due to PDF and

variations of the $\alpha_s(m_Z)$ value employed, as computed from the envelope of CT10, MMHT2014 [91] and NNPDF30 error sets; and the choice of renormalization and factorization scales. In addition, theoretical uncertainties in the predicted cross sections, including PDF and renormalization and factorization scale uncertainties, are computed separately for the different models.

VIII. RESULTS AND INTERPRETATION

The number of events in data and the expected background predictions in several inclusive and exclusive signal regions, as determined using the global fit discussed in Sec. VID, are presented in detail in Table VII. The results for all the signal regions are summarized in Table VIII. Good agreement is observed between the data and the SM predictions in each case. The SM predictions for the inclusive selections are determined with a total uncertainty of $\pm 4.0\%$, $\pm 6.8\%$, and $\pm 12\%$ for the IM1, IM5, and IM7 signal regions, respectively, which include correlations between uncertainties in the individual background contributions.

Figure 3 shows several measured distributions compared to the SM predictions for $E_T^{\text{miss}} > 250 \text{ GeV}$, for which the normalization factors applied to the MC predictions, and the related uncertainties, are determined from the global fit

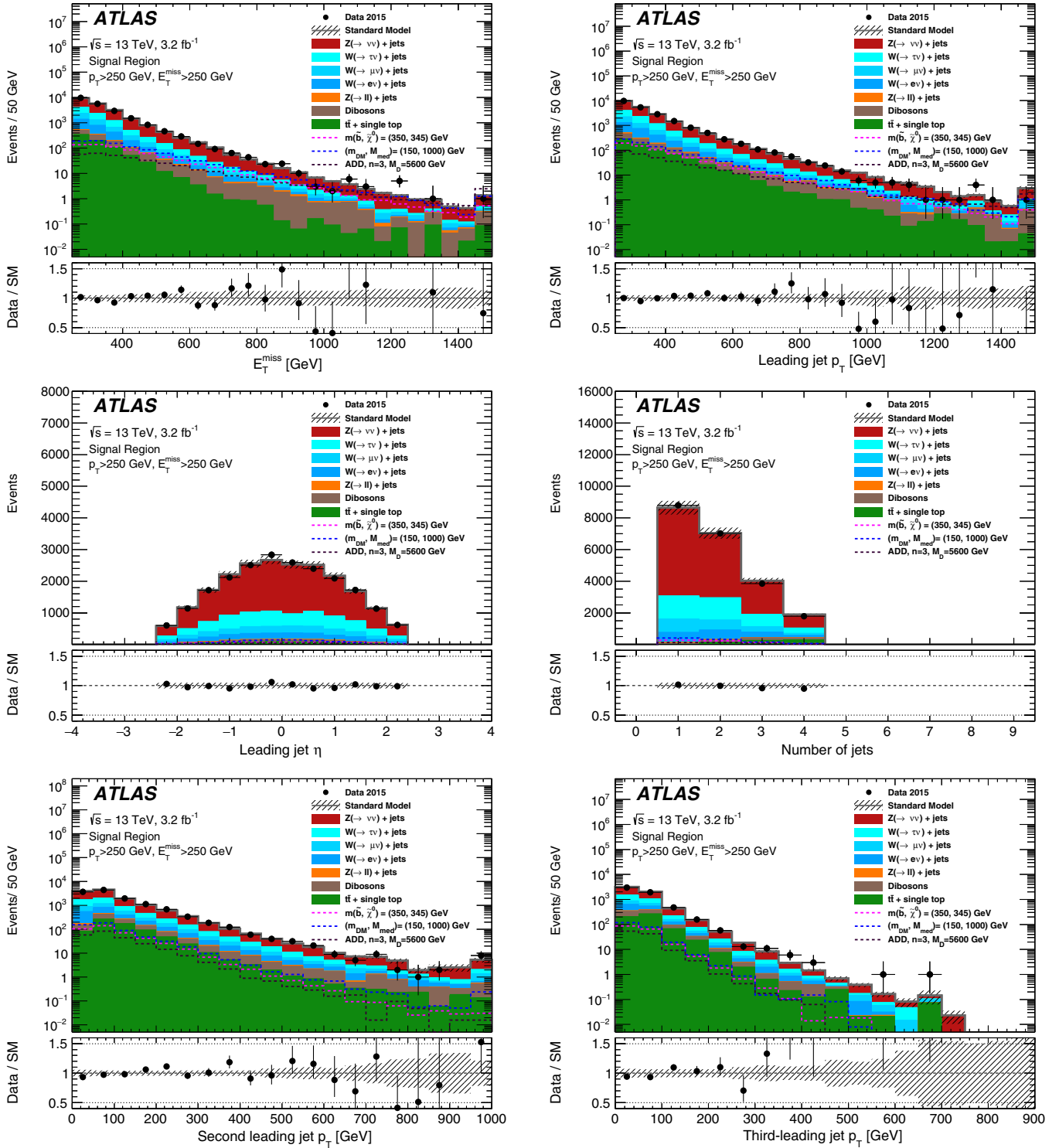


FIG. 3. Measured distributions of the E_T^{miss} , leading-jet p_T , leading-jet η , jet multiplicity, second-leading-jet p_T , and third-leading-jet p_T for the IM1 selection compared to the SM predictions. The latter are normalized with normalization factors as determined by the global fit that considers exclusive E_T^{miss} regions. For illustration purposes, the distributions of different ADD, SUSY, and WIMP scenarios are included. The error bands in the ratios shown in the lower panels include both the statistical and systematic uncertainties in the background predictions. The contributions from multijets and noncollision backgrounds are negligible and not shown in the figures.

TABLE IX. Observed and expected 95% C.L. upper limits on the number of signal events, S_{obs}^{95} and S_{exp}^{95} , and on the visible cross section, defined as the product of cross section, acceptance and efficiency, $\langle\sigma\rangle_{\text{obs}}^{95}$, for the IM1–IM7 selections.

Signal channel	$\langle\sigma\rangle_{\text{obs}}^{95}$ [fb]	S_{obs}^{95}	S_{exp}^{95}
IM1	553	1773	1864^{+829}_{-548}
IM2	308	988	1178^{+541}_{-348}
IM3	196	630	694^{+308}_{-204}
IM4	153	491	401^{+168}_{-113}
IM5	61	196	164^{+63}_{-45}
IM6	23	75	84^{+32}_{-23}
IM7	19	61	48^{+18}_{-13}

carried out in exclusive $E_{\text{T}}^{\text{miss}}$ bins. For illustration purposes, the distributions include the impact of different ADD, SUSY, and WIMP scenarios.

The level of agreement between the data and the SM predictions for the total number of events in the different inclusive signal regions IM1–IM7 is translated into upper limits for the presence of new phenomena. A simultaneous likelihood fit is performed in both the control and signal regions, separately for each of the inclusive regions IM1–IM7. As a result, model-independent 95% confidence level (C.L.) upper limits on the visible cross section, defined as the production cross section times acceptance times efficiency $\sigma \times A \times \epsilon$, are extracted using the CL_s modified frequentist approach [92] and considering the systematic uncertainties in the SM backgrounds and the uncertainty in the integrated luminosity. The results are presented in Table IX. Values of $\sigma \times A \times \epsilon$ above 553 fb (for IM1) and above 19 fb (for IM7) are excluded at 95% C.L. Typical event selection efficiencies ϵ varying from about 100% for IM1 to 96% for IM7 are found in simulated $Z(\rightarrow \nu\bar{\nu}) + \text{jets}$ background processes.

A. Large extra spatial dimensions

The level of agreement between the data and the SM predictions is translated into limits on the parameters of the ADD model. Only the signal regions with $E_{\text{T}}^{\text{miss}} > 400$ GeV, where the SM background is moderate and the shape difference between signal and the SM background becomes apparent, have an impact on the ADD limits. The typical $A \times \epsilon$ of the selection criteria varies, as the number of extra dimensions n increases from $n = 2$ to $n = 6$, between 5.5% and 6.6% for IM4 and between 2.9% and 4.2% for IM7.

The experimental uncertainties related to the jet and $E_{\text{T}}^{\text{miss}}$ scales and resolutions introduce uncertainties in the signal yields which vary between $\pm 1\%$ and $\pm 3\%$. The uncertainties related to the modeling of the initial- and final-state gluon radiation translate into uncertainties in the ADD signal acceptance which vary between $\pm 7\%$ and $\pm 10\%$. The uncertainties due to the PDFs, affecting the predicted signal cross sections, increase from $\pm 16\%$ at $n = 2$ to $\pm 42\%$ at $n = 6$. The effect of PDF uncertainties on the acceptance is between $\pm 10\%$ and $\pm 20\%$, mildly increasing with increasing n and $E_{\text{T}}^{\text{miss}}$. Similarly, the variations of the renormalization and factorization scales introduce a $\pm 23\%$ to $\pm 36\%$ uncertainty in the signal yields, with increasing n and $E_{\text{T}}^{\text{miss}}$ requirements, and about a $\pm 10\%$ variation in the signal acceptance.

Observed and expected 95% C.L. exclusion limits are set on M_D as a function of n using the CL_s approach, for which a simultaneous fit to the signal and control regions in the exclusive $E_{\text{T}}^{\text{miss}}$ bins is performed, including statistical and systematic uncertainties. Uncertainties in the signal acceptance times efficiency, the background predictions, and the luminosity are considered, and correlations between systematic uncertainties in signal and background predictions are taken into account. The fit accounts for the contamination of the control regions by signal events which *a priori* is estimated to be very small. In addition, observed limits are computed using $\pm 1\sigma$ variations of the theoretical

TABLE X. The 95% C.L. observed and expected lower limits on the fundamental Planck scale in $4 + n$ dimensions, M_D , as a function of the number of extra dimensions n , considering nominal LO signal cross sections. The impact of the $\pm 1\sigma$ theoretical uncertainty on the observed limits and the expected $\pm 1\sigma$ range of limits in the absence of a signal are also given. Finally, the 95% C.L. observed limits after damping of the signal cross section for $\hat{s} > M_D^2$ (see text) are quoted in parentheses.

n extra dimensions	95% C.L. lower limits on M_D [TeV]				
	95% C.L. observed limit		$\pm 1\sigma$ (theory)	95% C.L. expected limit	
	Nominal	(nominal after damping)		Nominal	$\pm 1\sigma$ (expected)
2	6.58	(6.58)	$+0.52$ -0.42	6.88	$+0.65$ -0.64
3	5.46	(5.44)	$+0.45$ -0.34	5.67	$+0.41$ -0.41
4	4.81	(4.74)	$+0.41$ -0.29	4.96	$+0.29$ -0.29
5	4.48	(4.34)	$+0.41$ -0.26	4.60	$+0.23$ -0.23
6	4.31	(4.10)	$+0.41$ -0.24	4.38	$+0.19$ -0.19

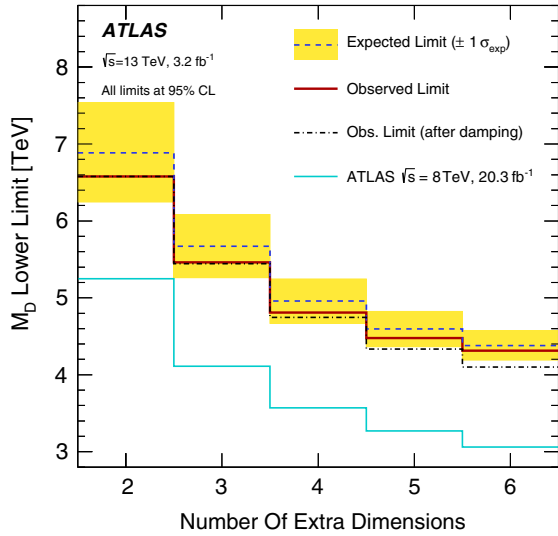


FIG. 4. Observed and expected 95% C.L. lower limits on the fundamental Planck scale in $4 + n$ dimensions, M_D , as a function of the number of extra dimensions. The shaded area around the expected limit indicates the expected $\pm 1\sigma$ range of limits in the absence of a signal. Finally, the thin dashed line shows the 95% C.L. observed limits after the suppression of the events with $\hat{s} > M_D^2$ (damping) is applied, as described in the text. The results from this analysis are compared to previous results from the ATLAS Collaboration at $\sqrt{s} = 8$ TeV [37].

predictions for the ADD cross sections. The -1σ variations of the ADD theoretical cross sections result in about a 6% decrease in the nominal observed limits. Figure 4 and Table X present the results in the case of the ADD model. Values of M_D below 6.58 TeV at $n = 2$ and below 4.31 TeV at $n = 6$ are excluded at 95% C.L., which extend the exclusion from previous results using 8 TeV data [37].

As discussed in Refs. [5,37], the analysis partially probes the phase-space region with $\hat{s} > M_D^2$, where $\sqrt{\hat{s}}$ is the center-of-mass energy of the hard interaction. This challenges the validity of model implementation and the lower bounds on M_D , as they depend on the unknown ultraviolet behavior of the effective theory. The observed 95% C.L. limits are recomputed after suppressing, with a weighting factor M_D^4/\hat{s}^2 , the signal events with $\hat{s} > M_D^2$, here referred to as damping. This results in a decrease of the quoted 95% C.L. lower limit on M_D which is negligible for $n = 2$ and about 5% for $n = 6$.

B. Squark pair production

The results are translated into exclusion limits computed separately for stop pair production with $\tilde{t}_1 \rightarrow c + \tilde{\chi}_1^0$, squark pair production with $\tilde{q} \rightarrow q + \tilde{\chi}_1^0$ ($q = u, d, c, s$), and sbottom pair production with $\tilde{b}_1 \rightarrow b + \tilde{\chi}_1^0$, as a function of the squark mass for different neutralino masses. As an example, in the case of stop pair production the typical $A \times \epsilon$ of the selection criteria varies, with increasing

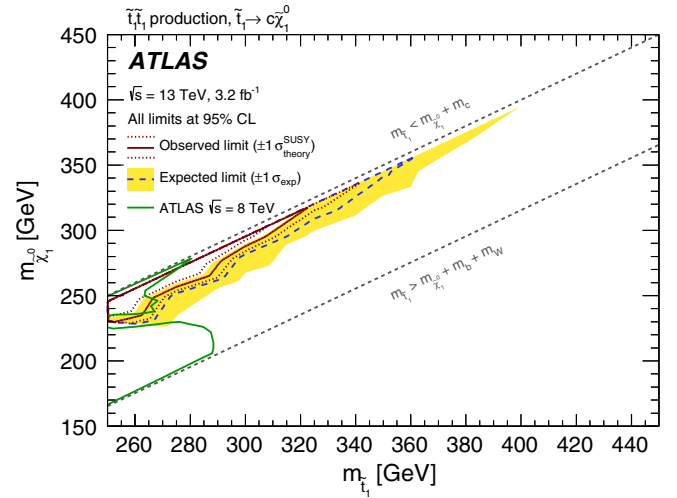


FIG. 5. Excluded region at the 95% C.L. in the $(\tilde{t}_1, \tilde{\chi}_1^0)$ mass plane for the decay channel $\tilde{t}_1 \rightarrow c + \tilde{\chi}_1^0$ (BR = 100%). The dotted lines around the observed limit indicate the range of observed limits corresponding to $\pm 1\sigma$ variations of the NLO SUSY cross-section predictions. The shaded area around the expected limit indicates the expected $\pm 1\sigma$ ranges of limits in the absence of a signal. The results from this analysis are compared to previous results from the ATLAS Collaboration at $\sqrt{s} = 8$ TeV [10].

stop and neutralino masses, between 0.7% and 1.4% for IM1 and between 0.06% and 0.8% for IM7. Observed and expected 95% C.L. exclusion limits are calculated using a simultaneous fit to the signal and control regions in exclusive E_T^{miss} bins, as in the case of the ADD models.

The systematic uncertainties in the SUSY signal yields are also determined following a procedure close to that for the ADD case. The uncertainties related to the jet and E_T^{miss} scales and resolutions introduce uncertainties in the signal yields which vary between $\pm 0.2\%$ and $\pm 7\%$ for different selections and squark and neutralino masses. In addition, the uncertainty in the integrated luminosity is included. The uncertainties related to the modeling of initial- and final-state gluon radiation translate into a $\pm 7\%$ to $\pm 17\%$ uncertainty in the signal yields. The uncertainties due to the PDFs result in a $\pm 5\%$ to $\pm 17\%$ uncertainty in the signal yields. Finally, the variations of the renormalization and factorization scales introduce a $\pm 4\%$ to $\pm 13\%$ uncertainty in the signal yields.

Figure 5 presents the results in the case of the $\tilde{t}_1 \rightarrow c + \tilde{\chi}_1^0$ signal. The previous limits from the ATLAS Collaboration [10] are also shown. As anticipated, the monojetlike selection improves significantly the sensitivity at very low Δm . In the compressed scenario with the stop and neutralino nearly degenerate in mass, the exclusion extends up to stop masses of 323 GeV. The region with $\Delta m < 5$ GeV is not considered in the exclusion since in this regime the stop could become long lived. Figure 6 (left) presents the observed and expected 95% C.L.

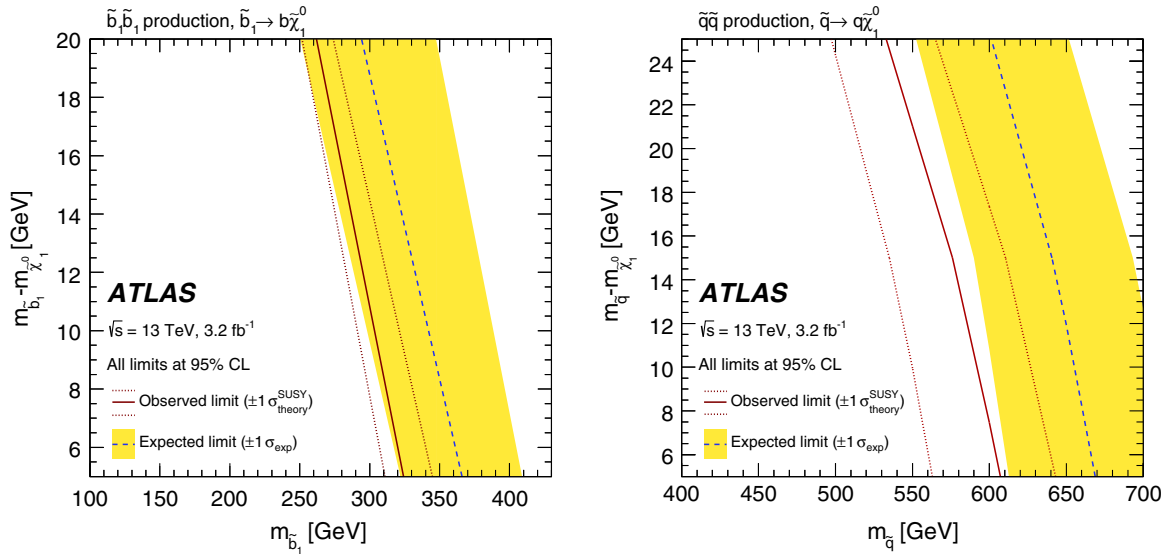


FIG. 6. Exclusion region at 95% C.L. as a function of squark mass and the squark-neutralino mass difference for (left) the decay channel $\tilde{b}_1 \rightarrow b + \tilde{\chi}_1^0$ and (right) $\tilde{q} \rightarrow q + \tilde{\chi}_1^0$ ($q = u, d, c, s$). The dotted lines around the observed limit indicate the range of observed limits corresponding to $\pm 1\sigma$ variations of the NLO SUSY cross-section predictions. The shaded area around the expected limit indicates the expected $\pm 1\sigma$ ranges of limits in the absence of a signal.

exclusion limits as a function of the sbottom mass and the sbottom-neutralino mass difference for the $\tilde{b}_1 \rightarrow b + \tilde{\chi}_1^0$ decay channel. In the scenario with $m_{\tilde{b}_1} - m_{\tilde{\chi}_1^0} \sim m_b$, this analysis extends the 95% C.L. exclusion limits up to a sbottom mass of 323 GeV. Similarly, Fig. 6 (right) presents the observed and expected 95% C.L. exclusion limits as a function of the squark mass and the squark-neutralino mass difference for $\tilde{q} \rightarrow q + \tilde{\chi}_1^0$ ($q = u, d, c, s$). In the compressed scenario with similar squark and neutralino masses, squark masses below 608 GeV are excluded at 95% C.L. These results significantly extend previous exclusion limits [10,93,94].

C. Weakly interacting massive particles

The results are translated into exclusion limits on the WIMP pair production, assuming the exchange of an axial-vector mediator in the s -channel. For on-shell WIMP pair production, where $m_A > 2m_\chi$, typical $A \times \epsilon$ values for the signal models with a 1 TeV mediator range from 25% to 2% for IM1 and IM7 selections, respectively.

The effect of experimental uncertainties related to jet and E_T^{miss} scales and resolutions is found to be similar to the effect in the ADD model. The uncertainty related to the modeling of the initial- and final-state radiation translates into $\pm 20\%$ uncertainty in the acceptance and is neglected for the cross section. The choice of different PDF sets results in up to $\pm 20\%$ uncertainty in the acceptance and $\pm 10\%$ uncertainty in the cross section. Varying the renormalization and factorization scales introduces $\pm 5\%$ variations of the cross section and a $\pm 3\%$ change in the

acceptance. In addition, the uncertainty in the integrated luminosity is included.

Figure 7 (left) shows the observed and expected 95% C.L. exclusion limits in the m_χ - m_A parameter plane for a simplified model with an axial-vector mediator, Dirac WIMPs, and couplings $g_q = 1/4$ and $g_\chi = 1$. A minimal mediator width is assumed. In addition, observed limits are shown using $\pm 1\sigma$ theoretical uncertainties in the signal cross sections. In the on-shell regime, the models with mediator masses up to 1 TeV are excluded. This analysis loses sensitivity to the models in the off-shell regime, where the decay into a pair of WIMPs is kinematically suppressed. The perturbative unitarity is violated in the parameter region defined by $m_\chi > \sqrt{\pi/2}m_A$ [95]. The masses corresponding to the correct relic density as measured by the Planck and WMAP satellites [35,36], in the absence of any interaction other than the one considered, are indicated in the figure as a line that crosses the excluded region at $m_A \sim 880$ GeV and $m_\chi \sim 270$ GeV. The region towards lower WIMP masses or higher mediator masses corresponds to dark matter overproduction. On the opposite side of the curve, other WIMP production mechanisms need to exist in order to explain the observed dark matter relic density.

In Fig. 7 (right) the results are translated into 90% C.L. exclusion limits on the spin-dependent WIMP-proton scattering cross section as a function of the WIMP mass, following the prescriptions explained in Refs. [41,42], and are compared to results from the direct-detection experiments XENON100 [96], LUX [97], and PICO [98,99]. This comparison is model dependent and solely valid in the context of this particular Z' -like model. In this case,

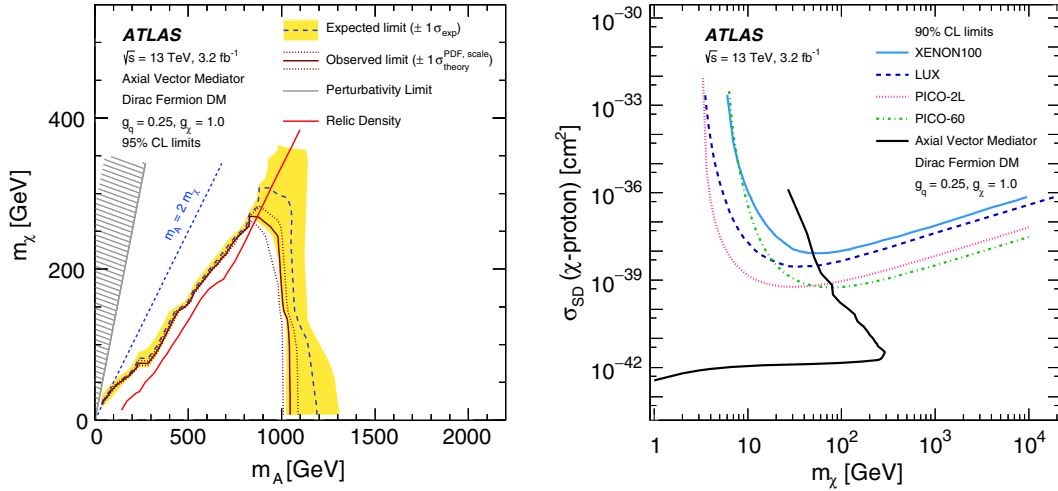


FIG. 7. Left: 95% C.L. exclusion contours in the m_χ - m_A parameter plane. The solid (dashed) curve shows the median of the observed (expected) limit, while the bands indicate the $\pm 1\sigma$ theory uncertainties in the observed limit and $\pm 1\sigma$ range of the expected limit in the absence of a signal. The red curve corresponds to the expected relic density. The region excluded due to perturbativity, defined by $m_\chi > \sqrt{\pi/2}m_A$, is indicated by the hatched area. Right: a comparison of the inferred limits to the constraints from direct detection experiments on the spin-dependent WIMP-proton scattering cross section in the context of the Z' -like simplified model with axial-vector couplings. Unlike in the m_χ - m_A parameter plane, the limits are shown at 90% C.L. The results from this analysis, excluding the region to the left of the contour, are compared with limits from the XENON100 [96], LUX [97], and PICO [98,99] experiments. The comparison is model dependent and solely valid in the context of this model, assuming minimal mediator width and the coupling values $g_q = 1/4$ and $g_\chi = 1$.

stringent limits on the scattering cross section of the order of 10^{-42} cm² up to WIMP masses of about 300 GeV are inferred from this analysis, and complement the results from direct-detection experiments for $m_\chi < 10$ GeV. The loss of sensitivity in models where WIMPs are produced off-shell is expressed by the turn of the exclusion line, reaching back to low WIMP masses and intercepting the exclusion lines from the direct-detection experiments at around $m_\chi = 80$ GeV.

IX. CONCLUSIONS

In summary, results are reported from a search for new phenomena in events with an energetic jet and large missing transverse momentum in proton-proton collisions at $\sqrt{s} = 13$ TeV at the LHC, based on data corresponding to an integrated luminosity of 3.2 fb^{-1} collected by the ATLAS experiment in 2015. The measurements are in agreement with the SM predictions.

The results are translated into model-independent 95% confidence-level upper limits on $\sigma \times A \times \epsilon$ in the range 553–19 fb, depending on the selection criteria considered. The results are presented in terms of lower limits on the fundamental Planck scale, M_D , versus the number of extra spatial dimensions in the ADD LED model. Values of M_D below 6.58 TeV at $n = 2$ and below 4.31 TeV at $n = 6$ are excluded at 95% C.L. Similarly, the results are interpreted in terms of the search for squark pair production in a compressed supersymmetric scenario. In the case of stop and sbottom pair production with $\tilde{t}_1 \rightarrow c + \tilde{\chi}_1^0$ and

$\tilde{b}_1 \rightarrow b + \tilde{\chi}_1^0$, respectively, squark masses below 323 GeV are excluded at 95% C.L. In the case of squark pair production with $\tilde{q} \rightarrow q + \tilde{\chi}_1^0$ ($q = u, d, c, s$) squark masses below 608 GeV are excluded. Altogether, these results extend the exclusion from previous analyses at the LHC.

Finally, the results are interpreted in terms of upper limits on the pair-production cross section of WIMPs. A simplified model is used with an axial-vector mediator, given couplings to fermions $g_\chi = 1$ and $g_q = 1/4$, and considering Dirac fermions as dark matter candidates. Mediator masses below 1 TeV are excluded at 95% C.L. for WIMP masses below 250 GeV. These results are translated, in a model-dependent manner, into upper limits on spin-dependent contributions to the WIMP-nucleon elastic cross section as a function of the WIMP mass. WIMP-proton cross sections above 10^{-42} cm² are excluded at 90% C.L. for WIMP masses below 10 GeV, complementing results from direct-detection experiments.

ACKNOWLEDGMENTS

We thank CERN for the very successful operation of the LHC, as well as the support staff from our institutions without whom ATLAS could not be operated efficiently. We acknowledge the support of ANPCyT, Argentina; YerPhI, Armenia; ARC, Australia; BMWFW and FWF, Austria; ANAS, Azerbaijan; SSTC, Belarus; CNPq and FAPESP, Brazil; NSERC, NRC and CFI, Canada; CERN; CONICYT,

Chile; CAS, MOST and NSFC, China; COLCIENCIAS, Colombia; MSMT CR, MPO CR and VSC CR, Czech Republic; DNRF and DNSRC, Denmark; IN2P3-CNRS, CEA-DSM/IRFU, France; GNSF, Georgia; BMBF, HGF, and MPG, Germany; GSRT, Greece; RGC, Hong Kong SAR, China; ISF, I-CORE and Benoziyo Center, Israel; INFN, Italy; MEXT and JSPS, Japan; CNRST, Morocco; FOM and NWO, Netherlands; RCN, Norway; MNiSW and NCN, Poland; FCT, Portugal; MNE/IFA, Romania; MES of Russia and NRC KI, Russian Federation; JINR; MESTD, Serbia; MSSR, Slovakia; ARRS and MIZŠ, Slovenia; DST/NRF, South Africa; MINECO, Spain; SRC and Wallenberg Foundation, Sweden; SERI, SNSF and Cantons of Bern and Geneva, Switzerland; MOST, Taiwan; TAEK, Turkey; STFC, United Kingdom; DOE and NSF, United States of America. In addition, individual groups and members have received support from BCKDF, the Canada Council,

CANARIE, CRC, Compute Canada, FQRNT, and the Ontario Innovation Trust, Canada; EPLANET, ERC, FP7, Horizon 2020 and Marie Skłodowska-Curie Actions, European Union; Investissements d'Avenir Labex and Idex, ANR, Région Auvergne and Fondation Partager le Savoir, France; DFG and AvH Foundation, Germany; Herakleitos, Thales and Aristeia programmes co-financed by EU-ESF and the Greek NSRF; BSF, GIF and Minerva, Israel; BRF, Norway; Generalitat de Catalunya, Generalitat Valenciana, Spain; the Royal Society and Leverhulme Trust, United Kingdom. The crucial computing support from all WLCG partners is acknowledged gratefully, in particular from CERN and the ATLAS Tier-1 facilities at TRIUMF (Canada), NDGF (Denmark, Norway, Sweden), CC-IN2P3 (France), KIT/GridKA (Germany), INFN-CNAF (Italy), NL-T1 (Netherlands), PIC (Spain), ASGC (Taiwan), RAL (UK) and BNL (USA) and in the Tier-2 facilities worldwide.

-
- [1] CMS Collaboration, Search for New Physics with a Mono-Jet and Missing Transverse Energy in pp Collisions at $\sqrt{s} = 7$ TeV, *Phys. Rev. Lett.* **107**, 201804 (2011).
- [2] CMS Collaboration, Search for dark matter and large extra dimensions in monojet events in pp collisions at $\sqrt{s} = 7$ TeV, *J. High Energy Phys.* **09** (2012) 094.
- [3] CMS Collaboration, Search for Dark Matter and Large Extra Dimensions in pp Collisions Yielding a Photon and Missing Transverse Energy, *Phys. Rev. Lett.* **108**, 261803 (2012).
- [4] ATLAS Collaboration, Search for new phenomena with the monojet and missing transverse momentum signature using the ATLAS detector in $\sqrt{s} = 7$ TeV proton-proton collisions, *Phys. Lett. B* **705**, 294 (2011).
- [5] ATLAS Collaboration, Search for dark matter candidates and large extra dimensions in events with a jet and missing transverse momentum with the ATLAS detector, *J. High Energy Phys.* **04** (2013) 075.
- [6] ATLAS Collaboration, Search for Dark Matter Candidates and Large Extra Dimensions in Events with a Photon and Missing Transverse Momentum in pp Collision Data at $\sqrt{s} = 7$ TeV with the ATLAS detector, *Phys. Rev. Lett.* **110**, 011802 (2013).
- [7] CMS Collaboration, Search for dark matter, extra dimensions, and unparticles in monojet events in proton-proton collisions at $\sqrt{s} = 8$ TeV, *Eur. Phys. J. C* **75**, 235 (2015).
- [8] CMS Collaboration, Search for new phenomena in mono-photon final states in proton-proton collisions at $\sqrt{s} = 8$ TeV, *Phys. Lett. B* **755**, 102 (2016).
- [9] T. Affolder *et al.* (CDF Collaboration), Limits on Gravitino Production and New Processes with Large Missing Transverse Energy in $p\bar{p}$ Collisions at $\sqrt{s} = 1.8$ TeV, *Phys. Rev. Lett.* **85**, 1378 (2000).
- [10] ATLAS Collaboration, Search for pair-produced third-generation squarks decaying via charm quarks or in compressed supersymmetric scenarios in pp collisions at $\sqrt{s} = 8$ TeV with the ATLAS detector, *Phys. Rev. D* **90**, 052008 (2014).
- [11] ATLAS Collaboration, Search for dark matter in events with heavy quarks and missing transverse momentum in pp collisions with the ATLAS detector, *Eur. Phys. J. C* **75**, 92 (2015).
- [12] ATLAS Collaboration, Search for dark matter in events with a Z boson and missing transverse momentum in pp collisions at $\sqrt{s} = 8$ TeV with the ATLAS detector, *Phys. Rev. D* **90**, 012004 (2014).
- [13] ATLAS Collaboration, Search for Dark Matter in Events with a Hadronically Decaying W or Z Boson and Missing Transverse Momentum in pp Collisions at $\sqrt{s} = 8$ TeV with the ATLAS Detector, *Phys. Rev. Lett.* **112**, 041802 (2014).
- [14] CMS Collaboration, Search for physics beyond the standard model in final states with a lepton and missing transverse energy in proton-proton collisions at $\sqrt{s} = 8$ TeV, *Phys. Rev. D* **91**, 092005 (2015).
- [15] CMS Collaboration, Searches for third-generation squark production in fully hadronic final states in proton-proton collisions at $\sqrt{s} = 8$ TeV, *J. High Energy Phys.* **06** (2015) 116.
- [16] N. Arkani-Hamed, S. Dimopoulos, and G. Dvali, The hierarchy problem and new dimensions at a millimeter, *Phys. Lett. B* **429**, 263 (1998).
- [17] H. Miyazawa, Baryon number changing currents, *Prog. Theor. Phys.* **36**, 1266 (1966).
- [18] P. Ramond, Dual theory for free fermions, *Phys. Rev. D* **3**, 2415 (1971).
- [19] Y. A. Golfand and E. P. Likhtman, Extension of the algebra of Poincare group generators and violation of p invariance, *JETP Lett.* **13**, 323 (1971).
- [20] A. Neveu and J. H. Schwarz, Factorizable dual model of pions, *Nucl. Phys.* **B31**, 86 (1971).

- [21] A. Neveu and J. H. Schwarz, Quark model of dual pions, *Phys. Rev. D* **4**, 1109 (1971).
- [22] J. Gervais and B. Sakita, Field theory interpretation of supergauge in dual models, *Nucl. Phys.* **B34**, 632 (1971).
- [23] D. V. Volkov and V. P. Akulov, Is the neutrino a Goldstone particle?, *Phys. Lett.* **46B**, 109 (1973).
- [24] J. Wess and B. Zumino, A Lagrangian model invariant under supergauge transformations, *Phys. Lett.* **49B**, 52 (1974).
- [25] J. Wess and B. Zumino, Supergauge transformations in four dimensions, *Nucl. Phys.* **B70**, 39 (1974).
- [26] R. Barbieri and G. Giudice, Upper bounds on supersymmetric particle masses, *Nucl. Phys.* **B306**, 63 (1988).
- [27] P. Fayet, Supersymmetry and weak, electromagnetic and strong interactions, *Phys. Lett.* **64B**, 159 (1976).
- [28] P. Fayet, Spontaneously broken supersymmetric theories of weak, electromagnetic and strong interactions, *Phys. Lett.* **69B**, 489 (1977).
- [29] G. R. Farrar and P. Fayet, Phenomenology of the production, decay, and detection of new hadronic states associated with supersymmetry, *Phys. Lett. B* **76**, 575 (1978).
- [30] P. Fayet, Relations between the masses of the superpartners of leptons and quarks, the Goldstino couplings and the neutral currents, *Phys. Lett. B* **84**, 416 (1979).
- [31] S. Dimopoulos and H. Georgi, Softly broken supersymmetry and SU(5), *Nucl. Phys.* **B193**, 150 (1981).
- [32] G. Bertone, D. Hooper, and J. Silk, Particle dark matter: Evidence, candidates and constraints, *Phys. Rep.* **405**, 279 (2005).
- [33] G. Steigman and M. S. Turner, Cosmological constraints on the properties of weakly interacting massive particles, *Nucl. Phys.* **B253**, 375 (1985).
- [34] E. W. Kolb and M. S. Turner, The early universe, *Front. Phys.* **69**, 1 (1990).
- [35] R. Adam *et al.* (Planck Collaboration), Planck 2015 results. I. Overview of products and scientific results, [arXiv:1502.01582](https://arxiv.org/abs/1502.01582).
- [36] G. Hinshaw *et al.*, Nine-year Wilkinson Microwave Anisotropy Probe (WMAP) observations: Cosmological parameter results, *Astrophys. J. Suppl. Ser.* **208**, 19 (2013).
- [37] ATLAS Collaboration, Search for new phenomena in final states with an energetic jet and large missing transverse momentum in pp collisions at $\sqrt{s} = 8$ TeV with the ATLAS detector, *Eur. Phys. J. C* **75**, 299 (2015); **75**, 408(E) (2015).
- [38] J. Goodman, M. Ibe, A. Rajaraman, W. Shepherd, T. M. P. Tait, and H.-B. Yu, Constraints on dark matter from colliders, *Phys. Rev. D* **82**, 116010 (2010).
- [39] J. Abdallah *et al.*, Simplified models for dark matter searches at the LHC, *Phys. Dark Univ.* **9–10**, 8 (2015).
- [40] D. Abercrombie *et al.*, Dark matter benchmark models for early LHC Run-2 searches: Report of the ATLAS/CMS Dark Matter Forum, [arXiv:1507.00966](https://arxiv.org/abs/1507.00966).
- [41] O. Buchmueller, M. J. Dolan, S. A. Malik, and C. McCabe, Characterising dark matter searches at colliders and direct detection experiments: Vector mediators, *J. High Energy Phys.* **01** (2015) 037.
- [42] G. Busoni *et al.*, Recommendations on presenting LHC searches for missing transverse energy signals using simplified s-channel models of dark matter, edited by A. Boveia *et al.*, [arXiv:1603.04156](https://arxiv.org/abs/1603.04156).
- [43] G. Busoni, A. De Simone, E. Morgante, and A. Riotto, On the validity of the effective field theory for dark matter searches at the LHC, *Phys. Lett. B* **728**, 412 (2014).
- [44] ATLAS Collaboration, The ATLAS Experiment at the CERN Large Hadron Collider, *J. Instrum.* **3** S08003 (2008).
- [45] ATLAS Collaboration, Tech. Reports No. CERN-LHCC-2010-013 and No. ATLAS-TDR-19, CERN, 2010, <http://cds.cern.ch/record/1291633>.
- [46] ATLAS Collaboration, Report No. ATL-DAQ-PUB-2016-001, 2016, <http://cds.cern.ch/record/2136007>.
- [47] T. Gleisberg, S. Höche, F. Krauss, M. Schönherr, S. Schumann, F. Siegert, and J. Winter, Event generation with SHERPA 1.1, *J. High Energy Phys.* **02** (2009) 007.
- [48] T. Gleisberg and S. Höche, Comix, a new matrix element generator, *J. High Energy Phys.* **12** (2008) 039.
- [49] F. Cascioli, P. Maierhofer, and S. Pozzorini, Scattering Amplitudes with Open Loops, *Phys. Rev. Lett.* **108**, 111601 (2012).
- [50] S. Schumann and F. Krauss, A Parton shower algorithm based on Catani-Seymour dipole factorisation, *J. High Energy Phys.* **03** (2008) 038.
- [51] S. Höche, F. Krauss, M. Schönherr, and F. Siegert, QCD matrix elements + parton showers: The NLO case, *J. High Energy Phys.* **04** (2013) 027.
- [52] H.-L. Lai, M. Guzzi, J. Huston, Z. Li, P. M. Nadolsky, J. Pumplin, and C.-P. Yuan, New parton distributions for collider physics, *Phys. Rev. D* **82**, 074024 (2010).
- [53] S. Catani, L. Cieri, G. Ferrera, D. de Florian, and M. Grazzini, Vector Boson Production at Hadron Colliders: A Fully Exclusive QCD Calculation at NNLO, *Phys. Rev. Lett.* **103**, 082001 (2009).
- [54] S. Catani and M. Grazzini, An NNLO Subtraction Formalism in Hadron Collisions and Its Application to Higgs Boson Production at the LHC, *Phys. Rev. Lett.* **98**, 222002 (2007).
- [55] A. D. Martin, W. J. Stirling, R. S. Thorne, and G. Watt, Parton distributions for the LHC, *Eur. Phys. J. C* **63**, 189 (2009).
- [56] S. Frixione, P. Nason, and G. Ridolfi, A positive-weight next-to-leading-order Monte Carlo for heavy Flavour hadroproduction, *J. High Energy Phys.* **09** (2007) 126.
- [57] T. Sjöstrand, S. Mrenna, and P. Z. Skands, PYTHIA 6.4 physics and manual, *J. High Energy Phys.* **05** (2006) 026.
- [58] J. Pumplin, D. R. Stump, J. Huston, H.-L. Lai, P. Nadolsky, and W.-K. Tung, New generation of parton distributions with uncertainties from global QCD analysis, *J. High Energy Phys.* **07** (2002) 012.
- [59] P. Z. Skands, Tuning Monte Carlo generators: The Perugia tunes, *Phys. Rev. D* **82**, 074018 (2010).
- [60] D. J. Lange, The EvtGen particle decay simulation package, *Nucl. Instrum. Methods Phys. Res., Sect. A* **462**, 152 (2001).
- [61] J. M. Campbell, R. K. Ellis, and C. Williams, Vector boson pair production at the LHC, *J. High Energy Phys.* **07** (2011) 018.
- [62] R. D. Ball *et al.*, Parton distributions with LHC data, *Nucl. Phys.* **B867**, 244 (2013).
- [63] J. Alwall, R. Frederix, S. Frixione, V. Hirschi, F. Maltoni, O. Mattelaer, H.-S. Shao, T. Stelzer, P. Torrielli, and M. Zaro, The automated computation of tree-level

- and next-to-leading order differential cross sections, and their matching to parton shower simulations, *J. High Energy Phys.* **07** (2014) 079.
- [64] ATLAS Collaboration, Report No. ATL-PHYS-PUB-2014-021, 2014, <http://cds.cern.ch/record/1966419>.
- [65] L. Lönnblad and S. Prestel, Matching tree-level matrix elements with interleaved showers, *J. High Energy Phys.* **03** (2012) 019.
- [66] W. Beenakker, M. Krämer, T. Plehn, M. Spira, and P. M. Zerwas, Stop production at hadron colliders, *Nucl. Phys.* **B515**, 3 (1998).
- [67] W. Beenakker, S. Brensing, M. Krämer, A. Kulesza, E. Laenen, and I. Niessen, Supersymmetric top and bottom squark production at hadron colliders, *J. High Energy Phys.* **08** (2010) 098.
- [68] W. Beenakker, S. Brensing, M. Krämer, A. Kulesza, E. Laenen, L. Motyka, and I. Niessen, Squark and gluino hadroproduction, *Int. J. Mod. Phys. A* **26**, 2637 (2011).
- [69] C. Borschensky, M. Krämer, A. Kulesza, M. Mangano, S. Padhi, T. Plehn, and X. Portell, Squark and gluino production cross sections in pp collisions at $\sqrt{s} = 13, 14, 33$ and 100 TeV, *Eur. Phys. J. C* **74**, 3174 (2014).
- [70] S. Alioli, P. Nason, C. Oleari, and E. Re, A general framework for implementing NLO calculations in shower Monte Carlo programs: The POWHEG BOX, *J. High Energy Phys.* **06** (2010) 043.
- [71] S. Frixione, P. Nason, and C. Oleari, Matching NLO QCD computations with parton shower simulations: The POWHEG method, *J. High Energy Phys.* **11** (2007) 070.
- [72] P. Nason, A new method for combining NLO QCD with shower Monte Carlo algorithms, *J. High Energy Phys.* **11** (2004) 040.
- [73] U. Haisch, F. Kahlhöfer, and E. Re, QCD effects in mono-jet searches for dark matter, *J. High Energy Phys.* **12** (2013) 007.
- [74] R. D. Ball *et al.*, Parton distributions for the LHC Run II, *J. High Energy Phys.* **04** (2015) 040.
- [75] ATLAS Collaboration, The ATLAS simulation infrastructure, *Eur. Phys. J. C* **70**, 823 (2010).
- [76] S. Agostinelli *et al.*, GEANT4: A Simulation toolkit, *Nucl. Instrum. Methods Phys. Res., Sect. A* **506**, 250 (2003).
- [77] M. Cacciari, G. P. Salam, and G. Soyez, The anti- k_t jet clustering algorithm, *J. High Energy Phys.* **04** (2008) 063.
- [78] ATLAS Collaboration, Jet energy measurement with the ATLAS detector in proton-proton collisions at $\sqrt{s} = 7$ TeV, *Eur. Phys. J. C* **73**, 2304 (2013).
- [79] ATLAS Collaboration, Report No. ATLASCONF-2014-018, 2014, <http://cds.cern.ch/record/1700870>.
- [80] ATLAS Collaboration, Muon reconstruction performance of the ATLAS detector in proton-proton collision data at $\sqrt{s} = 13$ TeV, *Eur. Phys. J. C* **76**, 292 (2016).
- [81] ATLAS Collaboration, Report No. ATLAS-CONF-2014-032, 2014, <http://cdsweb.cern.ch/record/1706245>.
- [82] ATLAS Collaboration, Performance of missing transverse momentum reconstruction in proton-proton collisions at 7 TeV with ATLAS, *Eur. Phys. J. C* **72**, 1844 (2012).
- [83] ATLAS Collaboration, Report No. ATLAS-CONF-2015-029, 2015, <http://cds.cern.ch/record/2037702>.
- [84] ATLAS Collaboration, Characterisation and mitigation of beam-induced backgrounds observed in the ATLAS detector during the 2011 proton-proton run, *J. Instrum.* **8**, P07004 (2013).
- [85] ATLAS Collaboration, Search for squarks and gluinos with the ATLAS detector in final states with jets and missing transverse momentum using 4.7 fb^{-1} of $\sqrt{s} = 7$ TeV proton-proton collision data, *Phys. Rev. D* **87**, 012008 (2013).
- [86] G. Cowan, K. Cranmer, E. Gross, and O. Vitells, Asymptotic formulae for likelihood-based tests of new physics, *Eur. Phys. J. C* **71**, 1554 (2011).
- [87] A. Denner, S. Dittmaier, T. Kasprzik, and A. Mück, Electroweak corrections to monojet production at the LHC, *Eur. Phys. J. C* **73**, 2297 (2013).
- [88] A. Denner, S. Dittmaier, T. Kasprzik, and A. Mück, Electroweak corrections to dilepton + jet production at hadron colliders, *J. High Energy Phys.* **06** (2011) 069.
- [89] A. Denner, S. Dittmaier, T. Kasprzik, and A. Mück, Electroweak corrections to $W + \text{jet}$ hadroproduction including leptonic W-boson decays, *J. High Energy Phys.* **08** (2009) 075.
- [90] ATLAS Collaboration, Improved luminosity determination in pp collisions at $\sqrt{s} = 7$ TeV using the ATLAS detector at the LHC, *Eur. Phys. J. C* **73**, 2518 (2013).
- [91] L. A. Harland-Lang, A. D. Martin, P. Motylinski, and R. S. Thorne, Parton distributions in the LHC era: MMHT 2014 PDFs, *Eur. Phys. J. C* **75**, 204 (2015).
- [92] A. L. Read, Presentation of search results: The CLs technique, *J. Phys. G* **28**, 2693 (2002).
- [93] T. Aaltonen *et al.* (CDF Collaboration), Search for Scalar Top Quark Production in $p\bar{p}$ Collisions at $\sqrt{s} = 1.96$ TeV, *J. High Energy Phys.* **10** (2012) 158.
- [94] V.M. Abazov *et al.* (D0 Collaboration), Search for scalar top quarks in the acoplanar charm jets and missing transverse energy final state in $p\bar{p}$ collisions at $\sqrt{s} = 1.96$ TeV, *Phys. Lett. B* **665**, 1 (2008).
- [95] F. Kahlhöfer, K. Schmidt-Hoberg, T. Schwetz, and S. Vogl, Implications of unitarity and gauge invariance for simplified dark matter models, *J. High Energy Phys.* **02** (2016) 016.
- [96] E. Aprile *et al.* (XENON100 Collaboration), Limits on Spin-Dependent WIMP-Nucleon Cross Sections from 225 Live Days of XENON100 Data, *Phys. Rev. Lett.* **111**, 021301 (2013).
- [97] D. S. Akerib *et al.* (LUX Collaboration), First Spin-Dependent WIMP-Nucleon Cross Section Limits from the LUX Experiment, *Phys. Rev. Lett.* **116**, 161302 (2016).
- [98] C. Amole *et al.*, Dark matter search results from the PICO-60 CF₃I bubble chamber, *Phys. Rev. D* **93**, 052014 (2016).
- [99] C. Amole *et al.* (PICO Collaboration), Improved dark matter search results from PICO-2L Run-2, [arXiv:1601.03729](https://arxiv.org/abs/1601.03729).

- M. Aaboud,^{136d} G. Aad,⁸⁷ B. Abbott,¹¹⁴ J. Abdallah,⁶⁵ O. Abidinov,¹² B. Abeloos,¹¹⁸ R. Aben,¹⁰⁸ O. S. AbouZeid,¹³⁸
 N. L. Abraham,¹⁵⁰ H. Abramowicz,¹⁵⁴ H. Abreu,¹⁵³ R. Abreu,¹¹⁷ Y. Abulaiti,^{147a,147b} B. S. Acharya,^{164a,164b}
 L. Adamczyk,^{40a} D. L. Adams,²⁷ J. Adelman,¹⁰⁹ S. Adomeit,¹⁰¹ T. Adye,¹³² A. A. Affolder,⁷⁶ T. Agatonovic-Jovin,¹⁴
 J. Agricola,⁵⁶ J. A. Aguilar-Saavedra,^{127a,127f} S. P. Ahlen,²⁴ F. Ahmadov,^{67,c} G. Aielli,^{134a,134b} H. Akerstedt,^{147a,147b}
 T. P. A. Åkesson,⁸³ A. V. Akimov,⁹⁷ G. L. Alberghi,^{22a,22b} J. Albert,¹⁶⁹ S. Albrand,⁵⁷ M. J. Alconada Verzini,⁷³ M. Aleksa,³²
 I. N. Aleksandrov,⁶⁷ C. Alexa,^{28b} G. Alexander,¹⁵⁴ T. Alexopoulos,¹⁰ M. Alhroob,¹¹⁴ M. Aliev,^{75a,75b} G. Alimonti,^{93a}
 J. Alison,³³ S. P. Alkire,³⁷ B. M. M. Allbrooke,¹⁵⁰ B. W. Allen,¹¹⁷ P. P. Allport,¹⁹ A. Aloisio,^{105a,105b} A. Alonso,³⁸
 F. Alonso,⁷³ C. Alpigiani,¹³⁹ M. Alstaty,⁸⁷ B. Alvarez Gonzalez,³² D. Álvarez Piqueras,¹⁶⁷ M. G. Alviggi,^{105a,105b}
 B. T. Amadio,¹⁶ K. Amako,⁶⁸ Y. Amaral Coutinho,^{26a} C. Amelung,²⁵ D. Amidei,⁹¹ S. P. Amor Dos Santos,^{127a,127c}
 A. Amorim,^{127a,127b} S. Amoroso,³² G. Amundsen,²⁵ C. Anastopoulos,¹⁴⁰ L. S. Ancu,⁵¹ N. Andari,¹⁰⁹ T. Andeen,¹¹
 C. F. Anders,^{60b} G. Anders,³² J. K. Anders,⁷⁶ K. J. Anderson,³³ A. Andreazza,^{93a,93b} V. Andrei,^{60a} S. Angelidakis,⁹
 I. Angelozzi,¹⁰⁸ P. Anger,⁴⁶ A. Angerami,³⁷ F. Anghinolfi,³² A. V. Anisenkov,^{110,d} N. Anjos,¹³ A. Annovi,^{125a,125b}
 M. Antonelli,⁴⁹ A. Antonov,⁹⁹ F. Anulli,^{133a} M. Aoki,⁶⁸ L. Aperio Bella,¹⁹ G. Arabidze,⁹² Y. Arai,⁶⁸ J. P. Araque,^{127a}
 A. T. H. Arce,⁴⁷ F. A. Arduh,⁷³ J-F. Arguin,⁹⁶ S. Argyropoulos,⁶⁵ M. Arik,^{20a} A. J. Armbruster,¹⁴⁴ L. J. Armitage,⁷⁸
 O. Arnaez,³² H. Arnold,⁵⁰ M. Arratia,³⁰ O. Arslan,²³ A. Artamonov,⁹⁸ G. Artoni,¹²¹ S. Artz,⁸⁵ S. Asai,¹⁵⁶ N. Asbah,⁴⁴
 A. Ashkenazi,¹⁵⁴ B. Åsman,^{147a,147b} L. Asquith,¹⁵⁰ K. Assamagan,²⁷ R. Astalos,^{145a} M. Atkinson,¹⁶⁶ N. B. Atlay,¹⁴²
 K. Augsten,¹²⁹ G. Avolio,³² B. Axen,¹⁶ M. K. Ayoub,¹¹⁸ G. Azuelos,^{96,e} M. A. Baak,³² A. E. Baas,^{60a} M. J. Baca,¹⁹
 H. Bachacou,¹³⁷ K. Bachas,^{75a,75b} M. Backes,³² M. Backhaus,³² P. Bagiacci,^{133a,133b} P. Bagnaia,^{133a,133b} Y. Bai,^{35a}
 J. T. Baines,¹³² O. K. Baker,¹⁷⁶ E. M. Baldin,^{110,d} P. Balek,¹³⁰ T. Balestri,¹⁴⁹ F. Balli,¹³⁷ W. K. Balunas,¹²³ E. Banas,⁴¹
 Sw. Banerjee,^{173,f} A. A. E. Bannoura,¹⁷⁵ L. Barak,³² E. L. Barberio,⁹⁰ D. Barberis,^{52a,52b} M. Barbero,⁸⁷ T. Barillari,¹⁰²
 T. Barklow,¹⁴⁴ N. Barlow,³⁰ S. L. Barnes,⁸⁶ B. M. Barnett,¹³² R. M. Barnett,¹⁶ Z. Barnovska,⁵ A. Baroncelli,^{135a} G. Barone,²⁵
 A. J. Barr,¹²¹ L. Barranco Navarro,¹⁶⁷ F. Barreiro,⁸⁴ J. Barreiro Guimarães da Costa,^{35a} R. Bartoldus,¹⁴⁴ A. E. Barton,⁷⁴
 P. Bartos,^{145a} A. Basalaeu,¹²⁴ A. Bassalat,¹¹⁸ R. L. Bates,⁵⁵ S. J. Batista,¹⁵⁹ J. R. Batley,³⁰ M. Battaglia,¹³⁸ M. Bauce,^{133a,133b}
 F. Bauer,¹³⁷ H. S. Bawa,^{144,g} J. B. Beacham,¹¹² M. D. Beattie,⁷⁴ T. Beau,⁸² P. H. Beauchemin,¹⁶² P. Bechtel,²³ H. P. Beck,^{18,h}
 K. Becker,¹²¹ M. Becker,⁸⁵ M. Beckingham,¹⁷⁰ C. Becot,¹¹¹ A. J. Beddall,^{20e} A. Beddall,^{20b} V. A. Bednyakov,⁶⁷
 M. Bedognetti,¹⁰⁸ C. P. Bee,¹⁴⁹ L. J. Beemster,¹⁰⁸ T. A. Beermann,³² M. Begel,²⁷ J. K. Behr,⁴⁴ C. Belanger-Champagne,⁸⁹
 A. S. Bell,⁸⁰ G. Bella,¹⁵⁴ L. Bellagamba,^{22a} A. Bellerive,³¹ M. Bellomo,⁸⁸ K. Belotskiy,⁹⁹ O. Beltramello,³² N. L. Belyaev,⁹⁹
 O. Benary,¹⁵⁴ D. Benchekroun,^{136a} M. Bender,¹⁰¹ K. Bendtz,^{147a,147b} N. Benekos,¹⁰ Y. Benhammou,¹⁵⁴
 E. Benhar Noccioli,¹⁷⁶ J. Benitez,⁶⁵ D. P. Benjamin,⁴⁷ J. R. Bensinger,²⁵ S. Bentvelsen,¹⁰⁸ L. Beresford,¹²¹ M. Beretta,⁴⁹
 D. Berge,¹⁰⁸ E. Bergeaas Kuutmann,¹⁶⁵ N. Berger,⁵ J. Beringer,¹⁶ S. Berlendis,⁵⁷ N. R. Bernard,⁸⁸ C. Bernius,¹¹¹
 F. U. Bernlochner,²³ T. Berry,⁷⁹ P. Berta,¹³⁰ C. Bertella,⁸⁵ G. Bertoli,^{147a,147b} F. Bertolucci,^{125a,125b} I. A. Bertram,⁷⁴
 C. Bertsche,⁴⁴ D. Bertsche,¹¹⁴ G. J. Besjes,³⁸ O. Bessidskaia Bylund,^{147a,147b} M. Bessner,⁴⁴ N. Besson,¹³⁷ C. Betancourt,⁵⁰
 S. Bethke,¹⁰² A. J. Bevan,⁷⁸ W. Bhimji,¹⁶ R. M. Bianchi,¹²⁶ L. Bianchini,²⁵ M. Bianco,³² O. Biebel,¹⁰¹ D. Biedermann,¹⁷
 R. Bielski,⁸⁶ N. V. Biesuz,^{125a,125b} M. Biglietti,^{135a} J. Bilbao De Mendizabal,⁵¹ H. Bilokon,⁴⁹ M. Bindi,⁵⁶ S. Binet,¹¹⁸
 A. Bingul,^{20b} C. Bini,^{133a,133b} S. Biondi,^{22a,22b} D. M. Bjergaard,⁴⁷ C. W. Black,¹⁵¹ J. E. Black,¹⁴⁴ K. M. Black,²⁴
 D. Blackburn,¹³⁹ R. E. Blair,⁶ J.-B. Blanchard,¹³⁷ J. E. Blanco,⁷⁹ T. Blazek,^{145a} I. Bloch,⁴⁴ C. Blocker,²⁵ W. Blum,^{85,a}
 U. Blumenschein,⁵⁶ S. Blunier,^{34a} G. J. Bobbink,¹⁰⁸ V. S. Bobrovnikov,^{110,d} S. S. Bocchetta,⁸³ A. Bocci,⁴⁷ C. Bock,¹⁰¹
 M. Boehler,⁵⁰ D. Boerner,¹⁷⁵ J. A. Bogaerts,³² D. Bogavac,¹⁴ A. G. Bogdanchikov,¹¹⁰ C. Bohm,^{147a} V. Boisvert,⁷⁹
 P. Bokan,¹⁴ T. Bold,^{40a} A. S. Boldyrev,^{164a,164c} M. Bomben,⁸² M. Bona,⁷⁸ M. Boonekamp,¹³⁷ A. Borisov,¹³¹ G. Borissov,⁷⁴
 J. Bortfeldt,¹⁰¹ D. Bortoletto,¹²¹ V. Bortolotto,^{62a,62b,62c} K. Bos,¹⁰⁸ D. Boscherini,^{22a} M. Bosman,¹³ J. D. Bossio Sola,²⁹
 J. Boudreau,¹²⁶ J. Bouffard,² E. V. Bouhova-Thacker,⁷⁴ D. Boumediene,³⁶ C. Bourdarios,¹¹⁸ S. K. Boutle,⁵⁵ A. Boveia,³²
 J. Boyd,³² I. R. Boyko,⁶⁷ J. Bracinik,¹⁹ A. Brandt,⁸ G. Brandt,⁵⁶ O. Brandt,^{60a} U. Bratzler,¹⁵⁷ B. Brau,⁸⁸ J. E. Brau,¹¹⁷
 H. M. Braun,^{175,a} W. D. Breaden Madden,⁵⁵ K. Brendlinger,¹²³ A. J. Brennan,⁹⁰ L. Brenner,¹⁰⁸ R. Brenner,¹⁶⁵ S. Bressler,¹⁷²
 T. M. Bristow,⁴⁸ D. Britton,⁵⁵ D. Britzger,⁴⁴ F. M. Brochu,³⁰ I. Brock,²³ R. Brock,⁹² G. Brooijmans,³⁷ T. Brooks,⁷⁹
 W. K. Brooks,^{34b} J. Brosamer,¹⁶ E. Brost,¹¹⁷ J. H. Broughton,¹⁹ P. A. Bruckman de Renstrom,⁴¹ D. Bruncko,^{145b}
 R. Bruneliere,⁵⁰ A. Bruni,^{22a} G. Bruni,^{22a} L. S. Bruni,¹⁰⁸ BH Brunt,³⁰ M. Bruschi,^{22a} N. Brusino,²³ P. Bryant,³³
 L. Bryngemark,⁸³ T. Buanes,¹⁵ Q. Buat,¹⁴³ P. Buchholz,¹⁴² A. G. Buckley,⁵⁵ I. A. Budagov,⁶⁷ F. Buehrer,⁵⁰ M. K. Bugge,¹²⁰
 O. Bulekov,⁹⁹ D. Bullock,⁸ H. Burckhart,³² S. Burdin,⁷⁶ C. D. Burgard,⁵⁰ B. Burghgrave,¹⁰⁹ K. Burka,⁴¹ S. Burke,¹³²
 I. Burmeister,⁴⁵ E. Busato,³⁶ D. Büscher,⁵⁰ V. Büscher,⁸⁵ P. Bussey,⁵⁵ J. M. Butler,²⁴ C. M. Buttar,⁵⁵ J. M. Butterworth,⁸⁰

P. Butti,¹⁰⁸ W. Buttinger,²⁷ A. Buzatu,⁵⁵ A. R. Buzykaev,^{110,d} S. Cabrera Urbán,¹⁶⁷ D. Caforio,¹²⁹ V. M. Cairo,^{39a,39b} O. Cakir,^{4a} N. Calace,⁵¹ P. Calafiura,¹⁶ A. Calandri,⁸⁷ G. Calderini,⁸² P. Calfayan,¹⁰¹ L. P. Caloba,^{26a} D. Calvet,³⁶ S. Calvet,³⁶ T. P. Calvet,⁸⁷ R. Camacho Toro,³³ S. Camarda,³² P. Camarri,^{134a,134b} D. Cameron,¹²⁰ R. Caminal Armadans,¹⁶⁶ C. Camincher,⁵⁷ S. Campana,³² M. Campanelli,⁸⁰ A. Camplani,^{93a,93b} A. Campoverde,¹⁴⁹ V. Canale,^{105a,105b} A. Canepa,^{160a} M. Cano Bret,^{35e} J. Cantero,¹¹⁵ R. Cantrill,^{127a} T. Cao,⁴² M. D. M. Capeans Garrido,³² I. Caprini,^{28b} M. Caprini,^{28b} M. Capua,^{39a,39b} R. Caputo,⁸⁵ R. M. Carbone,³⁷ R. Cardarelli,^{134a} F. Cardillo,⁵⁰ I. Carli,¹³⁰ T. Carli,³² G. Carlino,^{105a} L. Carminati,^{93a,93b} S. Caron,¹⁰⁷ E. Carquin,^{34b} G. D. Carrillo-Montoya,³² J. R. Carter,³⁰ J. Carvalho,^{127a,127c} D. Casadei,¹⁹ M. P. Casado,^{13,i} M. Casolino,¹³ D. W. Casper,¹⁶³ E. Castaneda-Miranda,^{146a} R. Castelijin,¹⁰⁸ A. Castelli,¹⁰⁸ V. Castillo Gimenez,¹⁶⁷ N. F. Castro,^{127aj} A. Catinaccio,³² J. R. Catmore,¹²⁰ A. Cattai,³² J. Caudron,⁸⁵ V. Cavaliere,¹⁶⁶ E. Cavallaro,¹³ D. Cavalli,^{93a} M. Cavalli-Sforza,¹³ V. Cavasinni,^{125a,125b} F. Ceradini,^{135a,135b} L. Cerda Alberich,¹⁶⁷ B. C. Cerio,⁴⁷ A. S. Cerqueira,^{26b} A. Cerri,¹⁵⁰ L. Cerrito,⁷⁸ F. Cerutti,¹⁶ M. Cerv,³² A. Cervelli,¹⁸ S. A. Cetin,^{20d} A. Chafaq,^{136a} D. Chakraborty,¹⁰⁹ S. K. Chan,⁵⁹ Y. L. Chan,^{62a} P. Chang,¹⁶⁶ J. D. Chapman,³⁰ D. G. Charlton,¹⁹ A. Chatterjee,⁵¹ C. C. Chau,¹⁵⁹ C. A. Chavez Barajas,¹⁵⁰ S. Che,¹¹² S. Cheatham,⁷⁴ A. Chegwidan,⁹² S. Chekanov,⁶ S. V. Chekulaev,^{160a} G. A. Chelkov,^{67,k} M. A. Chelstowska,⁹¹ C. Chen,⁶⁶ H. Chen,²⁷ K. Chen,¹⁴⁹ S. Chen,^{35c} S. Chen,¹⁵⁶ X. Chen,^{35f} Y. Chen,⁶⁹ H. C. Cheng,⁹¹ H. J. Cheng,^{35a} Y. Cheng,³³ A. Cheplakov,⁶⁷ E. Cheremushkina,¹³¹ R. Cherkaoui El Moursli,^{136e} V. Chernyatin,^{27,a} E. Cheu,⁷ L. Chevalier,¹³⁷ V. Chiarella,⁴⁹ G. Chiarelli,^{125a,125b} G. Chiodini,^{75a} A. S. Chisholm,¹⁹ A. Chitan,^{28b} M. V. Chizhov,⁶⁷ K. Choi,⁶³ A. R. Chomont,³⁶ S. Chouridou,⁹ B. K. B. Chow,¹⁰¹ V. Christodoulou,⁸⁰ D. Chromek-Burckhart,³² J. Chudoba,¹²⁸ A. J. Chuinard,⁸⁹ J. J. Chwastowski,⁴¹ L. Chytka,¹¹⁶ G. Ciapetti,^{133a,133b} A. K. Ciftci,^{4a} D. Cinca,⁵⁵ V. Cindro,⁷⁷ I. A. Cioara,²³ A. Ciocio,¹⁶ F. Ciroto,^{105a,105b} Z. H. Citron,¹⁷² M. Citterio,^{93a} M. Ciubancan,^{28b} A. Clark,⁵¹ B. L. Clark,⁵⁹ M. R. Clark,³⁷ P. J. Clark,⁴⁸ R. N. Clarke,¹⁶ C. Clement,^{147a,147b} Y. Coadou,⁸⁷ M. Cobal,^{164a,164c} A. Cocco,⁵¹ J. Cochran,⁶⁶ L. Coffey,²⁵ L. Colasurdo,¹⁰⁷ B. Cole,³⁷ A. P. Colijn,¹⁰⁸ J. Collot,⁵⁷ T. Colombo,³² G. Compostella,¹⁰² P. Conde Muño,^{127a,127b} E. Coniavitis,⁵⁰ S. H. Connell,^{146b} I. A. Connelly,⁷⁹ V. Consorti,⁵⁰ S. Constantinescu,^{28b} G. Conti,³² F. Conventi,^{105a,l} M. Cooke,¹⁶ B. D. Cooper,⁸⁰ A. M. Cooper-Sarkar,¹²¹ K. J. R. Cormier,¹⁵⁹ T. Cornelissen,¹⁷⁵ M. Corradi,^{133a,133b} F. Corriveau,^{89,m} A. Corso-Radu,¹⁶³ A. Cortes-Gonzalez,¹³ G. Cortiana,¹⁰² G. Costa,^{93a} M. J. Costa,¹⁶⁷ D. Costanzo,¹⁴⁰ G. Cottin,³⁰ G. Cowan,⁷⁹ B. E. Cox,⁸⁶ K. Cranmer,¹¹¹ S. J. Crawley,⁵⁵ G. Cree,³¹ S. Crépe-Renaudin,⁵⁷ F. Crescioli,⁸² W. A. Cribbs,^{147a,147b} M. Crispin Ortuzar,¹²¹ M. Cristinziani,²³ V. Croft,¹⁰⁷ G. Crosetti,^{39a,39b} T. Cuhadar Donszelmann,¹⁴⁰ J. Cummings,¹⁷⁶ M. Curatolo,⁴⁹ J. Cúth,⁸⁵ C. Cuthbert,¹⁵¹ H. Czirr,¹⁴² P. Czodrowski,³ G. D'amen,^{22a,22b} S. D'Auria,⁵⁵ M. D'Onofrio,⁷⁶ M. J. Da Cunha Sargedas De Sousa,^{127a,127b} C. Da Via,⁸⁶ W. Dabrowski,^{40a} T. Dado,^{145a} T. Dai,⁹¹ O. Dale,¹⁵ F. Dallaire,⁹⁶ C. Dallapiccola,⁸⁸ M. Dam,³⁸ J. R. Dandoy,³³ N. P. Dang,⁵⁰ A. C. Daniells,¹⁹ N. S. Dann,⁸⁶ M. Danninger,¹⁶⁸ M. Dano Hoffmann,¹³⁷ V. Dao,⁵⁰ G. Darbo,^{52a} S. Darmora,⁸ J. Dassoulas,³ A. Dattagupta,⁶³ W. Davey,²³ C. David,¹⁶⁹ T. Davidek,¹³⁰ M. Davies,¹⁵⁴ P. Davison,⁸⁰ E. Dawe,⁹⁰ I. Dawson,¹⁴⁰ R. K. Daya-Ishmukhametova,⁸⁸ K. De,⁸ R. de Asmundis,^{105a} A. De Benedetti,¹¹⁴ S. De Castro,^{22a,22b} S. De Cecco,⁸² N. De Groot,¹⁰⁷ P. de Jong,¹⁰⁸ H. De la Torre,⁸⁴ F. De Lorenzi,⁶⁶ A. De Maria,⁵⁶ D. De Pedis,^{133a} A. De Salvo,^{133a} U. De Sanctis,¹⁵⁰ A. De Santo,¹⁵⁰ J. B. De Vivie De Regie,¹¹⁸ W. J. Dearnaley,⁷⁴ R. Debbe,²⁷ C. Debenedetti,¹³⁸ D. V. Dedovich,⁶⁷ N. Dehghanian,³ I. Deigaard,¹⁰⁸ M. Del Gaudio,^{39a,39b} J. Del Peso,⁸⁴ T. Del Prete,^{125a,125b} D. Delgove,¹¹⁸ F. Deliot,¹³⁷ C. M. Delitzsch,⁵¹ M. Deliyergiyev,⁷⁷ A. Dell'Acqua,³² L. Dell'Asta,²⁴ M. Dell'Orso,^{125a,125b} M. Della Pietra,^{105a,l} D. della Volpe,⁵¹ M. Delmastro,⁵ P. A. Delsart,⁵⁷ C. Deluca,¹⁰⁸ D. A. DeMarco,¹⁵⁹ S. Demers,¹⁷⁶ M. Demichev,⁶⁷ A. Demilly,⁸² S. P. Denisov,¹³¹ D. Denysiuk,¹³⁷ D. Derendarz,⁴¹ J. E. Derkaoui,^{136d} F. Derue,⁸² P. Dervan,⁷⁶ K. Desch,²³ C. Deterre,⁴⁴ K. Dette,⁴⁵ P. O. Deviveiros,³² A. Dewhurst,¹³² S. Dhaliwal,²⁵ A. Di Ciaccio,^{134a,134b} L. Di Ciaccio,⁵ W. K. Di Clemente,¹²³ C. Di Donato,^{133a,133b} A. Di Girolamo,³² B. Di Girolamo,³² B. Di Micco,^{135a,135b} R. Di Nardo,³² A. Di Simone,⁵⁰ R. Di Sipio,¹⁵⁹ D. Di Valentino,³¹ C. Diaconu,⁸⁷ M. Diamond,¹⁵⁹ F. A. Dias,⁴⁸ M. A. Diaz,^{34a} E. B. Diehl,⁹¹ J. Dietrich,¹⁷ S. Diglio,⁸⁷ A. Dimitrievska,¹⁴ J. Dingfelder,²³ P. Dita,^{28b} S. Dita,^{28b} F. Dittus,³² F. Djama,⁸⁷ T. Djobava,^{53b} J. I. Djuvsland,^{60a} M. A. B. do Vale,^{26c} D. Dobos,³² M. Dobre,^{28b} C. Doglioni,⁸³ T. Dohmae,¹⁵⁶ J. Dolejsi,¹³⁰ Z. Dolezal,¹³⁰ B. A. Dolgoshein,^{99,a} M. Donadelli,^{26d} S. Donati,^{125a,125b} P. Dondero,^{122a,122b} J. Donini,³⁶ J. Dopke,¹³² A. Doria,^{105a} M. T. Dova,⁷³ A. T. Doyle,⁵⁵ E. Drechsler,⁵⁶ M. Dris,¹⁰ Y. Du,^{35d} J. Duarte-Campderros,¹⁵⁴ E. Duchovni,¹⁷² G. Duckeck,¹⁰¹ O. A. Ducu,^{96,n} D. Duda,¹⁰⁸ A. Dudarev,³² E. M. Duffield,¹⁶ L. Duflot,¹¹⁸ L. Duguid,⁷⁹ M. Dührssen,³² M. Dumancic,¹⁷² M. Dunford,^{60a} H. Duran Yildiz,^{4a} M. Düren,⁵⁴ A. Durglishvili,^{53b} D. Duschinger,⁴⁶ B. Dutta,⁴⁴ M. Dyndal,⁴⁴ C. Eckardt,⁴⁴ K. M. Ecker,¹⁰² R. C. Edgar,⁹¹ N. C. Edwards,⁴⁸ T. Eifert,³² G. Eigen,¹⁵ K. Einsweiler,¹⁶ T. Ekelof,¹⁶⁵ M. El Kacimi,^{136c}

V. Ellajosyula,⁸⁷ M. Ellert,¹⁶⁵ S. Elles,⁵ F. Ellinghaus,¹⁷⁵ A. A. Elliot,¹⁶⁹ N. Ellis,³² J. Elmsheuser,²⁷ M. Elsing,³² D. Emeliyanov,¹³² Y. Enari,¹⁵⁶ O. C. Endner,⁸⁵ M. Endo,¹¹⁹ J. S. Ennis,¹⁷⁰ J. Erdmann,⁴⁵ A. Ereditato,¹⁸ G. Ernis,¹⁷⁵ J. Ernst,² M. Ernst,²⁷ S. Errede,¹⁶⁶ E. Ertel,⁸⁵ M. Escalier,¹¹⁸ H. Esch,⁴⁵ C. Escobar,¹²⁶ B. Esposito,⁴⁹ A. I. Etienvre,¹³⁷ E. Etzion,¹⁵⁴ H. Evans,⁶³ A. Ezhilov,¹²⁴ F. Fabbri,^{22a,22b} L. Fabbri,^{22a,22b} G. Facini,³³ R. M. Fakhrutdinov,¹³¹ S. Falciano,^{133a} R. J. Falla,⁸⁰ J. Faltova,¹³⁰ Y. Fang,^{35a} M. Fanti,^{93a,93b} A. Farbin,⁸ A. Farilla,^{135a} C. Farina,¹²⁶ T. Farooque,¹³ S. Farrell,¹⁶ S. M. Farrington,¹⁷⁰ P. Farthouat,³² F. Fassi,^{136e} P. Fassnacht,³² D. Fassouliotis,⁹ M. Fauci Giannelli,⁷⁹ A. Favareto,^{52a,52b} W. J. Fawcett,¹²¹ L. Fayard,¹¹⁸ O. L. Fedin,^{124,o} W. Fedorko,¹⁶⁸ S. Feigl,¹²⁰ L. Feligioni,⁸⁷ C. Feng,^{35d} E. J. Feng,³² H. Feng,⁹¹ A. B. Fenyuk,¹³¹ L. Feremenga,⁸ P. Fernandez Martinez,¹⁶⁷ S. Fernandez Perez,¹³ J. Ferrando,⁵⁵ A. Ferrari,¹⁶⁵ P. Ferrari,¹⁰⁸ R. Ferrari,^{122a} D. E. Ferreira de Lima,^{60b} A. Ferrer,¹⁶⁷ D. Ferrere,⁵¹ C. Ferretti,⁹¹ A. Ferretto Parodi,^{52a,52b} F. Fiedler,⁸⁵ A. Filipčič,⁷⁷ M. Filipuzzi,⁴⁴ F. Filthaut,¹⁰⁷ M. Fincke-Keeler,¹⁶⁹ K. D. Finelli,¹⁵¹ M. C. N. Fiolhais,^{127a,127c} L. Fiorini,¹⁶⁷ A. Firan,⁴² A. Fischer,² C. Fischer,¹³ J. Fischer,¹⁷⁵ W. C. Fisher,⁹² N. Flaschel,⁴⁴ I. Fleck,¹⁴² P. Fleischmann,⁹¹ G. T. Fletcher,¹⁴⁰ R. R. M. Fletcher,¹²³ T. Flick,¹⁷⁵ A. Floderus,⁸³ L. R. Flores Castillo,^{62a} M. J. Flowerdew,¹⁰² G. T. Forcolin,⁸⁶ A. Formica,¹³⁷ A. Forti,⁸⁶ A. G. Foster,¹⁹ D. Fournier,¹¹⁸ H. Fox,⁷⁴ S. Fracchia,¹³ P. Francavilla,⁸² M. Franchini,^{22a,22b} D. Francis,³² L. Franconi,¹²⁰ M. Franklin,⁵⁹ M. Frate,¹⁶³ M. Fraternali,^{122a,122b} D. Freeborn,⁸⁰ S. M. Fressard-Batranceanu,³² F. Friedrich,⁴⁶ D. Froidevaux,³² J. A. Frost,¹²¹ C. Fukunaga,¹⁵⁷ E. Fullana Torregrosa,⁸⁵ T. Fusayasu,¹⁰³ J. Fuster,¹⁶⁷ C. Gabaldon,⁵⁷ O. Gabizon,¹⁷⁵ A. Gabrielli,^{22a,22b} A. Gabrielli,¹⁶ G. P. Gach,^{40a} S. Gadatsch,³² S. Gadomski,⁵¹ G. Gagliardi,^{52a,52b} L. G. Gagnon,⁹⁶ P. Gagnon,⁶³ C. Galea,¹⁰⁷ B. Galhardo,^{127a,127c} E. J. Gallas,¹²¹ B. J. Gallop,¹³² P. Gallus,¹²⁹ G. Galster,³⁸ K. K. Gan,¹¹² J. Gao,^{35b,87} Y. Gao,⁴⁸ Y. S. Gao,^{144,g} F. M. Garay Walls,⁴⁸ C. García,¹⁶⁷ J. E. García Navarro,¹⁶⁷ M. Garcia-Sciveres,¹⁶ R. W. Gardner,³³ N. Garelli,¹⁴⁴ V. Garonne,¹²⁰ A. Gascon Bravo,⁴⁴ C. Gatti,⁴⁹ A. Gaudiello,^{52a,52b} G. Gaudio,^{122a} B. Gaur,¹⁴² L. Gauthier,⁹⁶ I. L. Gavrilenko,⁹⁷ C. Gay,¹⁶⁸ G. Gaycken,²³ E. N. Gazis,¹⁰ Z. Gece,¹⁶⁸ C. N. P. Gee,¹³² Ch. Geich-Gimbel,²³ M. Geisen,⁸⁵ M. P. Geisler,^{60a} C. Gemme,^{52a} M. H. Genest,⁵⁷ C. Geng,^{35b,p} S. Gentile,^{133a,133b} S. George,⁷⁹ D. Gerbaudo,¹³ A. Gershon,¹⁵⁴ S. Ghasemi,¹⁴² H. Ghazlane,^{136b} M. Ghneimat,²³ B. Giacobbe,^{22a} S. Giagu,^{133a,133b} P. Giannetti,^{125a,125b} B. Gibbard,²⁷ S. M. Gibson,⁷⁹ M. Gignac,¹⁶⁸ M. Gilchriese,¹⁶ T. P. S. Gillam,³⁰ D. Gillberg,³¹ G. Gilles,¹⁷⁵ D. M. Gingrich,^{3,e} N. Giokaris,⁹ M. P. Giordani,^{164a,164c} F. M. Giorgi,^{22a} F. M. Giorgi,¹⁷ P. F. Giraud,¹³⁷ P. Giromini,⁵⁹ D. Giugni,^{93a} F. Giuli,¹²¹ C. Giuliani,¹⁰² M. Giulini,^{60b} B. K. Gjelsten,¹²⁰ S. Gkaitatzis,¹⁵⁵ I. Gkialas,¹⁵⁵ E. L. Gkougkousis,¹¹⁸ L. K. Gladilin,¹⁰⁰ C. Glasman,⁸⁴ J. Glatzer,³² P. C. F. Glaysheer,⁴⁸ A. Glazov,⁴⁴ M. Goblirsch-Kolb,¹⁰² J. Godlewski,⁴¹ S. Goldfarb,⁹¹ T. Golling,⁵¹ D. Golubkov,¹³¹ A. Gomes,^{127a,127b,127d} R. Gonçalo,^{127a} J. Goncalves Pinto Firmino Da Costa,¹³⁷ G. Gonella,⁵⁰ L. Gonella,¹⁹ A. Gongadze,⁶⁷ S. González de la Hoz,¹⁶⁷ G. Gonzalez Parra,¹³ S. Gonzalez-Sevilla,⁵¹ L. Goossens,³² P. A. Gorbounov,⁹⁸ H. A. Gordon,²⁷ I. Gorelov,¹⁰⁶ B. Gorini,³² E. Gorini,^{75a,75b} A. Gorišek,⁷⁷ E. Gornicki,⁴¹ A. T. Goshaw,⁴⁷ C. Gössling,⁴⁵ M. I. Gostkin,⁶⁷ C. R. Goudet,¹¹⁸ D. Goujdami,^{136c} A. G. Goussiou,¹³⁹ N. Govender,^{146b,q} E. Gozani,¹⁵³ L. Graber,⁵⁶ I. Grabowska-Bold,^{40a} P. O. J. Gradin,⁵⁷ P. Grafström,^{22a,22b} J. Gramling,⁵¹ E. Gramstad,¹²⁰ S. Grancagnolo,¹⁷ V. Gratchev,¹²⁴ P. M. Gravila,^{28e} H. M. Gray,³² E. Graziani,^{135a} Z. D. Greenwood,^{81,r} C. Grefe,²³ K. Gregersen,⁸⁰ I. M. Gregor,⁴⁴ P. Grenier,¹⁴⁴ K. Grevtsov,⁵ J. Griffiths,⁸ A. A. Grillo,¹³⁸ K. Grimm,⁷⁴ S. Grinstein,^{13,s} Ph. Gris,³⁶ J.-F. Grivaz,¹¹⁸ S. Groh,⁸⁵ J. P. Grohs,⁴⁶ E. Gross,¹⁷² J. Grosse-Knetter,⁵⁶ G. C. Grossi,⁸¹ Z. J. Grout,¹⁵⁰ L. Guan,⁹¹ W. Guan,¹⁷³ J. Guenther,¹²⁹ F. Guescini,⁵¹ D. Guest,¹⁶³ O. Gueta,¹⁵⁴ E. Guido,^{52a,52b} T. Guillemin,⁵ S. Guindon,² U. Gul,⁵⁵ C. Gumpert,³² J. Guo,^{35e} Y. Guo,^{35b,p} S. Gupta,¹²¹ G. Gustavino,^{133a,133b} P. Gutierrez,¹¹⁴ N. G. Gutierrez Ortiz,⁸⁰ C. Gutsche,⁴⁶ C. Guyot,¹³⁷ C. Gwenlan,¹²¹ C. B. Gwilliam,⁷⁶ A. Haas,¹¹¹ C. Haber,¹⁶ H. K. Hadavand,⁸ N. Haddad,^{136e} A. Hadeef,⁸⁷ P. Haefner,²³ S. Hageböck,²³ Z. Hajduk,⁴¹ H. Hakobyan,^{177,a} M. Haleem,⁴⁴ J. Haley,¹¹⁵ G. Halladjian,⁹² G. D. Hallewell,⁸⁷ K. Hamacher,¹⁷⁵ P. Hamal,¹¹⁶ K. Hamano,¹⁶⁹ A. Hamilton,^{146a} G. N. Hamity,¹⁴⁰ P. G. Hamnett,⁴⁴ L. Han,^{35b} K. Hanagaki,^{68,t} K. Hanawa,¹⁵⁶ M. Hance,¹³⁸ B. Haney,¹²³ P. Hanke,^{60a} R. Hanna,¹³⁷ J. B. Hansen,³⁸ J. D. Hansen,³⁸ M. C. Hansen,²³ P. H. Hansen,³⁸ K. Hara,¹⁶¹ A. S. Hard,¹⁷³ T. Harenberg,¹⁷⁵ F. Hariri,¹¹⁸ S. Harkusha,⁹⁴ R. D. Harrington,⁴⁸ P. F. Harrison,¹⁷⁰ F. Hartjes,¹⁰⁸ N. M. Hartmann,¹⁰¹ M. Hasegawa,⁶⁹ Y. Hasegawa,¹⁴¹ A. Hasib,¹¹⁴ S. Hassani,¹³⁷ S. Haug,¹⁸ R. Hauser,⁹² L. Hauswald,⁴⁶ M. Havranek,¹²⁸ C. M. Hawkes,¹⁹ R. J. Hawkings,³² D. Hayden,⁹² C. P. Hays,¹²¹ J. M. Hays,⁷⁸ H. S. Hayward,⁷⁶ S. J. Haywood,¹³² S. J. Head,¹⁹ T. Heck,⁸⁵ V. Hedberg,⁸³ L. Heelan,⁸ S. Heim,¹²³ T. Heim,¹⁶ B. Heinemann,¹⁶ J. J. Heinrich,¹⁰¹ L. Heinrich,¹¹¹ C. Heinz,⁵⁴ J. Hejbal,¹²⁸ L. Helary,²⁴ S. Hellman,^{147a,147b} C. Helsen,³² J. Henderson,¹²¹ R. C. W. Henderson,⁷⁴ Y. Heng,¹⁷³ S. Henkelmann,¹⁶⁸ A. M. Henriques Correia,³² S. Henrot-Versille,¹¹⁸ G. H. Herbert,¹⁷ Y. Hernández Jiménez,¹⁶⁷ G. Herten,⁵⁰ R. Hertenberger,¹⁰¹ L. Hervas,³² G. G. Hesketh,⁸⁰ N. P. Hessay,¹⁰⁸ J. W. Hetherly,⁴² R. Hickling,⁷⁸ E. Higón-Rodríguez,¹⁶⁷

E. Hill,¹⁶⁹ J. C. Hill,³⁰ K. H. Hiller,⁴⁴ S. J. Hillier,¹⁹ I. Hinchliffe,¹⁶ E. Hines,¹²³ R. R. Hinman,¹⁶ M. Hirose,¹⁵⁸ D. Hirschbuehl,¹⁷⁵ J. Hobbs,¹⁴⁹ N. Hod,^{160a} M. C. Hodgkinson,¹⁴⁰ P. Hodgson,¹⁴⁰ A. Hoecker,³² M. R. Hoferkamp,¹⁰⁶ F. Hoenic,¹⁰¹ D. Hohn,²³ T. R. Holmes,¹⁶ M. Homann,⁴⁵ T. M. Hong,¹²⁶ B. H. Hooberman,¹⁶⁶ W. H. Hopkins,¹¹⁷ Y. Horii,¹⁰⁴ A. J. Horton,¹⁴³ J.-Y. Hostachy,⁵⁷ S. Hou,¹⁵² A. Hoummada,^{136a} J. Howarth,⁴⁴ M. Hrabovsky,¹¹⁶ I. Hristova,¹⁷ J. Hrivnac,¹¹⁸ T. Hryn'ova,⁵ A. Hrynevich,⁹⁵ C. Hsu,^{146c} P. J. Hsu,^{152,u} S.-C. Hsu,¹³⁹ D. Hu,³⁷ Q. Hu,^{35b} Y. Huang,⁴⁴ Z. Hubacek,¹²⁹ F. Hubaut,⁸⁷ F. Huegging,²³ T. B. Huffman,¹²¹ E. W. Hughes,³⁷ G. Hughes,⁷⁴ M. Huhtinen,³² T. A. Hülsing,⁸⁵ P. Huo,¹⁴⁹ N. Huseynov,^{67,c} J. Huston,⁹² J. Huth,⁵⁹ G. Iacobucci,⁵¹ G. Iakovidis,²⁷ I. Ibragimov,¹⁴² L. Iconomidou-Fayard,¹¹⁸ E. Ideal,¹⁷⁶ Z. Idrissi,^{136e} P. Iengo,³² O. Igonkina,^{108,v} T. Iizawa,¹⁷¹ Y. Ikegami,⁶⁸ M. Ikeno,⁶⁸ Y. Ilchenko,^{11,w} D. Iliadis,¹⁵⁵ N. Ilic,¹⁴⁴ T. Ince,¹⁰² G. Introzzi,^{122a,122b} P. Ioannou,^{9,a} M. Iodice,^{135a} K. Iordanidou,³⁷ V. Ippolito,⁵⁹ M. Ishino,⁷⁰ M. Ishitsuka,¹⁵⁸ R. Ishmukhametov,¹¹² C. Issever,¹²¹ S. Istin,^{20a} F. Ito,¹⁶¹ J. M. Iturbe Ponce,⁸⁶ R. Iuppa,^{134a,134b} W. Iwanski,⁴¹ H. Iwasaki,⁶⁸ J. M. Izen,⁴³ V. Izzo,^{105a} S. Jabbar,³ B. Jackson,¹²³ M. Jackson,⁷⁶ P. Jackson,¹ V. Jain,² K. B. Jakobi,⁸⁵ K. Jakobs,⁵⁰ S. Jakobsen,³² T. Jakoubek,¹²⁸ D. O. Jamin,¹¹⁵ D. K. Jana,⁸¹ E. Jansen,⁸⁰ R. Jansky,⁶⁴ J. Janssen,²³ M. Janus,⁵⁶ G. Jarlskog,⁸³ N. Javadov,^{67,c} T. Javůrek,⁵⁰ F. Jeanneau,¹³⁷ L. Jeanty,¹⁶ J. Jejelava,^{53a,x} G.-Y. Jeng,¹⁵¹ D. Jennens,⁹⁰ P. Jenni,^{50,y} J. Jentsch,⁴⁵ C. Jeske,¹⁷⁰ S. Jézéquel,⁵ H. Ji,¹⁷³ J. Jia,¹⁴⁹ H. Jiang,⁶⁶ Y. Jiang,^{35b} S. Jiggins,⁸⁰ J. Jimenez Pena,¹⁶⁷ S. Jin,^{35a} A. Jinaru,^{28b} O. Jinnouchi,¹⁵⁸ P. Johansson,¹⁴⁰ K. A. Johns,⁷ W. J. Johnson,¹³⁹ K. Jon-And,^{147a,147b} G. Jones,¹⁷⁰ R. W. L. Jones,⁷⁴ S. Jones,⁷ T. J. Jones,⁷⁶ J. Jongmanns,^{60a} P. M. Jorge,^{127a,127b} J. Jovicevic,^{160a} X. Ju,¹⁷³ A. Juste Rozas,^{13,s} M. K. Köhler,¹⁷² A. Kaczmarek,⁴¹ M. Kado,¹¹⁸ H. Kagan,¹¹² M. Kagan,¹⁴⁴ S. J. Kahn,⁸⁷ E. Kajomovitz,⁴⁷ C. W. Kalderon,¹²¹ A. Kaluza,⁸⁵ S. Kama,⁴² A. Kamenshchikov,¹³¹ N. Kanaya,¹⁵⁶ S. Kaneti,³⁰ L. Kanjir,⁷⁷ V. A. Kantsеров,⁹⁹ J. Kanzaki,⁶⁸ B. Kaplan,¹¹¹ L. S. Kaplan,¹⁷³ A. Kapliy,³³ D. Kar,^{146c} K. Karakostas,¹⁰ A. Karamaoun,³ N. Karastathis,¹⁰ M. J. Kareem,⁵⁶ E. Karentzos,¹⁰ M. Karnevskiy,⁸⁵ S. N. Karpov,⁶⁷ Z. M. Karpova,⁶⁷ K. Karthik,¹¹¹ V. Kartvelishvili,⁷⁴ A. N. Karyukhin,¹³¹ K. Kasahara,¹⁶¹ L. Kashif,¹⁷³ R. D. Kass,¹¹² A. Kastanas,¹⁵ Y. Kataoka,¹⁵⁶ C. Kato,¹⁵⁶ A. Katre,⁵¹ J. Katzy,⁴⁴ K. Kawagoe,⁷² T. Kawamoto,¹⁵⁶ G. Kawamura,⁵⁶ S. Kazama,¹⁵⁶ V. F. Kazanin,^{110,d} R. Keeler,¹⁶⁹ R. Kehoe,⁴² J. S. Keller,⁴⁴ J. J. Kempster,⁷⁹ K. Kentaro,¹⁰⁴ H. Keoshkerian,¹⁵⁹ O. Kepka,¹²⁸ B. P. Kerševan,⁷⁷ S. Kersten,¹⁷⁵ R. A. Keyes,⁸⁹ F. Khalil-zada,¹² A. Khanov,¹¹⁵ A. G. Kharlamov,^{110,d} T. J. Khoo,⁵¹ V. Khovanskiy,⁹⁸ E. Khramov,⁶⁷ J. Khubua,^{53b,z} S. Kido,⁶⁹ H. Y. Kim,⁸ S. H. Kim,¹⁶¹ Y. K. Kim,³³ N. Kimura,¹⁵⁵ O. M. Kind,¹⁷ B. T. King,⁷⁶ M. King,¹⁶⁷ S. B. King,¹⁶⁸ J. Kirk,¹³² A. E. Kiryunin,¹⁰² T. Kishimoto,⁶⁹ D. Kisielewska,^{40a} F. Kiss,⁵⁰ K. Kiuchi,¹⁶¹ O. Kivernyk,¹³⁷ E. Kladiva,^{145b} M. H. Klein,³⁷ M. Klein,⁷⁶ U. Klein,⁷⁶ K. Kleinknecht,⁸⁵ P. Klimek,^{147a,147b} A. Klimentov,²⁷ R. Klingenberg,⁴⁵ J. A. Klinger,¹⁴⁰ T. Klioutchnikova,³² E.-E. Kluge,^{60a} P. Kluit,¹⁰⁸ S. Kluth,¹⁰² J. Knapik,⁴¹ E. Kneringer,⁶⁴ E. B. F. G. Knoops,⁸⁷ A. Knue,⁵⁵ A. Kobayashi,¹⁵⁶ D. Kobayashi,¹⁵⁸ T. Kobayashi,¹⁵⁶ M. Kobel,⁴⁶ M. Kocian,¹⁴⁴ P. Kodys,¹³⁰ T. Koffas,³¹ E. Koffeman,¹⁰⁸ T. Koi,¹⁴⁴ H. Kolanoski,¹⁷ M. Kolb,^{60b} I. Koletsou,⁵ A. A. Komar,^{97,a} Y. Komori,¹⁵⁶ T. Kondo,⁶⁸ N. Kondrashova,⁴⁴ K. Köneke,⁵⁰ A. C. König,¹⁰⁷ T. Kono,^{68,aa} R. Konoplich,^{111,bb} N. Konstantinidis,⁸⁰ R. Kopeliansky,⁶³ S. Koperny,^{40a} L. Köpke,⁸⁵ A. K. Kopp,⁵⁰ K. Korcyl,⁴¹ K. Kordas,¹⁵⁵ A. Korn,⁸⁰ A. A. Korol,^{110,d} I. Korolkov,¹³ E. V. Korolkova,¹⁴⁰ O. Kortner,¹⁰² S. Kortner,¹⁰² T. Kosek,¹³⁰ V. V. Kostyukhin,²³ A. Kotwal,⁴⁷ A. Kourkouveli-Charalampidi,¹⁵⁵ C. Kourkouvelis,⁹ V. Kouskoura,²⁷ A. B. Kowalewska,⁴¹ R. Kowalewski,¹⁶⁹ T. Z. Kowalski,^{40a} C. Kozakai,¹⁵⁶ W. Kozanecki,¹³⁷ A. S. Kozhin,¹³¹ V. A. Kramarenko,¹⁰⁰ G. Kramberger,⁷⁷ D. Krasnopevtsev,⁹⁹ M. W. Krasny,⁸² A. Krasznahorkay,³² J. K. Kraus,²³ A. Kravchenko,²⁷ M. Kretz,^{60c} J. Kretzschmar,⁷⁶ K. Kreutzfeldt,⁵⁴ P. Krieger,¹⁵⁹ K. Krizka,³³ K. Kroeninger,⁴⁵ H. Kroha,¹⁰² J. Kroll,¹²³ J. Kröseberg,²³ J. Krstic,¹⁴ U. Kruchonak,⁶⁷ H. Krüger,²³ N. Krumnack,⁶⁶ A. Kruse,¹⁷³ M. C. Kruse,⁴⁷ M. Kruskal,²⁴ T. Kubota,⁹⁰ H. Kucuk,⁸⁰ S. Kuday,^{4b} J. T. Kuechler,¹⁷⁵ S. Kuehn,⁵⁰ A. Kugel,^{60c} F. Kuger,¹⁷⁴ A. Kuhl,¹³⁸ T. Kuhl,⁴⁴ V. Kukhtin,⁶⁷ R. Kukla,¹³⁷ Y. Kulchitsky,⁹⁴ S. Kuleshov,^{34b} M. Kuna,^{133a,133b} T. Kunigo,⁷⁰ A. Kupco,¹²⁸ H. Kurashige,⁶⁹ Y. A. Kurochkin,⁹⁴ V. Kus,¹²⁸ E. S. Kuwertz,¹⁶⁹ M. Kuze,¹⁵⁸ J. Kvita,¹¹⁶ T. Kwan,¹⁶⁹ D. Kyriazopoulos,¹⁴⁰ A. La Rosa,¹⁰² J. L. La Rosa Navarro,^{26d} L. La Rotonda,^{39a,39b} C. Lacasta,¹⁶⁷ F. Lacava,^{133a,133b} J. Lacey,³¹ H. Lacker,¹⁷ D. Lacour,⁸² V. R. Lacuesta,¹⁶⁷ E. Ladygin,⁶⁷ R. Lafaye,⁵ B. Laforge,⁸² T. Lagouri,¹⁷⁶ S. Lai,⁵⁶ S. Lammers,⁶³ W. Lampl,⁷ E. Lançon,¹³⁷ U. Landgraf,⁵⁰ M. P. J. Landon,⁷⁸ V. S. Lang,^{60a} J. C. Lange,¹³ A. J. Lankford,¹⁶³ F. Lanni,²⁷ K. Lantsch,²³ A. Lanza,^{122a} S. Laplace,⁸² C. Lapoire,³² J. F. Laporte,¹³⁷ T. Lari,^{93a} F. Lasagni Manghi,^{22a,22b} M. Lassnig,³² P. Laurelli,⁴⁹ W. Lavrijsen,¹⁶ A. T. Law,¹³⁸ P. Laycock,⁷⁶ T. Lazovich,⁵⁹ M. Lazzaroni,^{93a,93b} B. Le,⁹⁰ O. Le Dortz,⁸² E. Le Guirriec,⁸⁷ E. P. Le Quilleuc,¹³⁷ M. LeBlanc,¹⁶⁹ T. LeCompte,⁶ F. Ledroit-Guillon,⁵⁷ C. A. Lee,²⁷ S. C. Lee,¹⁵² L. Lee,¹ G. Lefebvre,⁸² M. Lefebvre,¹⁶⁹ F. Legger,¹⁰¹ C. Leggett,¹⁶ A. Lehan,⁷⁶ G. Lehmann Miotto,³² X. Lei,⁷ W. A. Leight,³¹ A. Leisos,^{155,cc} A. G. Leister,¹⁷⁶ M. A. L. Leite,^{26d} R. Leitner,¹³⁰ D. Lellouch,¹⁷² B. Lemmer,⁵⁶ K. J. C. Leney,⁸⁰ T. Lenz,²³ B. Lenzi,³²

R. Leone,⁷ S. Leone,^{125a,125b} C. Leonidopoulos,⁴⁸ S. Leontsinis,¹⁰ G. Lerner,¹⁵⁰ C. Leroy,⁹⁶ A. A. J. Lesage,¹³⁷ C. G. Lester,³⁰ M. Levchenko,¹²⁴ J. Levêque,⁵ D. Levin,⁹¹ L. J. Levinson,¹⁷² M. Levy,¹⁹ D. Lewis,⁷⁸ A. M. Leyko,²³ M. Leyton,⁴³ B. Li,^{35b,p} H. Li,¹⁴⁹ H. L. Li,³³ L. Li,⁴⁷ L. Li,^{35e} Q. Li,^{35a} S. Li,⁴⁷ X. Li,⁸⁶ Y. Li,¹⁴² Z. Liang,^{35a} B. Liberti,^{134a} A. Liblong,¹⁵⁹ P. Lichard,³² K. Lie,¹⁶⁶ J. Liebal,²³ W. Liebig,¹⁵ A. Limosani,¹⁵¹ S. C. Lin,^{152,dd} T. H. Lin,⁸⁵ B. E. Lindquist,¹⁴⁹ A. E. Lioni,⁵¹ E. Lipeles,¹²³ A. Lipniacka,¹⁵ M. Lisovsky,^{60b} T. M. Liss,¹⁶⁶ A. Lister,¹⁶⁸ A. M. Litke,¹³⁸ B. Liu,^{152,ee} D. Liu,¹⁵² H. Liu,⁹¹ H. Liu,²⁷ J. Liu,⁸⁷ J. B. Liu,^{35b} K. Liu,⁸⁷ L. Liu,¹⁶⁶ M. Liu,⁴⁷ M. Liu,^{35b} Y. L. Liu,^{35b} Y. Liu,^{35b} M. Livan,^{122a,122b} A. Lleres,⁵⁷ J. Llorente Merino,^{35a} S. L. Lloyd,⁷⁸ F. Lo Sterzo,¹⁵² E. Lobodzinska,⁴⁴ P. Loch,⁷ W. S. Lockman,¹³⁸ F. K. Loebinger,⁸⁶ A. E. Loevschall-Jensen,³⁸ K. M. Loew,²⁵ A. Loginov,¹⁷⁶ T. Lohse,¹⁷ K. Lohwasser,⁴⁴ M. Lokajicek,¹²⁸ B. A. Long,²⁴ J. D. Long,¹⁶⁶ R. E. Long,⁷⁴ L. Longo,^{75a,75b} K. A. Looper,¹¹² L. Lopes,^{127a} D. Lopez Mateos,⁵⁹ B. Lopez Paredes,¹⁴⁰ I. Lopez Paz,¹³ A. Lopez Solis,⁸² J. Lorenz,¹⁰¹ N. Lorenzo Martinez,⁶³ M. Losada,²¹ P. J. Lösel,¹⁰¹ X. Lou,^{35a} A. Lounis,¹¹⁸ J. Love,⁶ P. A. Love,⁷⁴ H. Lu,^{62a} N. Lu,⁹¹ H. J. Lubatti,¹³⁹ C. Luci,^{133a,133b} A. Lucotte,⁵⁷ C. Luedtke,⁵⁰ F. Luehring,⁶³ W. Lukas,⁶⁴ L. Luminari,^{133a} O. Lundberg,^{147a,147b} B. Lund-Jensen,¹⁴⁸ P. M. Luzi,⁸² D. Lynn,²⁷ R. Lysak,¹²⁸ E. Lytken,⁸³ V. Lyubushkin,⁶⁷ H. Ma,²⁷ L. L. Ma,^{35d} Y. Ma,^{35d} G. Maccarrone,⁴⁹ A. Macchiolo,¹⁰² C. M. Macdonald,¹⁴⁰ B. Maček,⁷⁷ J. Machado Miguens,^{123,127b} D. Madaffari,⁸⁷ R. Madar,³⁶ H. J. Maddocks,¹⁶⁵ W. F. Mader,⁴⁶ A. Madsen,⁴⁴ J. Maeda,⁶⁹ S. Maeland,¹⁵ T. Maeno,²⁷ A. Maevskiy,¹⁰⁰ E. Magradze,⁵⁶ J. Mahlstedt,¹⁰⁸ C. Maiani,¹¹⁸ C. Maidantchik,^{26a} A. A. Maier,¹⁰² T. Maier,¹⁰¹ A. Maio,^{127a,127b,127d} S. Majewski,¹¹⁷ Y. Makida,⁶⁸ N. Makovec,¹¹⁸ B. Malaescu,⁸² Pa. Malecki,⁴¹ V. P. Maleev,¹²⁴ F. Malek,⁵⁷ U. Mallik,⁶⁵ D. Malon,⁶ C. Malone,¹⁴⁴ S. Maltezos,¹⁰ S. Malyukov,³² J. Mamuzic,¹⁶⁷ G. Mancini,⁴⁹ B. Mandelli,³² L. Mandelli,^{93a} I. Mandić,⁷⁷ J. Maneira,^{127a,127b} L. Manhaes de Andrade Filho,^{26b} J. Manjarres Ramos,^{160b} A. Mann,¹⁰¹ A. Manousos,³² B. Mansoulie,¹³⁷ J. D. Mansour,^{35a} R. Mantifel,⁸⁹ M. Mantoani,⁵⁶ S. Manzoni,^{93a,93b} L. Mapelli,³² G. Marceca,²⁹ L. March,⁵¹ G. Marchiori,⁸² M. Marcisovsky,¹²⁸ M. Marjanovic,¹⁴ D. E. Marley,⁹¹ F. Marroquim,^{26a} S. P. Marsden,⁸⁶ Z. Marshall,¹⁶ S. Marti-Garcia,¹⁶⁷ B. Martin,⁹² T. A. Martin,¹⁷⁰ V. J. Martin,⁴⁸ B. Martin dit Latour,¹⁵ M. Martinez,^{13,s} S. Martin-Haugh,¹³² V. S. Martoiu,^{28b} A. C. Martyniuk,⁸⁰ M. Marx,¹³⁹ A. Marzin,³² L. Masetti,⁸⁵ T. Mashimo,¹⁵⁶ R. Mashinistov,⁹⁷ J. Masik,⁸⁶ A. L. Maslennikov,^{110,d} I. Massa,^{22a,22b} L. Massa,^{22a,22b} P. Mastrandrea,⁵ A. Mastroberardino,^{39a,39b} T. Masubuchi,¹⁵⁶ P. Mättig,¹⁷⁵ J. Mattmann,⁸⁵ J. Maurer,^{28b} S. J. Maxfield,⁷⁶ D. A. Maximov,^{110,d} R. Mazini,¹⁵² S. M. Mazza,^{93a,93b} N. C. Mc Fadden,¹⁰⁶ G. Mc Goldrick,¹⁵⁹ S. P. Mc Kee,⁹¹ A. McCar, ⁹¹ R. L. McCarthy,¹⁴⁹ T. G. McCarthy,¹⁰² L. I. McClymont,⁸⁰ E. F. McDonald,⁹⁰ K. W. McFarlane,^{58,a} J. A. McFayden,⁸⁰ G. Mchedlidze,⁵⁶ S. J. McMahon,¹³² R. A. McPherson,^{169,m} M. Medinnis,⁴⁴ S. Meehan,¹³⁹ S. Mehlhase,¹⁰¹ A. Mehta,⁷⁶ K. Meier,^{60a} C. Meineck,¹⁰¹ B. Meirose,⁴³ D. Melini,¹⁶⁷ B. R. Mellado Garcia,^{146c} M. Melo,^{145a} F. Meloni,¹⁸ A. Mengarelli,^{22a,22b} S. Menke,¹⁰² E. Meoni,¹⁶² S. Mergelmeyer,¹⁷ P. Mermod,⁵¹ L. Merola,^{105a,105b} C. Meroni,^{93a} F. S. Merritt,³³ A. Messina,^{133a,133b} J. Metcalfe,⁶ A. S. Mete,¹⁶³ C. Meyer,⁸⁵ C. Meyer,¹²³ J-P. Meyer,¹³⁷ J. Meyer,¹⁰⁸ H. Meyer Zu Theenhausen,^{60a} F. Miano,¹⁵⁰ R. P. Middleton,¹³² S. Miglioranza,^{52a,52b} L. Mijović,²³ G. Mikenberg,¹⁷² M. Mikestikova,¹²⁸ M. Mikuž,⁷⁷ M. Milesi,⁹⁰ A. Milic,⁶⁴ D. W. Miller,³³ C. Mills,⁴⁸ A. Milov,¹⁷² D. A. Milstead,^{147a,147b} A. A. Minaenko,¹³¹ Y. Minami,¹⁵⁶ I. A. Minashvili,⁶⁷ A. I. Mincer,¹¹¹ B. Mindur,^{40a} M. Mineev,⁶⁷ Y. Ming,¹⁷³ L. M. Mir,¹³ K. P. Mistry,¹²³ T. Mitani,¹⁷¹ J. Mitrevski,¹⁰¹ V. A. Mitsou,¹⁶⁷ A. Miucci,⁵¹ P. S. Miyagawa,¹⁴⁰ J. U. Mjörnmark,⁸³ T. Moe,^{147a,147b} K. Mochizuki,⁹⁶ S. Mohapatra,³⁷ S. Molander,^{147a,147b} R. Moles-Valls,²³ R. Monden,⁷⁰ M. C. Mondragon,⁹² K. Mönig,⁴⁴ J. Monk,³⁸ E. Monnier,⁸⁷ A. Montalbano,¹⁴⁹ J. Montejo Berlingen,³² F. Monticelli,⁷³ S. Monzani,^{93a,93b} R. W. Moore,³ N. Morange,¹¹⁸ D. Moreno,²¹ M. Moreno Llácer,⁵⁶ P. Morettini,^{52a} D. Mori,¹⁴³ T. Mori,¹⁵⁶ M. Morii,⁵⁹ M. Morinaga,¹⁵⁶ V. Morisbak,¹²⁰ S. Moritz,⁸⁵ A. K. Morley,¹⁵¹ G. Mornacchi,³² J. D. Morris,⁷⁸ S. S. Mortensen,³⁸ L. Morvaj,¹⁴⁹ M. Mosidze,^{53b} J. Moss,¹⁴⁴ K. Motohashi,¹⁵⁸ R. Mount,¹⁴⁴ E. Mountricha,²⁷ S. V. Mouraviev,^{97,a} E. J. W. Moyses,⁸⁸ S. Muanza,⁸⁷ R. D. Mudd,¹⁹ F. Mueller,¹⁰² J. Mueller,¹²⁶ R. S. P. Mueller,¹⁰¹ T. Mueller,³⁰ D. Muenstermann,⁷⁴ P. Mullen,⁵⁵ G. A. Mullier,¹⁸ F. J. Munoz Sanchez,⁸⁶ J. A. Murillo Quijada,¹⁹ W. J. Murray,^{170,132} H. Musheghyan,⁵⁶ M. Muškinja,⁷⁷ A. G. Myagkov,^{131,ff} M. Myska,¹²⁹ B. P. Nachman,¹⁴⁴ O. Nackenhorst,⁵¹ K. Nagai,¹²¹ R. Nagai,^{68,aa} K. Nagano,⁶⁸ Y. Nagasaka,⁶¹ K. Nagata,¹⁶¹ M. Nagel,⁵⁰ E. Nagy,⁸⁷ A. M. Nairz,³² Y. Nakahama,³² K. Nakamura,⁶⁸ T. Nakamura,¹⁵⁶ I. Nakano,¹¹³ H. Namasivayam,⁴³ R. F. Naranjo Garcia,⁴⁴ R. Narayan,¹¹ D. I. Narrias Villar,^{60a} I. Naryshkin,¹²⁴ T. Naumann,⁴⁴ G. Navarro,²¹ R. Nayyar,⁷ H. A. Neal,⁹¹ P. Yu. Nechaeva,⁹⁷ T. J. Neep,⁸⁶ P. D. Nef,¹⁴⁴ A. Negri,^{122a,122b} M. Negrini,^{22a} S. Nektarijevic,¹⁰⁷ C. Nellist,¹¹⁸ A. Nelson,¹⁶³ S. Nemecek,¹²⁸ P. Nemethy,¹¹¹ A. A. Nepomuceno,^{26a} M. Nessi,^{32,gg} M. S. Neubauer,¹⁶⁶ M. Neumann,¹⁷⁵ R. M. Neves,¹¹¹ P. Nevski,²⁷ P. R. Newman,¹⁹ D. H. Nguyen,⁶ T. Nguyen Manh,⁹⁶ R. B. Nickerson,¹²¹ R. Nicolaidou,¹³⁷ J. Nielsen,¹³⁸ A. Nikiforov,¹⁷ V. Nikolaenko,^{131,ff} I. Nikolic-Audit,⁸² K. Nikolopoulos,¹⁹ J. K. Nilsen,¹²⁰ P. Nilsson,²⁷ Y. Ninomiya,¹⁵⁶

A. Nisati,^{133a} R. Nisius,¹⁰² T. Nobe,¹⁵⁶ L. Nodulman,⁶ M. Nomachi,¹¹⁹ I. Nomidis,³¹ T. Nooney,⁷⁸ S. Norberg,¹¹⁴ M. Nordberg,³² N. Norjoharuddeen,¹²¹ O. Novgorodova,⁴⁶ S. Nowak,¹⁰² M. Nozaki,⁶⁸ L. Nozka,¹¹⁶ K. Ntekas,¹⁰ E. Nurse,⁸⁰ F. Nuti,⁹⁰ F. O'grady,⁷ D. C. O'Neil,¹⁴³ A. A. O'Rourke,⁴⁴ V. O'Shea,⁵⁵ F. G. Oakham,^{31,e} H. Oberlack,¹⁰² T. Obermann,²³ J. Ocariz,⁸² A. Ochi,⁶⁹ I. Ochoa,³⁷ J. P. Ochoa-Ricoux,^{34a} S. Oda,⁷² S. Odaka,⁶⁸ H. Ogren,⁶³ A. Oh,⁸⁶ S. H. Oh,⁴⁷ C. C. Ohm,¹⁶ H. Ohman,¹⁶⁵ H. Oide,³² H. Okawa,¹⁶¹ Y. Okumura,³³ T. Okuyama,⁶⁸ A. Olariu,^{28b} L. F. Oleiro Seabra,^{127a} S. A. Olivares Pino,⁴⁸ D. Oliveira Damazio,²⁷ A. Olszewski,⁴¹ J. Olszowska,⁴¹ A. Onofre,^{127a,127e} K. Onogi,¹⁰⁴ P. U. E. Onyisi,^{11,w} M. J. Oreglia,³³ Y. Oren,¹⁵⁴ D. Orestano,^{135a,135b} N. Orlando,^{62b} R. S. Orr,¹⁵⁹ B. Osculati,^{52a,52b} R. Ospanov,⁸⁶ G. Otero y Garzon,²⁹ H. Otono,⁷² M. Ouchrif,^{136d} F. Ould-Saada,¹²⁰ A. Ouraou,¹³⁷ K. P. Oussoren,¹⁰⁸ Q. Ouyang,^{35a} M. Owen,⁵⁵ R. E. Owen,¹⁹ V. E. Ozcan,^{20a} N. Ozturk,⁸ K. Pachal,¹⁴³ A. Pacheco Pages,¹³ C. Padilla Aranda,¹³ M. Pagáčová,⁵⁰ S. Pagan Griso,¹⁶ F. Paige,²⁷ P. Pais,⁸⁸ K. Pajchel,¹²⁰ G. Palacino,^{160b} S. Palestini,³² M. Palka,^{40b} D. Pallin,³⁶ A. Palma,^{127a,127b} E. St. Panagiotopoulou,¹⁰ C. E. Pandini,⁸² J. G. Panduro Vazquez,⁷⁹ P. Pani,^{147a,147b} S. Panitkin,²⁷ D. Pantea,^{28b} L. Paolozzi,⁵¹ Th. D. Papadopoulos,¹⁰ K. Papageorgiou,¹⁵⁵ A. Paramonov,⁶ D. Paredes Hernandez,¹⁷⁶ A. J. Parker,⁷⁴ M. A. Parker,³⁰ K. A. Parker,¹⁴⁰ F. Parodi,^{52a,52b} J. A. Parsons,³⁷ U. Parzefall,⁵⁰ V. R. Pascuzzi,¹⁵⁹ E. Pasqualucci,^{133a} S. Passaggio,^{52a} Fr. Pastore,⁷⁹ G. Pásztor,^{31,hh} S. Patariaia,¹⁷⁵ J. R. Pater,⁸⁶ T. Pauly,³² J. Pearce,¹⁶⁹ B. Pearson,¹¹⁴ L. E. Pedersen,³⁸ M. Pedersen,¹²⁰ S. Pedraza Lopez,¹⁶⁷ R. Pedro,^{127a,127b} S. V. Peleganchuk,^{110,d} D. Pelikan,¹⁶⁵ O. Penc,¹²⁸ C. Peng,^{35a} H. Peng,^{35b} J. Penwell,⁶³ B. S. Peralva,^{26b} M. M. Perego,¹³⁷ D. V. Perepelitsa,²⁷ E. Perez Codina,^{160a} L. Perini,^{93a,93b} H. Pernegger,³² S. Perrella,^{105a,105b} R. Peschke,⁴⁴ V. D. Peshekhonov,⁶⁷ K. Peters,⁴⁴ R. F. Y. Peters,⁸⁶ B. A. Petersen,³² T. C. Petersen,³⁸ E. Petit,⁵⁷ A. Petridis,¹ C. Petridou,¹⁵⁵ P. Petroff,¹¹⁸ E. Petrolo,^{133a} M. Petrov,¹²¹ F. Petrucci,^{135a,135b} N. E. Pettersson,⁸⁸ A. Peyaud,¹³⁷ R. Pezoa,^{34b} P. W. Phillips,¹³² G. Piacquadio,¹⁴⁴ E. Pianori,¹⁷⁰ A. Picazio,⁸⁸ E. Piccaro,⁷⁸ M. Piccinini,^{22a,22b} M. A. Pickering,¹²¹ R. Piegaiia,²⁹ J. E. Pilcher,³³ A. D. Pilkington,⁸⁶ A. W. J. Pin,⁸⁶ M. Pinamonti,^{164a,164c,ii} J. L. Pinfold,³ A. Pingel,³⁸ S. Pires,⁸² H. Pirumov,⁴⁴ M. Pitt,¹⁷² L. Plazak,^{145a} M.-A. Pleier,²⁷ V. Pleskot,⁸⁵ E. Plotnikova,⁶⁷ P. Plucinski,⁹² D. Pluth,⁶⁶ R. Poettgen,^{147a,147b} L. Poggioli,¹¹⁸ D. Pohl,²³ G. Polesello,^{122a} A. Poley,⁴⁴ A. Policicchio,^{39a,39b} R. Polifka,¹⁵⁹ A. Polini,^{22a} C. S. Pollard,⁵⁵ V. Polychronakos,²⁷ K. Pommès,³² L. Pontecorvo,^{133a} B. G. Pope,⁹² G. A. Popeneciu,^{28c} D. S. Popovic,¹⁴ A. Poppleton,³² S. Pospisil,¹²⁹ K. Potamianos,¹⁶ I. N. Potrap,⁶⁷ C. J. Potter,³⁰ C. T. Potter,¹¹⁷ G. Poulard,³² J. Poveda,³² V. Pozdnyakov,⁶⁷ M. E. Pozo Astigarraga,³² P. Pralavorio,⁸⁷ A. Pranko,¹⁶ S. Prell,⁶⁶ D. Price,⁸⁶ L. E. Price,⁶ M. Primavera,^{75a} S. Prince,⁸⁹ M. Proissl,⁴⁸ K. Prokofiev,^{62c} F. Prokoshin,^{34b} S. Protopopescu,²⁷ J. Proudfoot,⁶ M. Przybycien,^{40a} D. Puddu,^{135a,135b} M. Purohit,^{27,ji} P. Puzo,¹¹⁸ J. Qian,⁹¹ G. Qin,⁵⁵ Y. Qin,⁸⁶ A. Quadt,⁵⁶ W. B. Quayle,^{164a,164b} M. Queitsch-Maitland,⁸⁶ D. Quilty,⁵⁵ S. Raddum,¹²⁰ V. Radeka,²⁷ V. Radescu,^{60b} S. K. Radhakrishnan,¹⁴⁹ P. Radloff,¹¹⁷ P. Rados,⁹⁰ F. Ragusa,^{93a,93b} G. Rahal,¹⁷⁸ J. A. Raine,⁸⁶ S. Rajagopalan,²⁷ M. Rammensee,³² C. Rangel-Smith,¹⁶⁵ M. G. Ratti,^{93a,93b} F. Rauscher,¹⁰¹ S. Rave,⁸⁵ T. Ravenscroft,⁵⁵ I. Ravinovich,¹⁷² M. Raymond,³² A. L. Read,¹²⁰ N. P. Readioff,⁷⁶ M. Reale,^{75a,75b} D. M. Rebuffi,^{122a,122b} A. Redelbach,¹⁷⁴ G. Redlinger,²⁷ R. Reece,¹³⁸ K. Reeves,⁴³ L. Rehnisch,¹⁷ J. Reichert,¹²³ H. Reisin,²⁹ C. Rembser,³² H. Ren,^{35a} M. Rescigno,^{133a} S. Resconi,^{93a} O. L. Rezanova,^{110,d} P. Reznicek,¹³⁰ R. Rezvani,⁹⁶ R. Richter,¹⁰² S. Richter,⁸⁰ E. Richter-Was,^{40b} O. Ricken,²³ M. Ridel,⁸² P. Rieck,¹⁷ C. J. Riegel,¹⁷⁵ J. Rieger,⁵⁶ O. Rifki,¹¹⁴ M. Rijssenbeek,¹⁴⁹ A. Rimoldi,^{122a,122b} M. Rimoldi,¹⁸ L. Rinaldi,^{22a} B. Ristić,⁵¹ E. Ritsch,³² I. Riu,¹³ F. Rizatdinova,¹¹⁵ E. Rizvi,⁷⁸ C. Rizzi,¹³ S. H. Robertson,^{89,m} A. Robichaud-Veronneau,⁸⁹ D. Robinson,³⁰ J. E. M. Robinson,⁴⁴ A. Robson,⁵⁵ C. Roda,^{125a,125b} Y. Rodina,⁸⁷ A. Rodriguez Perez,¹³ D. Rodriguez Rodriguez,¹⁶⁷ S. Roe,³² C. S. Rogan,⁵⁹ O. Røhne,¹²⁰ A. Romaniouk,⁹⁹ M. Romano,^{22a,22b} S. M. Romano Saez,³⁶ E. Romero Adam,¹⁶⁷ N. Rompotis,¹³⁹ M. Ronzani,⁵⁰ L. Roos,⁸² E. Ros,¹⁶⁷ S. Rosati,^{133a} K. Rosbach,⁵⁰ P. Rose,¹³⁸ O. Rosenthal,¹⁴² N.-A. Rosien,⁵⁶ V. Rossetti,^{147a,147b} E. Rossi,^{105a,105b} L. P. Rossi,^{52a} J. H. N. Rosten,³⁰ R. Rosten,¹³⁹ M. Rotaru,^{28b} I. Roth,¹⁷² J. Rothberg,¹³⁹ D. Rousseau,¹¹⁸ C. R. Royon,¹³⁷ A. Rozanov,⁸⁷ Y. Rozen,¹⁵³ X. Ruan,^{146c} F. Rubbo,¹⁴⁴ M. S. Rudolph,¹⁵⁹ F. Rühr,⁵⁰ A. Ruiz-Martinez,³¹ Z. Rurikova,⁵⁰ N. A. Rusakovich,⁶⁷ A. Ruschke,¹⁰¹ H. L. Russell,¹³⁹ J. P. Rutherford,⁷ N. Ruthmann,³² Y. F. Ryabov,¹²⁴ M. Rybar,¹⁶⁶ G. Rybkin,¹¹⁸ S. Ryu,⁶ A. Ryzhov,¹³¹ G. F. Rzehorz,⁵⁶ A. F. Saavedra,¹⁵¹ G. Sabato,¹⁰⁸ S. Sacerdoti,²⁹ H. F.-W. Sadrozinski,¹³⁸ R. Sadykov,⁶⁷ F. Safai Tehrani,^{133a} P. Saha,¹⁰⁹ M. Sahinsoy,^{60a} M. Saimpert,¹³⁷ T. Saito,¹⁵⁶ H. Sakamoto,¹⁵⁶ Y. Sakurai,¹⁷¹ G. Salamanna,^{135a,135b} A. Salamon,^{134a,134b} J. E. Salazar Loyola,^{34b} D. Salek,¹⁰⁸ P. H. Sales De Bruin,¹³⁹ D. Salihagic,¹⁰² A. Salnikov,¹⁴⁴ J. Salt,¹⁶⁷ D. Salvatore,^{39a,39b} F. Salvatore,¹⁵⁰ A. Salvucci,^{62a} A. Salzburger,³² D. Sammel,⁵⁰ D. Sampsonidis,¹⁵⁵ A. Sanchez,^{105a,105b} J. Sánchez,¹⁶⁷ V. Sanchez Martinez,¹⁶⁷ H. Sandaker,¹²⁰ R. L. Sandbach,⁷⁸ H. G. Sander,⁸⁵ M. Sandhoff,¹⁷⁵ C. Sandoval,²¹ R. Sandstroem,¹⁰² D. P. C. Sankey,¹³² M. Sannino,^{52a,52b} A. Sansoni,⁴⁹ C. Santoni,³⁶ R. Santonico,^{134a,134b} H. Santos,^{127a} I. Santoyo Castillo,¹⁵⁰ K. Sapp,¹²⁶

A. Sapronov,⁶⁷ J. G. Saraiva,^{127a,127d} B. Sarrazin,²³ O. Sasaki,⁶⁸ Y. Sasaki,¹⁵⁶ K. Sato,¹⁶¹ G. Sauvage,^{5,a} E. Sauvan,⁵ G. Savage,⁷⁹ P. Savard,^{159,e} C. Sawyer,¹³² L. Sawyer,^{81,r} J. Saxon,³³ C. Sbarra,^{22a} A. Sbrizzi,^{22a,22b} T. Scanlon,⁸⁰ D. A. Scannicchio,¹⁶³ M. Scarcella,¹⁵¹ V. Scarfone,^{39a,39b} J. Schaarschmidt,¹⁷² P. Schacht,¹⁰² B. M. Schachtner,¹⁰¹ D. Schaefer,³² R. Schaefer,⁴⁴ J. Schaeffer,⁸⁵ S. Schaepe,²³ S. Schaezel,^{60b} U. Schäfer,⁸⁵ A. C. Schaffer,¹¹⁸ D. Schaile,¹⁰¹ R. D. Schamberger,¹⁴⁹ V. Scharf,^{60a} V. A. Schegelsky,¹²⁴ D. Scheirich,¹³⁰ M. Schernau,¹⁶³ C. Schiavi,^{52a,52b} S. Schier,¹³⁸ C. Schillo,⁵⁰ M. Schioppa,^{39a,39b} S. Schlenker,³² K. R. Schmidt-Sommerfeld,¹⁰² K. Schmieden,³² C. Schmitt,⁸⁵ S. Schmitt,⁴⁴ S. Schmitz,⁸⁵ B. Schneider,^{160a} U. Schnoor,⁵⁰ L. Schoeffel,¹³⁷ A. Schoening,^{60b} B. D. Schoenrock,⁹² E. Schopf,²³ M. Schott,⁸⁵ J. Schovancova,⁸ S. Schramm,⁵¹ M. Schreyer,¹⁷⁴ N. Schuh,⁸⁵ M. J. Schultens,²³ H.-C. Schultz-Coulon,^{60a} H. Schulz,¹⁷ M. Schumacher,⁵⁰ B. A. Schumm,¹³⁸ Ph. Schune,¹³⁷ A. Schwartzman,¹⁴⁴ T. A. Schwarz,⁹¹ Ph. Schwegler,¹⁰² H. Schweiger,⁸⁶ Ph. Schwemling,¹³⁷ R. Schwienhorst,⁹² J. Schwindling,¹³⁷ T. Schwindt,²³ G. Sciolla,²⁵ F. Scuri,^{125a,125b} F. Scutti,⁹⁰ J. Searcy,⁹¹ P. Seema,²³ S. C. Seidel,¹⁰⁶ A. Seiden,¹³⁸ F. Seifert,¹²⁹ J. M. Seixas,^{26a} G. Sekhniaidze,^{105a} K. Sekhon,⁹¹ S. J. Sekula,⁴² D. M. Seliverstov,^{124,a} N. Semprini-Cesari,^{22a,22b} C. Serfon,¹²⁰ L. Serin,¹¹⁸ L. Serkin,^{164a,164b} M. Sessa,^{135a,135b} R. Seuster,¹⁶⁹ H. Severini,¹¹⁴ T. Sfiligoj,⁷⁷ F. Sforza,³² A. Sfyrla,⁵¹ E. Shabalina,⁵⁶ N. W. Shaikh,^{147a,147b} L. Y. Shan,^{35a} R. Shang,¹⁶⁶ J. T. Shank,²⁴ M. Shapiro,¹⁶ P. B. Shatalov,⁹⁸ K. Shaw,^{164a,164b} S. M. Shaw,⁸⁶ A. Shcherbakova,^{147a,147b} C. Y. Shehu,¹⁵⁰ P. Sherwood,⁸⁰ L. Shi,^{152,kk} S. Shimizu,⁶⁹ C. O. Shimmmin,¹⁶³ M. Shimojima,¹⁰³ M. Shiyakova,^{67,ll} A. Shmeleva,⁹⁷ D. Shoaleh Saadi,⁹⁶ M. J. Shochet,³³ S. Shojaii,^{93a,93b} S. Shrestha,¹¹² E. Shulga,⁹⁹ M. A. Shupe,⁷ P. Sicho,¹²⁸ A. M. Sickles,¹⁶⁶ P. E. Sidebo,¹⁴⁸ O. Sidiropoulou,¹⁷⁴ D. Sidorov,¹¹⁵ A. Sidoti,^{22a,22b} F. Siegert,⁴⁶ Dj. Sijacki,¹⁴ J. Silva,^{127a,127d} S. B. Silverstein,^{147a} V. Simak,¹²⁹ O. Simard,⁵ Lj. Simic,¹⁴ S. Simion,¹¹⁸ E. Simioni,⁸⁵ B. Simmons,⁸⁰ D. Simon,³⁶ M. Simon,⁸⁵ P. Sinervo,¹⁵⁹ N. B. Sinev,¹¹⁷ M. Sioli,^{22a,22b} G. Siragusa,¹⁷⁴ S. Yu. Sivoklokov,¹⁰⁰ J. Sjölin,^{147a,147b} T. B. Sjursen,¹⁵ M. B. Skinner,⁷⁴ H. P. Skottowe,⁵⁹ P. Skubic,¹¹⁴ M. Slater,¹⁹ T. Slavicek,¹²⁹ M. Slawinska,¹⁰⁸ K. Sliwa,¹⁶² R. Slovak,¹³⁰ V. Smakhtin,¹⁷² B. H. Smart,⁵ L. Smestad,¹⁵ J. Smiesko,^{145a} S. Yu. Smirnov,⁹⁹ Y. Smirnov,⁹⁹ L. N. Smirnova,^{100,mmm} O. Smirnova,⁸³ M. N. K. Smith,³⁷ R. W. Smith,³⁷ M. Smizanska,⁷⁴ K. Smolek,¹²⁹ A. A. Snesarev,⁹⁷ S. Snyder,²⁷ R. Sobie,^{169,m} F. Socher,⁴⁶ A. Soffer,¹⁵⁴ D. A. Soh,¹⁵² G. Sokhrannyi,⁷⁷ C. A. Solans Sanchez,³² M. Solar,¹²⁹ E. Yu. Soldatov,⁹⁹ U. Soldevila,¹⁶⁷ A. A. Solodkov,¹³¹ A. Soloshenko,⁶⁷ O. V. Solovyanov,¹³¹ V. Solovyev,¹²⁴ P. Sommer,⁵⁰ H. Son,¹⁶² H. Y. Song,^{35b,nn} A. Sood,¹⁶ A. Sopczak,¹²⁹ V. Sopko,¹²⁹ V. Sorin,¹³ D. Sosa,^{60b} C. L. Sotiropoulou,^{125a,125b} R. Soualah,^{164a,164c} A. M. Soukharev,^{110,d} D. South,⁴⁴ B. C. Sowden,⁷⁹ S. Spagnolo,^{75a,75b} M. Spalla,^{125a,125b} M. Spangenberg,¹⁷⁰ F. Spanò,⁷⁹ D. Sperlich,¹⁷ F. Spettel,¹⁰² R. Spighi,^{22a} G. Spigo,³² L. A. Spiller,⁹⁰ M. Spousta,¹³⁰ R. D. St. Denis,^{55,a} A. Stabile,^{93a} R. Stamen,^{60a} S. Stamm,¹⁷ E. Stanecka,⁴¹ R. W. Staneck,⁶ C. Stanescu,^{135a} M. Stanescu-Bellu,⁴⁴ M. M. Stanitzki,⁴⁴ S. Stapnes,¹²⁰ E. A. Starchenko,¹³¹ G. H. Stark,³³ J. Stark,⁵⁷ P. Staroba,¹²⁸ P. Starovoitov,^{60a} S. Stärz,³² R. Staszewski,⁴¹ P. Steinberg,²⁷ B. Stelzer,¹⁴³ H. J. Stelzer,³² O. Stelzer-Chilton,^{160a} H. Stenzel,⁵⁴ G. A. Stewart,⁵⁵ J. A. Stillings,²³ M. C. Stockton,⁸⁹ M. Stoebe,⁸⁹ G. Stoicea,^{28b} P. Stolte,⁵⁶ S. Stonjek,¹⁰² A. R. Stradling,⁸ A. Straessner,⁴⁶ M. E. Stramaglia,¹⁸ J. Strandberg,¹⁴⁸ S. Strandberg,^{147a,147b} A. Strandlie,¹²⁰ M. Strauss,¹¹⁴ P. Strizeneč,^{145b} R. Ströhmer,¹⁷⁴ D. M. Strom,¹¹⁷ R. Stroynowski,⁴² A. Strubig,¹⁰⁷ S. A. Stucci,¹⁸ B. Stugu,¹⁵ N. A. Styles,⁴⁴ D. Su,¹⁴⁴ J. Su,¹²⁶ R. Subramaniam,⁸¹ S. Suchek,^{60a} Y. Sugaya,¹¹⁹ M. Suk,¹²⁹ V. V. Sulin,⁹⁷ S. Sultansoy,^{4c} T. Sumida,⁷⁰ S. Sun,⁵⁹ X. Sun,^{35a} J. E. Sundermann,⁵⁰ K. Suruliz,¹⁵⁰ G. Susinno,^{39a,39b} M. R. Sutton,¹⁵⁰ S. Suzuki,⁶⁸ M. Svatos,¹²⁸ M. Swiatlowski,³³ I. Sykora,^{145a} T. Sykora,¹³⁰ D. Ta,⁵⁰ C. Taccini,^{135a,135b} K. Tackmann,⁴⁴ J. Taenzer,¹⁵⁹ A. Taffard,¹⁶³ R. Tahirout,^{160a} N. Taiblum,¹⁵⁴ H. Takai,²⁷ R. Takashima,⁷¹ T. Takeshita,¹⁴¹ Y. Takubo,⁶⁸ M. Talby,⁸⁷ A. A. Talyshev,^{110,d} K. G. Tan,⁹⁰ J. Tanaka,¹⁵⁶ R. Tanaka,¹¹⁸ S. Tanaka,⁶⁸ B. B. Tannenwald,¹¹² S. Tapia Araya,^{34b} S. Tapprogge,⁸⁵ S. Tarem,¹⁵³ G. F. Tartarelli,^{93a} P. Tas,¹³⁰ M. Tasevsky,¹²⁸ T. Tashiro,⁷⁰ E. Tassi,^{39a,39b} A. Tavares Delgado,^{127a,127b} Y. Tayalati,^{136d} A. C. Taylor,¹⁰⁶ G. N. Taylor,⁹⁰ P. T. E. Taylor,⁹⁰ W. Taylor,^{160b} F. A. Teischinger,³² P. Teixeira-Dias,⁷⁹ K. K. Temming,⁵⁰ D. Temple,¹⁴³ H. Ten Kate,³² P. K. Teng,¹⁵² J. J. Teoh,¹¹⁹ F. Tepel,¹⁷⁵ S. Terada,⁶⁸ K. Terashi,¹⁵⁶ J. Terron,⁸⁴ S. Terzo,¹⁰² M. Testa,⁴⁹ R. J. Teuscher,^{159,m} T. Theveneaux-Pelzer,⁸⁷ J. P. Thomas,¹⁹ J. Thomas-Wilsker,⁷⁹ E. N. Thompson,³⁷ P. D. Thompson,¹⁹ A. S. Thompson,⁵⁵ L. A. Thomsen,¹⁷⁶ E. Thomson,¹²³ M. Thomson,³⁰ M. J. Tibbetts,¹⁶ R. E. Ticse Torres,⁸⁷ V. O. Tikhomirov,^{97,oo} Yu. A. Tikhonov,^{110,d} S. Timoshenko,⁹⁹ P. Tipton,¹⁷⁶ S. Tisserant,⁸⁷ K. Todome,¹⁵⁸ T. Todorov,^{5,a} S. Todorova-Nova,¹³⁰ J. Tojo,⁷² S. Tokár,^{145a} K. Tokushuku,⁶⁸ E. Tolley,⁵⁹ L. Tomlinson,⁸⁶ M. Tomoto,¹⁰⁴ L. Tompkins,^{144,pp} K. Toms,¹⁰⁶ B. Tong,⁵⁹ E. Torrence,¹¹⁷ H. Torres,¹⁴³ E. Torró Pastor,¹³⁹ J. Toth,^{87,qq} F. Touchard,⁸⁷ D. R. Tovey,¹⁴⁰ T. Trefzger,¹⁷⁴ A. Tricoli,²⁷ I. M. Trigger,^{160a} S. Trincaz-Duvold,⁸² M. F. Tripiana,¹³ W. Trischuk,¹⁵⁹ B. Trocme,⁵⁷ A. Trofymov,⁴⁴ C. Troncon,^{93a} M. Trottier-McDonald,¹⁶ M. Trovatelli,¹⁶⁹ L. Truong,^{164a,164c} M. Trzebinski,⁴¹ A. Trzupek,⁴¹ J. C.-L. Tseng,¹²¹

P. V. Tsiareshka,⁹⁴ G. Tsipolitis,¹⁰ N. Tsirintanis,⁹ S. Tsiskaridze,¹³ V. Tsiskaridze,⁵⁰ E. G. Tskhadadze,^{53a} K. M. Tsui,^{62a}
 I. I. Tsukerman,⁹⁸ V. Tsulaia,¹⁶ S. Tsuno,⁶⁸ D. Tsybychev,¹⁴⁹ A. Tudorache,^{28b} V. Tudorache,^{28b} A. N. Tuna,⁵⁹
 S. A. Tuppusti,^{22a,22b} S. Turchikhin,^{100,mm} D. Turecek,¹²⁹ D. Turgeman,¹⁷² R. Turra,^{93a,93b} A. J. Turvey,⁴² P. M. Tuts,³⁷
 M. Tyndel,¹³² G. Uccielli,^{22a,22b} I. Ueda,¹⁵⁶ R. Ueno,³¹ M. Ughetto,^{147a,147b} F. Ukegawa,¹⁶¹ G. Unal,³² A. Undrus,²⁷
 G. Unel,¹⁶³ F. C. Ungaro,⁹⁰ Y. Unno,⁶⁸ C. Unverdorben,¹⁰¹ J. Urban,^{145b} P. Urquijo,⁹⁰ P. Urrejola,⁸⁵ G. Usai,⁸ A. Usanova,⁶⁴
 L. Vacavant,⁸⁷ V. Vacek,¹²⁹ B. Vachon,⁸⁹ C. Valderanis,¹⁰¹ E. Valdes Santurio,^{147a,147b} N. Valencic,¹⁰⁸ S. Valentinetti,^{22a,22b}
 A. Valero,¹⁶⁷ L. Valery,¹³ S. Valkar,¹³⁰ S. Vallecorsa,⁵¹ J. A. Valls Ferrer,¹⁶⁷ W. Van Den Wollenberg,¹⁰⁸
 P. C. Van Der Deijl,¹⁰⁸ R. van der Geer,¹⁰⁸ H. van der Graaf,¹⁰⁸ N. van Eldik,¹⁵³ P. van Gemmeren,⁶ J. Van Nieuwkoop,¹⁴³
 I. van Vulpen,¹⁰⁸ M. C. van Woerden,³² M. Vanadia,^{133a,133b} W. Vandelli,³² R. Vanguri,¹²³ A. Vaniachine,¹³¹ P. Vankov,¹⁰⁸
 G. Vardanyan,¹⁷⁷ R. Vari,^{133a} E. W. Varnes,⁷ T. Varol,⁴² D. Varouchas,⁸² A. Vartapetian,⁸ K. E. Varvell,¹⁵¹ J. G. Vasquez,¹⁷⁶
 F. Vazeille,³⁶ T. Vazquez Schroeder,⁸⁹ J. Veatch,⁵⁶ L. M. Veloce,¹⁵⁹ F. Veloso,^{127a,127c} S. Veneziano,^{133a} A. Ventura,^{75a,75b}
 M. Venturi,¹⁶⁹ N. Venturi,¹⁵⁹ A. Venturini,²⁵ V. Vercesi,^{122a} M. Verducci,^{133a,133b} W. Verkerke,¹⁰⁸ J. C. Vermeulen,¹⁰⁸
 A. Vest,^{46,rr} M. C. Vetterli,^{143,e} O. Viazlo,⁸³ I. Vichou,¹⁶⁶ T. Vickey,¹⁴⁰ O. E. Vickey Boeriu,¹⁴⁰ G. H. A. Viehhauser,¹²¹
 S. Viel,¹⁶ L. Vigani,¹²¹ R. Vigne,⁶⁴ M. Villa,^{22a,22b} M. Villaplana Perez,^{93a,93b} E. Vilucchi,⁴⁹ M. G. Vincter,³¹
 V. B. Vinogradov,⁶⁷ C. Vittori,^{22a,22b} I. Vivarelli,¹⁵⁰ S. Vlachos,¹⁰ M. Vlasak,¹²⁹ M. Vogel,¹⁷⁵ P. Vokac,¹²⁹ G. Volpi,^{125a,125b}
 M. Volpi,⁹⁰ H. von der Schmitt,¹⁰² E. von Toerne,²³ V. Vorobel,¹³⁰ K. Vorobev,⁹⁹ M. Vos,¹⁶⁷ R. Voss,³² J. H. Vossebeld,⁷⁶
 N. Vranjes,¹⁴ M. Vranjes Milosavljevic,¹⁴ V. Vrba,¹²⁸ M. Vreeswijk,¹⁰⁸ R. Vuillermet,³² I. Vukotic,³³ Z. Vykydal,¹²⁹
 P. Wagner,²³ W. Wagner,¹⁷⁵ H. Wahlberg,⁷³ S. Wahrenand,⁴⁶ J. Wakabayashi,¹⁰⁴ J. Walder,⁷⁴ R. Walker,¹⁰¹ W. Walkowiak,¹⁴²
 V. Wallangen,^{147a,147b} C. Wang,^{35c} C. Wang,^{35d,87} F. Wang,¹⁷³ H. Wang,¹⁶ H. Wang,⁴² J. Wang,⁴⁴ J. Wang,¹⁵¹ K. Wang,⁸⁹
 R. Wang,⁶ S. M. Wang,¹⁵² T. Wang,²³ T. Wang,³⁷ W. Wang,^{35b} X. Wang,¹⁷⁶ C. Wanotayaroj,¹¹⁷ A. Warburton,⁸⁹ C. P. Ward,³⁰
 D. R. Wardrope,⁸⁰ A. Washbrook,⁴⁸ P. M. Watkins,¹⁹ A. T. Watson,¹⁹ M. F. Watson,¹⁹ G. Watts,¹³⁹ S. Watts,⁸⁶
 B. M. Waugh,⁸⁰ S. Webb,⁸⁵ M. S. Weber,¹⁸ S. W. Weber,¹⁷⁴ J. S. Webster,⁶ A. R. Weidberg,¹²¹ B. Weinert,⁶³ J. Weingarten,⁵⁶
 C. Weiser,⁵⁰ H. Weits,¹⁰⁸ P. S. Wells,³² T. Wenaus,²⁷ T. Wengler,³² S. Wenig,³² N. Wermes,²³ M. Werner,⁵⁰ P. Werner,³²
 M. Wessels,^{60a} J. Wetter,¹⁶² K. Whalen,¹¹⁷ N. L. Whallon,¹³⁹ A. M. Wharton,⁷⁴ A. White,⁸ M. J. White,¹ R. White,^{34b}
 D. Whiteson,¹⁶³ F. J. Wickens,¹³² W. Wiedenmann,¹⁷³ M. Wielers,¹³² P. Wienemann,²³ C. Wiglesworth,³⁸
 L. A. M. Wiik-Fuchs,²³ A. Wildauer,¹⁰² F. Wilk,⁸⁶ H. G. Wilkens,³² H. H. Williams,¹²³ S. Williams,¹⁰⁸ C. Willis,⁹²
 S. Willocq,⁸⁸ J. A. Wilson,¹⁹ I. Wingerter-Seez,⁵ F. Winklmeier,¹¹⁷ O. J. Winston,¹⁵⁰ B. T. Winter,²³ M. Wittgen,¹⁴⁴
 J. Wittkowski,¹⁰¹ S. J. Wollstadt,⁸⁵ M. W. Wolter,⁴¹ H. Wolters,^{127a,127c} B. K. Wosiek,⁴¹ J. Wotschack,³² M. J. Woudstra,⁸⁶
 K. W. Wozniak,⁴¹ M. Wu,⁵⁷ M. Wu,³³ S. L. Wu,¹⁷³ X. Wu,⁵¹ Y. Wu,⁹¹ T. R. Wyatt,⁸⁶ B. M. Wynne,⁴⁸ S. Xella,³⁸ D. Xu,^{35a}
 L. Xu,²⁷ B. Yabsley,¹⁵¹ S. Yacoub,^{146a} R. Yakabe,⁶⁹ D. Yamaguchi,¹⁵⁸ Y. Yamaguchi,¹¹⁹ A. Yamamoto,⁶⁸ S. Yamamoto,¹⁵⁶
 T. Yamanaka,¹⁵⁶ K. Yamauchi,¹⁰⁴ Y. Yamazaki,⁶⁹ Z. Yan,²⁴ H. Yang,^{35e} H. Yang,¹⁷³ Y. Yang,¹⁵² Z. Yang,¹⁵ W-M. Yao,¹⁶
 Y. C. Yap,⁸² Y. Yasu,⁶⁸ E. Yatsenko,⁵ K. H. Yau Wong,²³ J. Ye,⁴² S. Ye,²⁷ I. Yeletsikh,⁶⁷ A. L. Yen,⁵⁹ E. Yildirim,⁸⁵
 K. Yorita,¹⁷¹ R. Yoshida,⁶ K. Yoshihara,¹²³ C. Young,¹⁴⁴ C. J. S. Young,³² S. Youssef,²⁴ D. R. Yu,¹⁶ J. Yu,⁸ J. M. Yu,⁹¹
 J. Yu,⁶⁶ L. Yuan,⁶⁹ S. P. Y. Yuen,²³ I. Yusuff,^{30,ss} B. Zabinski,⁴¹ R. Zaidan,^{35d} A. M. Zaitsev,^{131,ff} N. Zakharchuk,⁴⁴
 J. Zalieckas,¹⁵ A. Zaman,¹⁴⁹ S. Zambito,⁵⁹ L. Zanello,^{133a,133b} D. Zanzi,⁹⁰ C. Zeitnitz,¹⁷⁵ M. Zeman,¹²⁹ A. Zemla,^{40a}
 J. C. Zeng,¹⁶⁶ Q. Zeng,¹⁴⁴ K. Zengel,²⁵ O. Zenin,¹³¹ T. Ženiš,^{145a} D. Zerwas,¹¹⁸ D. Zhang,⁹¹ F. Zhang,¹⁷³ G. Zhang,^{35b,nn}
 H. Zhang,^{35c} J. Zhang,⁶ L. Zhang,⁵⁰ R. Zhang,²³ R. Zhang,^{35b,tt} X. Zhang,^{35d} Z. Zhang,¹¹⁸ X. Zhao,⁴² Y. Zhao,^{35d} Z. Zhao,^{35b}
 A. Zhemchugov,⁶⁷ J. Zhong,¹²¹ B. Zhou,⁹¹ C. Zhou,⁴⁷ L. Zhou,³⁷ L. Zhou,⁴² M. Zhou,¹⁴⁹ N. Zhou,^{35f} C. G. Zhu,^{35d}
 H. Zhu,^{35a} J. Zhu,⁹¹ Y. Zhu,^{35b} X. Zhuang,^{35a} K. Zhukov,⁹⁷ A. Zibell,¹⁷⁴ D. Zieminska,⁶³ N. I. Zimine,⁶⁷ C. Zimmermann,⁸⁵
 S. Zimmermann,⁵⁰ Z. Zinonos,⁵⁶ M. Zinser,⁸⁵ M. Ziolkowski,¹⁴² L. Živković,¹⁴ G. Zobernig,¹⁷³ A. Zoccoli,^{22a,22b}
 M. zur Nedden,¹⁷ G. Zurzolo,^{105a,105b} and L. Zwalinski³²

(ATLAS Collaboration)

¹Department of Physics, University of Adelaide, Adelaide, Australia²Physics Department, SUNY Albany, Albany NY, USA³Department of Physics, University of Alberta, Edmonton AB, Canada^{4a}Department of Physics, Ankara University, Ankara, Turkey^{4b}Istanbul Aydın University, Istanbul, Turkey^{4c}Division of Physics, TOBB University of Economics and Technology, Ankara, Turkey

- ⁵LAPP, CNRS/IN2P3 and Université Savoie Mont Blanc, Annecy-le-Vieux, France
- ⁶High Energy Physics Division, Argonne National Laboratory, Argonne IL, USA
- ⁷Department of Physics, University of Arizona, Tucson AZ, USA
- ⁸Department of Physics, The University of Texas at Arlington, Arlington TX, USA
- ⁹Physics Department, University of Athens, Athens, Greece
- ¹⁰Physics Department, National Technical University of Athens, Zografou, Greece
- ¹¹Department of Physics, The University of Texas at Austin, Austin TX, USA
- ¹²Institute of Physics, Azerbaijan Academy of Sciences, Baku, Azerbaijan
- ¹³Institut de Física d'Altes Energies (IFAE), The Barcelona Institute of Science and Technology, Barcelona, Spain
- ¹⁴Institute of Physics, University of Belgrade, Belgrade, Serbia
- ¹⁵Department for Physics and Technology, University of Bergen, Bergen, Norway
- ¹⁶Physics Division, Lawrence Berkeley National Laboratory and University of California, Berkeley CA, USA
- ¹⁷Department of Physics, Humboldt University, Berlin, Germany
- ¹⁸Albert Einstein Center for Fundamental Physics and Laboratory for High Energy Physics, University of Bern, Bern, Switzerland
- ¹⁹School of Physics and Astronomy, University of Birmingham, Birmingham, United Kingdom
- ^{20a}Department of Physics, Bogazici University, Istanbul, Turkey
- ^{20b}Department of Physics Engineering, Gaziantep University, Gaziantep, Turkey
- ^{20d}Istanbul Bilgi University, Faculty of Engineering and Natural Sciences, Istanbul, Turkey, Turkey
- ^{20c}Bahcesehir University, Faculty of Engineering and Natural Sciences, Istanbul, Turkey, Turkey
- ²¹Centro de Investigaciones, Universidad Antonio Narino, Bogota, Colombia
- ^{22a}INFN Sezione di Bologna, Italy
- ^{22b}Dipartimento di Fisica e Astronomia, Università di Bologna, Bologna, Italy
- ²³Physikalisches Institut, University of Bonn, Bonn, Germany
- ²⁴Department of Physics, Boston University, Boston MA, USA
- ²⁵Department of Physics, Brandeis University, Waltham MA, USA
- ^{26a}Universidade Federal do Rio De Janeiro COPPE/EE/IF, Rio de Janeiro, Brazil
- ^{26b}Electrical Circuits Department, Federal University of Juiz de Fora (UFJF), Juiz de Fora, Brazil
- ^{26c}Federal University of Sao Joao del Rei (UFSJ), Sao Joao del Rei, Brazil
- ^{26d}Instituto de Física, Universidade de Sao Paulo, Sao Paulo, Brazil
- ²⁷Physics Department, Brookhaven National Laboratory, Upton NY, USA
- ^{28a}Transilvania University of Brasov, Brasov, Romania
- ^{28b}National Institute of Physics and Nuclear Engineering, Bucharest, Romania
- ^{28c}National Institute for Research and Development of Isotopic and Molecular Technologies, Physics Department, Cluj Napoca, Romania
- ^{28d}University Politehnica Bucharest, Bucharest, Romania
- ^{28e}West University in Timisoara, Timisoara, Romania
- ²⁹Departamento de Física, Universidad de Buenos Aires, Buenos Aires, Argentina
- ³⁰Cavendish Laboratory, University of Cambridge, Cambridge, United Kingdom
- ³¹Department of Physics, Carleton University, Ottawa ON, Canada
- ³²CERN, Geneva, Switzerland
- ³³Enrico Fermi Institute, University of Chicago, Chicago IL, USA
- ^{34a}Departamento de Física, Pontificia Universidad Católica de Chile, Santiago, Chile
- ^{34b}Departamento de Física, Universidad Técnica Federico Santa María, Valparaíso, Chile
- ^{35a}Institute of High Energy Physics, Chinese Academy of Sciences, Beijing, China
- ^{35b}Department of Modern Physics, University of Science and Technology of China, Anhui, China
- ^{35c}Department of Physics, Nanjing University, Jiangsu, China
- ^{35d}School of Physics, Shandong University, Shandong, China
- ^{35e}Department of Physics and Astronomy, Shanghai Key Laboratory for Particle Physics and Cosmology, Shanghai Jiao Tong University, Shanghai; (also affiliated with PKU-CHEP), China
- ^{35f}Physics Department, Tsinghua University, Beijing 100084, China
- ³⁶Laboratoire de Physique Corpusculaire, Clermont Université and Université Blaise Pascal and CNRS/IN2P3, Clermont-Ferrand, France
- ³⁷Nevis Laboratory, Columbia University, Irvington NY, USA
- ³⁸Niels Bohr Institute, University of Copenhagen, Kobenhavn, Denmark
- ^{39a}INFN Gruppo Collegato di Cosenza, Laboratori Nazionali di Frascati, Italy
- ^{39b}Dipartimento di Fisica, Università della Calabria, Rende, Italy

- ^{40a}AGH University of Science and Technology, Faculty of Physics and Applied Computer Science, Krakow, Poland
- ^{40b}Marian Smoluchowski Institute of Physics, Jagiellonian University, Krakow, Poland
- ⁴¹Institute of Nuclear Physics Polish Academy of Sciences, Krakow, Poland
- ⁴²Physics Department, Southern Methodist University, Dallas TX, USA
- ⁴³Physics Department, University of Texas at Dallas, Richardson TX, USA
- ⁴⁴DESY, Hamburg and Zeuthen, Germany
- ⁴⁵Institut für Experimentelle Physik IV, Technische Universität Dortmund, Dortmund, Germany
- ⁴⁶Institut für Kern- und Teilchenphysik, Technische Universität Dresden, Dresden, Germany
- ⁴⁷Department of Physics, Duke University, Durham NC, USA
- ⁴⁸SUPA - School of Physics and Astronomy, University of Edinburgh, Edinburgh, United Kingdom
- ⁴⁹INFN Laboratori Nazionali di Frascati, Frascati, Italy
- ⁵⁰Fakultät für Mathematik und Physik, Albert-Ludwigs-Universität, Freiburg, Germany
- ⁵¹Section de Physique, Université de Genève, Geneva, Switzerland
- ^{52a}INFN Sezione di Genova, Italy
- ^{52b}Dipartimento di Fisica, Università di Genova, Genova, Italy
- ^{53a}E. Andronikashvili Institute of Physics, Iv. Javakishvili Tbilisi State University, Tbilisi, Georgia
- ^{53b}High Energy Physics Institute, Tbilisi State University, Tbilisi, Georgia
- ⁵⁴II Physikalisches Institut, Justus-Liebig-Universität Giessen, Giessen, Germany
- ⁵⁵SUPA - School of Physics and Astronomy, University of Glasgow, Glasgow, United Kingdom
- ⁵⁶II Physikalisches Institut, Georg-August-Universität, Göttingen, Germany
- ⁵⁷Laboratoire de Physique Subatomique et de Cosmologie, Université Grenoble-Alpes, CNRS/IN2P3, Grenoble, France
- ⁵⁸Department of Physics, Hampton University, Hampton VA, USA
- ⁵⁹Laboratory for Particle Physics and Cosmology, Harvard University, Cambridge MA, USA
- ^{60a}Kirchhoff-Institut für Physik, Ruprecht-Karls-Universität Heidelberg, Heidelberg, Germany
- ^{60b}Physikalisches Institut, Ruprecht-Karls-Universität Heidelberg, Heidelberg, Germany
- ^{60c}ZITI Institut für technische Informatik, Ruprecht-Karls-Universität Heidelberg, Mannheim, Germany
- ⁶¹Faculty of Applied Information Science, Hiroshima Institute of Technology, Hiroshima, Japan
- ^{62a}Department of Physics, The Chinese University of Hong Kong, Shatin, N.T., Hong Kong, China
- ^{62b}Department of Physics, The University of Hong Kong, Hong Kong, China
- ^{62c}Department of Physics, The Hong Kong University of Science and Technology, Clear Water Bay, Kowloon, Hong Kong, China
- ⁶³Department of Physics, Indiana University, Bloomington IN, USA
- ⁶⁴Institut für Astro- und Teilchenphysik, Leopold-Franzens-Universität, Innsbruck, Austria
- ⁶⁵University of Iowa, Iowa City IA, USA
- ⁶⁶Department of Physics and Astronomy, Iowa State University, Ames IA, USA
- ⁶⁷Joint Institute for Nuclear Research, JINR Dubna, Dubna, Russia
- ⁶⁸KEK, High Energy Accelerator Research Organization, Tsukuba, Japan
- ⁶⁹Graduate School of Science, Kobe University, Kobe, Japan
- ⁷⁰Faculty of Science, Kyoto University, Kyoto, Japan
- ⁷¹Kyoto University of Education, Kyoto, Japan
- ⁷²Department of Physics, Kyushu University, Fukuoka, Japan
- ⁷³Instituto de Física La Plata, Universidad Nacional de La Plata and CONICET, La Plata, Argentina
- ⁷⁴Physics Department, Lancaster University, Lancaster, United Kingdom
- ^{75a}INFN Sezione di Lecce, Italy
- ^{75b}Dipartimento di Matematica e Fisica, Università del Salento, Lecce, Italy
- ⁷⁶Oliver Lodge Laboratory, University of Liverpool, Liverpool, United Kingdom
- ⁷⁷Department of Physics, Jožef Stefan Institute and University of Ljubljana, Ljubljana, Slovenia
- ⁷⁸School of Physics and Astronomy, Queen Mary University of London, London, United Kingdom
- ⁷⁹Department of Physics, Royal Holloway University of London, Surrey, United Kingdom
- ⁸⁰Department of Physics and Astronomy, University College London, London, United Kingdom
- ⁸¹Louisiana Tech University, Ruston LA, USA
- ⁸²Laboratoire de Physique Nucléaire et de Hautes Energies, UPMC and Université Paris-Diderot and CNRS/IN2P3, Paris, France
- ⁸³Fysiska institutionen, Lunds universitet, Lund, Sweden
- ⁸⁴Departamento de Física Teórica C-15, Universidad Autónoma de Madrid, Madrid, Spain
- ⁸⁵Institut für Physik, Universität Mainz, Mainz, Germany
- ⁸⁶School of Physics and Astronomy, University of Manchester, Manchester, United Kingdom
- ⁸⁷CPPM, Aix-Marseille Université and CNRS/IN2P3, Marseille, France

- ⁸⁸*Department of Physics, University of Massachusetts, Amherst MA, USA*
- ⁸⁹*Department of Physics, McGill University, Montreal QC, Canada*
- ⁹⁰*School of Physics, University of Melbourne, Victoria, Australia*
- ⁹¹*Department of Physics, The University of Michigan, Ann Arbor MI, USA*
- ⁹²*Department of Physics and Astronomy, Michigan State University, East Lansing MI, USA*
- ^{93a}*INFN Sezione di Milano, Italy*
- ^{93b}*Dipartimento di Fisica, Università di Milano, Milano, Italy*
- ⁹⁴*B.I. Stepanov Institute of Physics, National Academy of Sciences of Belarus, Minsk, Republic of Belarus*
- ⁹⁵*National Scientific and Educational Centre for Particle and High Energy Physics, Minsk, Republic of Belarus*
- ⁹⁶*Group of Particle Physics, University of Montreal, Montreal QC, Canada*
- ⁹⁷*P.N. Lebedev Physical Institute of the Russian Academy of Sciences, Moscow, Russia*
- ⁹⁸*Institute for Theoretical and Experimental Physics (ITEP), Moscow, Russia*
- ⁹⁹*National Research Nuclear University MEPhI, Moscow, Russia*
- ¹⁰⁰*D.V. Skobeltsyn Institute of Nuclear Physics, M.V. Lomonosov Moscow State University, Moscow, Russia*
- ¹⁰¹*Fakultät für Physik, Ludwig-Maximilians-Universität München, München, Germany*
- ¹⁰²*Max-Planck-Institut für Physik (Werner-Heisenberg-Institut), München, Germany*
- ¹⁰³*Nagasaki Institute of Applied Science, Nagasaki, Japan*
- ¹⁰⁴*Graduate School of Science and Kobayashi-Maskawa Institute, Nagoya University, Nagoya, Japan*
- ^{105a}*INFN Sezione di Napoli, Italy*
- ^{105b}*Dipartimento di Fisica, Università di Napoli, Napoli, Italy*
- ¹⁰⁶*Department of Physics and Astronomy, University of New Mexico, Albuquerque NM, USA*
- ¹⁰⁷*Institute for Mathematics, Astrophysics and Particle Physics, Radboud University Nijmegen/Nikhef, Nijmegen, Netherlands*
- ¹⁰⁸*Nikhef National Institute for Subatomic Physics and University of Amsterdam, Amsterdam, Netherlands*
- ¹⁰⁹*Department of Physics, Northern Illinois University, DeKalb IL, USA*
- ¹¹⁰*Budker Institute of Nuclear Physics, SB RAS, Novosibirsk, Russia*
- ¹¹¹*Department of Physics, New York University, New York NY, USA*
- ¹¹²*Ohio State University, Columbus OH, USA*
- ¹¹³*Faculty of Science, Okayama University, Okayama, Japan*
- ¹¹⁴*Homer L. Dodge Department of Physics and Astronomy, University of Oklahoma, Norman OK, USA*
- ¹¹⁵*Department of Physics, Oklahoma State University, Stillwater OK, USA*
- ¹¹⁶*Palacký University, RCPTM, Olomouc, Czech Republic*
- ¹¹⁷*Center for High Energy Physics, University of Oregon, Eugene OR, USA*
- ¹¹⁸*LAL, Univ. Paris-Sud, CNRS/IN2P3, Université Paris-Saclay, Orsay, France*
- ¹¹⁹*Graduate School of Science, Osaka University, Osaka, Japan*
- ¹²⁰*Department of Physics, University of Oslo, Oslo, Norway*
- ¹²¹*Department of Physics, Oxford University, Oxford, United Kingdom*
- ^{122a}*INFN Sezione di Pavia, Italy*
- ^{122b}*Dipartimento di Fisica, Università di Pavia, Pavia, Italy*
- ¹²³*Department of Physics, University of Pennsylvania, Philadelphia PA, USA*
- ¹²⁴*National Research Centre “Kurchatov Institute” B.P.Konstantinov Petersburg Nuclear Physics Institute, St. Petersburg, Russia*
- ^{125a}*INFN Sezione di Pisa, Italy*
- ^{125b}*Dipartimento di Fisica E. Fermi, Università di Pisa, Pisa, Italy*
- ¹²⁶*Department of Physics and Astronomy, University of Pittsburgh, Pittsburgh PA, USA*
- ^{127a}*Laboratório de Instrumentação e Física Experimental de Partículas - LIP, Lisboa, Portugal*
- ^{127b}*Faculdade de Ciências, Universidade de Lisboa, Lisboa, Portugal*
- ^{127c}*Department of Physics, University of Coimbra, Coimbra, Portugal*
- ^{127d}*Centro de Física Nuclear da Universidade de Lisboa, Lisboa, Portugal*
- ^{127e}*Departamento de Física, Universidade do Minho, Braga, Portugal*
- ^{127f}*Departamento de Física Teórica y del Cosmos and CAFPE, Universidad de Granada, Granada, Spain*
- ^{127g}*Dep Física and CEFITEC of Faculdade de Ciências e Tecnologia, Universidade Nova de Lisboa, Caparica, Portugal*
- ¹²⁸*Institute of Physics, Academy of Sciences of the Czech Republic, Praha, Czech Republic*
- ¹²⁹*Czech Technical University in Prague, Praha, Czech Republic*
- ¹³⁰*Faculty of Mathematics and Physics, Charles University in Prague, Praha, Czech Republic*
- ¹³¹*State Research Center Institute for High Energy Physics (Protvino), NRC KI, Russia*
- ¹³²*Particle Physics Department, Rutherford Appleton Laboratory, Didcot, United Kingdom*

- ^{133a}*INFN Sezione di Roma, Italy*
- ^{133b}*Dipartimento di Fisica, Sapienza Università di Roma, Roma, Italy*
- ^{134a}*INFN Sezione di Roma Tor Vergata, Italy*
- ^{134b}*Dipartimento di Fisica, Università di Roma Tor Vergata, Roma, Italy*
- ^{135a}*INFN Sezione di Roma Tre, Italy*
- ^{135b}*Dipartimento di Matematica e Fisica, Università Roma Tre, Roma, Italy*
- ^{136a}*Faculté des Sciences Ain Chock, Réseau Universitaire de Physique des Hautes Energies - Université Hassan II, Casablanca, Morocco*
- ^{136b}*Centre National de l'Energie des Sciences Techniques Nucleaires, Rabat, Morocco*
- ^{136c}*Faculté des Sciences Semlalia, Université Cadi Ayyad, LPHEA-Marrakech, Morocco*
- ^{136d}*Faculté des Sciences, Université Mohamed Premier and LTPM, Oujda, Morocco*
- ^{136e}*Faculté des sciences, Université Mohammed V, Rabat, Morocco*
- ¹³⁷*DSM/IRFU (Institut de Recherches sur les Lois Fondamentales de l'Univers), CEA Saclay (Commissariat à l'Energie Atomique et aux Energies Alternatives), Gif-sur-Yvette, France*
- ¹³⁸*Santa Cruz Institute for Particle Physics, University of California Santa Cruz, Santa Cruz CA, USA*
- ¹³⁹*Department of Physics, University of Washington, Seattle WA, USA*
- ¹⁴⁰*Department of Physics and Astronomy, University of Sheffield, Sheffield, United Kingdom*
- ¹⁴¹*Department of Physics, Shinshu University, Nagano, Japan*
- ¹⁴²*Fachbereich Physik, Universität Siegen, Siegen, Germany*
- ¹⁴³*Department of Physics, Simon Fraser University, Burnaby BC, Canada*
- ¹⁴⁴*SLAC National Accelerator Laboratory, Stanford CA, USA*
- ^{145a}*Faculty of Mathematics, Physics & Informatics, Comenius University, Bratislava, Slovak Republic*
- ^{145b}*Department of Subnuclear Physics, Institute of Experimental Physics of the Slovak Academy of Sciences, Kosice, Slovak Republic*
- ^{146a}*Department of Physics, University of Cape Town, Cape Town, South Africa*
- ^{146b}*Department of Physics, University of Johannesburg, Johannesburg, South Africa*
- ^{146c}*School of Physics, University of the Witwatersrand, Johannesburg, South Africa*
- ^{147a}*Department of Physics, Stockholm University, Sweden*
- ^{147b}*The Oskar Klein Centre, Stockholm, Sweden*
- ¹⁴⁸*Physics Department, Royal Institute of Technology, Stockholm, Sweden*
- ¹⁴⁹*Departments of Physics & Astronomy and Chemistry, Stony Brook University, Stony Brook NY, USA*
- ¹⁵⁰*Department of Physics and Astronomy, University of Sussex, Brighton, United Kingdom*
- ¹⁵¹*School of Physics, University of Sydney, Sydney, Australia*
- ¹⁵²*Institute of Physics, Academia Sinica, Taipei, Taiwan*
- ¹⁵³*Department of Physics, Technion: Israel Institute of Technology, Haifa, Israel*
- ¹⁵⁴*Raymond and Beverly Sackler School of Physics and Astronomy, Tel Aviv University, Tel Aviv, Israel*
- ¹⁵⁵*Department of Physics, Aristotle University of Thessaloniki, Thessaloniki, Greece*
- ¹⁵⁶*International Center for Elementary Particle Physics and Department of Physics, The University of Tokyo, Tokyo, Japan*
- ¹⁵⁷*Graduate School of Science and Technology, Tokyo Metropolitan University, Tokyo, Japan*
- ¹⁵⁸*Department of Physics, Tokyo Institute of Technology, Tokyo, Japan*
- ¹⁵⁹*Department of Physics, University of Toronto, Toronto ON, Canada*
- ^{160a}*TRIUMF, Vancouver BC, Canada*
- ^{160b}*Department of Physics and Astronomy, York University, Toronto ON, Canada*
- ¹⁶¹*Faculty of Pure and Applied Sciences, and Center for Integrated Research in Fundamental Science and Engineering, University of Tsukuba, Tsukuba, Japan*
- ¹⁶²*Department of Physics and Astronomy, Tufts University, Medford MA, USA*
- ¹⁶³*Department of Physics and Astronomy, University of California Irvine, Irvine CA, USA*
- ^{164a}*INFN Gruppo Collegato di Udine, Sezione di Trieste, Udine, Italy*
- ^{164b}*ICTP, Trieste, Italy*
- ^{164c}*Dipartimento di Chimica, Fisica e Ambiente, Università di Udine, Udine, Italy*
- ¹⁶⁵*Department of Physics and Astronomy, University of Uppsala, Uppsala, Sweden*
- ¹⁶⁶*Department of Physics, University of Illinois, Urbana IL, USA*
- ¹⁶⁷*Instituto de Física Corpuscular (IFIC) and Departamento de Física Atomica, Molecular y Nuclear and Departamento de Ingeniería Electrónica and Instituto de Microelectrónica de Barcelona (IMB-CNM), University of Valencia and CSIC, Valencia, Spain*
- ¹⁶⁸*Department of Physics, University of British Columbia, Vancouver BC, Canada*
- ¹⁶⁹*Department of Physics and Astronomy, University of Victoria, Victoria BC, Canada*
- ¹⁷⁰*Department of Physics, University of Warwick, Coventry, United Kingdom*
- ¹⁷¹*Waseda University, Tokyo, Japan*

¹⁷²*Department of Particle Physics, The Weizmann Institute of Science, Rehovot, Israel*¹⁷³*Department of Physics, University of Wisconsin, Madison WI, USA*¹⁷⁴*Fakultät für Physik und Astronomie, Julius-Maximilians-Universität, Würzburg, Germany*¹⁷⁵*Fakultät für Mathematik und Naturwissenschaften, Fachgruppe Physik, Bergische Universität Wuppertal, Wuppertal, Germany*¹⁷⁶*Department of Physics, Yale University, New Haven CT, USA*¹⁷⁷*Yerevan Physics Institute, Yerevan, Armenia*¹⁷⁸*Centre de Calcul de l'Institut National de Physique Nucléaire et de Physique des Particules (IN2P3), Villeurbanne, France*^aDeceased.^bAlso at Department of Physics, King's College London, London, United Kingdom.^cAlso at Institute of Physics, Azerbaijan Academy of Sciences, Baku, Azerbaijan.^dAlso at Novosibirsk State University, Novosibirsk, Russia.^eAlso at TRIUMF, Vancouver BC, Canada.^fAlso at Department of Physics & Astronomy, University of Louisville, Louisville, KY, USA.^gAlso at Department of Physics, California State University, Fresno CA, USA.^hAlso at Department of Physics, University of Fribourg, Fribourg, Switzerland.ⁱAlso at Departament de Física de la Universitat Autònoma de Barcelona, Barcelona, Spain.^jAlso at Departamento de Física e Astronomia, Faculdade de Ciências, Universidade do Porto, Portugal.^kAlso at Tomsk State University, Tomsk, Russia.^lAlso at Università di Napoli Parthenope, Napoli, Italy.^mAlso at Institute of Particle Physics (IPP), Canada.ⁿAlso at National Institute of Physics and Nuclear Engineering, Bucharest, Romania.^oAlso at Department of Physics, St. Petersburg State Polytechnical University, St. Petersburg, Russia.^pAlso at Department of Physics, The University of Michigan, Ann Arbor MI, USA.^qAlso at Centre for High Performance Computing, CSIR Campus, Rosebank, Cape Town, South Africa.^rAlso at Louisiana Tech University, Ruston LA, USA.^sAlso at Institutio Catalana de Recerca i Estudis Avancats, ICREA, Barcelona, Spain.^tAlso at Graduate School of Science, Osaka University, Osaka, Japan.^uAlso at Department of Physics, National Tsing Hua University, Taiwan.^vAlso at Institute for Mathematics, Astrophysics and Particle Physics, Radboud University Nijmegen/Nikhef, Nijmegen, Netherlands.^wAlso at Department of Physics, The University of Texas at Austin, Austin TX, USA.^xAlso at Institute of Theoretical Physics, Ilia State University, Tbilisi, Georgia.^yAlso at CERN, Geneva, Switzerland.^zAlso at Georgian Technical University (GTU), Tbilisi, Georgia.^{aa}Also at Ochadai Academic Production, Ochanomizu University, Tokyo, Japan.^{bb}Also at Manhattan College, New York NY, USA.^{cc}Also at Hellenic Open University, Patras, Greece.^{dd}Also at Academia Sinica Grid Computing, Institute of Physics, Academia Sinica, Taipei, Taiwan.^{ee}Also at School of Physics, Shandong University, Shandong, China.^{ff}Also at Moscow Institute of Physics and Technology State University, Dolgoprudny, Russia.^{gg}Also at Section de Physique, Université de Genève, Geneva, Switzerland.^{hh}Also at Eotvos Lorand University, Budapest, Hungary.ⁱⁱAlso at International School for Advanced Studies (SISSA), Trieste, Italy.^{jj}Also at Department of Physics and Astronomy, University of South Carolina, Columbia SC, USA.^{kk}Also at School of Physics and Engineering, Sun Yat-sen University, Guangzhou, China.^{ll}Also at Institute for Nuclear Research and Nuclear Energy (INRNE) of the Bulgarian Academy of Sciences, Sofia, Bulgaria.^{mm}Also at Faculty of Physics, M.V.Lomonosov Moscow State University, Moscow, Russia.ⁿⁿAlso at Institute of Physics, Academia Sinica, Taipei, Taiwan.^{oo}Also at National Research Nuclear University MEPhI, Moscow, Russia.^{pp}Also at Department of Physics, Stanford University, Stanford CA, USA.^{qq}Also at Institute for Particle and Nuclear Physics, Wigner Research Centre for Physics, Budapest, Hungary.^{rr}Also at Flensburg University of Applied Sciences, Flensburg, Germany.^{ss}Also at University of Malaya, Department of Physics, Kuala Lumpur, Malaysia.^{tt}Also at CPPM, Aix-Marseille Université and CNRS/IN2P3, Marseille, France.